LOCALIZATION, TRACKING, AND ANTENNA ALLOCATION IN
MULTIPLE-INPUT MULTIPLE-OUTPUT RADARS

LOCALIZATION, TRACKING, AND ANTENNA ALLOCATION IN MULTIPLE-INPUT MULTIPLE-OUTPUT RADARS

By

ALIAKBAR GORJI DARONKOLAEI, B.Sc., M.Sc.

A Thesis

Submitted to the School of Graduate Studies

in Partial Fulfillment of the Requirements

for the Degree

Doctor of Philosophy

McMaster University

DOCTOR OF PHILOSOPHY (2012)   MCMASTER UNIVERSITY

(Electrical and Computer Engineering)   Hamilton, Ontario

TITLE: **Localization, Tracking, And Antenna Allocation
                          in Multiple-input Multiple-output Radars**

AUTHOR: Aliakbar Gorji Daronkolaei

                          B.Sc., M.Sc.

SUPERVISOR: Dr. Thia Kirubarajan

NUMBER OF PAGES: xx, 159

To my lovely parents who were my main supporters

Abstract

This thesis concerns with the localization, tracking, and sensor management in the Multiple-Input Multiple-Output (MIMO) radar systems. The collocated and widely-separated MIMO radars are separately discussed and the signal models are derived for both structures. The first chapter of the thesis is dedicated to the tracking and localization in collocated MIMO radars. A novel signal model is first formulated and the localization algorithm is developed for the derived signal model to estimate the location of multiple targets falling in the same resolution cell. Furthermore, a novel tracking algorithm is proposed in which the maximum bound on the number of uniquely detectable targets in the same cell is relaxed. The performance of the tracking and localization algorithms is finally evaluated using the tracking Posterior Cramer-Rao Lower Bound (PCRLB). After showing the impact of the antennas position on the localization CRLB, a novel sensor management technique is developed for the collocated MIMO radars in Chapter 4. A convex optimization technique is proposed for the antenna allocation in a single-target scenario. When multiple targets fall inside the same cell, a sampling-based technique is formulated to tackle the non-convexity of the optimization problem.

The third chapter of this thesis also proposes new approaches for detection, localization, and tracking using a widely-separated MIMO radar. A scenario with multiple-scatterer targets is considered and the detection performance of

both MIMO and multistatic radars will be evaluated in the designed scenario. To estimate the location of the multiple-scatterer target, a Multiple-Hypothesis (MH) based approach is proposed where the number and the location of multiple targets are both estimated. A particle filter based approach is also formulated for the dynamic tracking by a widely-separated MIMO radar. Finally, the performance of the MIMO radar and the miultistatic radar in detecting and localizing multiple-scatterer targets is studied.

Acknowledgements

During writing this thesis I have met and interacted with many people who have influenced and contributed to the path of my research. I first would like to express my deepest gratitude to Professor Thia Kirubarajan, who has been my thesis supervisor during the past four years. He introduced me to the field of target tracking, radar systems and many interesting ideas in a very relaxed atmosphere. Defining and writing this thesis would not be certainly possible without professor Kirubarajan's supervision and encouragements.

I am also grateful to Dr. Ratnasingham Tharmarasa for contributing enormously towards my understanding of radar systems and tracking algorithms. A significant part of my thesis contributions is a result of Thamas' great ideas and helpful suggestions. I really enjoyed interacting with you, Thamas!

I would like to specially thank Professor Brian Anderson, who was my supervisor during my visit to the Australian National University (ANU). Brian has been the most humble, resourceful, and the gentlest person who I have ever met in my life. I learnt many things from Brian in both academic and ethical points of view. I always wish I could have another opportunity to work with Brian.

Besides my supervisors, I have been also fortunate to collaborate with some other academic members at McMaster. I am specially indebted to Professor

Jim Reilly and Dr. Jian-Kang Zhang as the members of my graduate committee. I also thank Professor Tim Davidson for his constructive and helpful comments on the optimization and signal processing aspects of MIMO radars.

Many other people have helped me, directly or indirectly, at different stages of my PhD study. I would like to thank my friends and colleagues at McMaster including Nima Zarif, Keyvan Hosseinkhani, Reza Haghshenas, Sina Naderi, Hamed Afshari, Mina Attari, Kasra Asadzadeh, Sadegh Dadash, Bahram Marami, Ramin Mafi, Mehdi Nabaee, Cheryl Gies, Dr. Nandakumaran Nadarajah, Xin Chen, Darcy Dunne, and Biruk Habtemariam. My special thanks also go to Dr. Brad Yu, Dr. Adrian Bishop, Dr. Mark Reed, Mohsen Zamani, Mohammad Deghat, Morteza Azad, Alireza Motevallian, and Elspeth Davis who helped me during my visit at ANU. My whole PhD study would never be finalized without the help of above people.

Over the last four years, I was supported by two McMaster university graduate scholarship, and prestigious Sherman Clifford scholarship. I am most grateful for this financial assistance.

At the end, I want to thank my wife, parents and my brother for all love, support, and motivation.

List of Acronyms

2D	Two Dimensional
RCS	Radar-target Cross-section
MIMO	Multipl-input Multiple-output
CRLB	Cramer-Rao Lower Bound
FIM	Fisher Information Matrix
PCRLB	Posterior Cramer-Rao Lower Bound
DOA	Direction of Arrival
SDP	Semi-definite Programming
MSE	Mean Squared Error
MMSE	Minimum Mean Squared Error
RMSE	Root Mean Squared Error
MHT	Multiple-hypothesi Tracking
MH	Multiple Hypothesis
TBD	Track-Before-Detect
SNR	Signal-to-Noise Ratio
KF	Kalman Filter
EKF	Extended Kalman Filter
UKF	Unscented Kalman Filter
GRLT	Generalized Likelihood Ratio Test
BLUE	Best Linear Unbiased Estimator
ML	Maximum Likelihood
MDL	Minimum Distance Length
ROC	Receiver Operating Characteristic
TOT	Time-On-Target
TOA	Time of Arrival

List of Notations and Symbols

$\| \cdot \|_2$ Second Euclidian norm of a vector

x Scalar

$\mathbf{x}$ Vector

A Matrix

$\mathbf{x}_i$ i0-th entry of $\mathbf{x}$

A_{ij} (i, j)-th entry of A

$A(:, i)$ i-th column of A

$\Re(x)$ Real part of x

$\Im(x)$ Imaginary part of x

Operators and Functions

A'	Matrix transpose
A^{-1}	Inverse of matrix
A^H	Matrix Hermition transpose
$\|A\|$	Matrix determinant
$\mathcal{T}(A)$	Trace of matrix A
$A = \mathcal{D}(\mathbf{x})$	A diagonal matrix with $A_{ii} = \mathbf{x}_i$ and $A_{ij} = 0,\ i \neq j$
$\odot$	Kronicker product
$\langle \mathbf{x}, \mathbf{y} \rangle$	inner product of two vectors $\mathbf{x}$ and $\mathbf{y}$
$E(x)$	Expected value of the random variable x
$\mathcal{CN}(\mu, \Sigma)$	Complex Gaussian distribution with mean and covariance Σ
$\mathbf{a} = VEC(A)$	A vector constructed by stacking all columns of matrix A

Contents

List of Figures

xviii

List of Tables

Chapter 1

Introduction

This chapter is dedicated to review the basic concepts of the MIMO systems and their equivalence in the radar community. The MIMO concept is first discussed in Section 1.1. The benefits of the new emerging MIMO communication systems to the traditional SISO models are presented in this section. The MIMO radar systems are described in Section 1.2. Two different structures of the recently-proposed MIMO radars are first introduced and their advantages to the traditional phased-array and multistatic radars are summarized. The main contributions of this thesis are also demonstrated in Section 1.3.

1.1   MIMO Concept

MIMO is designated to the use of multiple antennas in both the transmitter and receiver stations [9]. The new MIMO concept has been originally proposed to improve the communication performance in wireless systems. The critical performances in the wireless community particularly include the power, bandwidth, complexity, and the rate of data transmission. The new emerging

MIMO technology has therefore attracted much attention due to the huge impact on the improvement of the communication performance. Compared to the traditional SISO structures, the MIMO antennas provide increased coverage, higher capacity and data rate, improved spectral efficiency, reduced power consumption, and reduced cost of wireless network [31]. These remarkable benefits ignited much interest among researchers to explore different aspects of MIMO communication systems such as channel capacity [41] [77], power and resource allocation [73] [86], and beam-forming [23].

A multiple antenna system might be represented in different configurations. As Figure 1.1 shows, the MIMO system is designed by placing multiple transmitters and receivers while other structures can be also created by creating single or multiple antennas in the transmitter or receiver sections. Now, consider the MIMO structure with M transmitters and N receivers. The received signal vector for a single-user MIMO system can be written as follows [41]:

$$\mathbf{y} = H\mathbf{s} + \mathbf{w} \tag{1.1}$$

where $\mathbf{w}$ denotes the white circularly symmetric complex Gaussian noise vector, normalized so that its covariance matrix is the identity matrix, and H is the $N \times M$ stochastic channel matrix. The amount of knowledge about the channel matrix depends on the availability of channel information in the transmitters and receivers. With the perfect channel state information at the transmitter (CSIT) and the perfect channel state information at the receiver (CSIR), the channel state information (CSI) or the system matrix H is fully known [41]. However, when the partial information is present at each or the transmitter or receiver sections, it is assumed that the channel distribution to the transmitter (CDIT) or to the receiver (CDIR) is available. It was shown by [27] [77] that under the perfect CSIR and CDIT where the channel

2

is assumed to be zero-mean spatially white (ZMSW) [41], the capacity grows linearly with the rate $\min(M, N)$ if the channel fading changes slowly by time. Alternatively, when the perfect CSIR and CSIT are available, the growth rate is reduced at higher SNRs while still increased at low SNRs [19]. In other words, the assumption of the perfect CSIR plays an important role in the capacity improvement of the MIMO communication system [41]. In this case, a set of training symbols is sent to the receiver section to estimate the channel state. With the perfect CSIR, the MIMO communication system shows a significant improvement in the capacity to the traditional SISO model whose information theoretic and communication aspects were explored in [8].

Besides the higher capacity, MIMO systems enjoy the spatial diversity in the signal paths by using multiple independent channel fading h_{ij}. The diversity gain is defined as the amount of a diversity scheme that reduces the required transmitted power without any performance loss. Ideally, a MIMO system with M transmitters and N receivers achieves MN as the maximum possible diversity gain. For the classical MIMO model given by (1.1), a space-time coding that achieves the maximum diversity gain meets the following condition [88]:

$$P_e(SNR) \sim SNR^{-MN} \qquad (1.2)$$

with P_e being the probability of error and SNR as the receiver signal-to-noise ratio. An analysis of the diversity gain for the block coded Ricean MIMO channels was also conducted in [64]. It was shown that there is a minimum rate (R_{crit}) under which if the data are transmitted the Ricean channel behaves like a Rayleigh one. Then, the relation of the diversity order to the slope of the average probability of error versus SNR curve and the diversity order to the slope of the outage probability versus SNR curve was derived. The diversity gain of the MIMO system was also calculated for double-scattering channels

3

in [70]. For the orthogonal spacetime block codes, it was shown in [70] that the diversity gain is of order $\frac{MNN_s}{\max(M,N,N_s)}$ with N_e being the number of effective scatterers. It was also mentioned in [91] that the lack of the knowledge about the channel state affects the diversity gain of a MIMO channel. With the joint power and rate control, analysis in [91] shows a significant improvement in the diversity gain of the MIMO fading channel. While there are many other works being done on the analysis of the diversity gain in MIMO communication systems, they finally show that under suitable conditions the MIMO system achieves a higher diversity gain compared to the SISO systems.

It is now inferred that channel estimation and equalization are two main concerns in MIMO systems. The main philosophy behind the invention of the MIMO system is to enjoy the diversity gain leading to a higher capacity and probability of error in the receiver. The research on different aspects of MIMO communication systems still carries on with several open problems in calculating the capacity of the MIMO channel [41] and the effect of different system parameters on the diversity gain and outage probability. In the next section, the MIMO idea is extended to the radar systems. It will be shown how the ideas like the diversity gain can be exploited in radar community. A potential comparison between the MIMO communication and radar systems will be finally provided.

1.2   MIMO in Radar Community

Recently, the idea of MIMO communication systems was exploited in the radar community to mitigate some drawbacks in the traditional phase-array and multistatic radar systems [72]. The idea is to design a multiple antenna radar system with M transmitters and N receivers that provides the benefits of
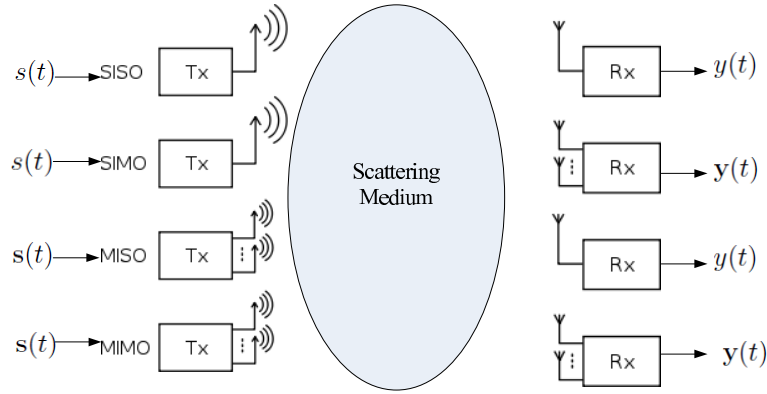
Figure 1.1: The schematic of different multiple antenna configurations. Here, the $M \times 1$ vector $\mathbf{s}(t)$ and the $N \times 1$ vector $\mathbf{y}(t)$ refer to the transmitted and received signals, respectively, with M and N being the number of antennas at each array.

MIMO communication systems such as the diversity gain. The MIMO radar systems are classified into two different configurations based on the mutual distances between each antenna and the target as:

- **Collocated MIMO radars**:

  When the distance between each two antennas in the array of transmitters and receivers is much less than the distance of the antennas to the targets, the underlying structure is called the collocated MIMO system. The collocated MIMO radars are introduced as an alternative to the traditional phased-array radars in which all antennas transmit the same signal with only a phase-shift.

- **Widely-separated MIMO radars**:

  Unlike the collocated structure, in widely separated MIMO radars, the antennas are separated in a way that the mutual distances between each

two antennas is larger that the distance between the target and the antenna. In this case, the MIMO radar is compared to the common multistatic radar model in which antennas might be also widely separated.

In the following subsections, each of the above structures is introduced and recent attempts in the signal processing and target estimation using each of the proposed structures are summarized.

1.2.1 MIMO Radars With Collocated Antennas

Collocated MIMO radars were offered [58] as a new structure of multiple antenna radars to achieve some benefits to the traditional phased-array systems [54]. In a typical phased-array system, the transmitted waveform at each antenna is written as

$$\mathbf{s}[k] = \mathbf{b}'s[k] \tag{1.3}$$

where $\mathbf{b}$ denotes the transmitter steering vector. In other words, the signal transmitted by the m_1-th antenna is the phase shifted version of the signal sent by the m_2-th antenna, which leads to a fully-coherent cross-correlation matrix for the array of transmitters. Conversely, MIMO radars enjoy multiple independent signal paths by sending orthogonal signals with the full-rank cross-correlation matrix R defined as follows:

$$R = \frac{1}{K}\sum_{k=1}^{K}\mathbf{s}[k]\mathbf{s}^{H}[k] \tag{1.4}$$

with K denoting the total number of snapshots. Recently, it has been therefore a great interest in exploring potential benefits exploited in MIMO radars by transmitting orthogonal signals.

The MIMO radar with orthogonal transmitted waveform achieves virtual aperture and spatial coverage extension, beampattern improvement, and increase on the number of uniquely detectable targets when they are compared

to a phased-array system [7]. As discussed in [7], a MIMO radar with M transmitters and N receivers can be equivalently considered as a distributed radar system with $M \times N$ virtual sensors, which are the combinations of transmitters and receivers locations. The virtual array consequently increases the array aperture. On the other hand, the orthogonality of transmitter waveform makes the MIMO antennas omnidirectional. This also leads to the increase of the spatial coverage of each antenna. In this case, the TOT of each transmitted beam is equal to the time required to scan the region of interest, which is smaller than that of the fully-coherent phased-array radar [7].

It is known that the beam-pattern of a multiple antennas system is a function of the cross-correlation matrix R [28]. In a phased-array system with a rank one matrix R, the beam-pattern achieves the maximum power around the transmitted DOA with several side-lopes in other DOAs. However, an orthogonal cross-correlation matrix provides a flat beam-pattern with the same power allocated to different potential DOAs. Figures 1.2 and 1.3 present the transmitted power and the transmit/receive pattern for cases with the fully-coherent and orthogonal transmitted signals, respectively. It can be observed that the MIMO radar achieves a flat transmit beam-pattern. In addition, the transmit/receive beam-pattern of the MIMO shows narrower beam width as well as lower side-lobes [7]. Although the results show an improvement in the beam-pattern when the orthogonal signals are transmitted, the MIMO system suffers from the loss in the transmit antenna gain [22]. It is mentioned in [22] that unlike the phased-array radar providing M^3 as the transmit gain, the MIMO's gain is only M^2 where M denotes the number of antennas. Therefore, a new structure was recently proposed in [48] in which the benefits of both MIMO and phased-array structures are incorporated in a new structure called the phased-MIMO radar. The main idea in [48] is to divide the array of

transmitter to some subarrays where each subarray coherently processes the signals. However, the overall structure works as a MIMO radar where the transmitted signals by different subarrays are still orthogonal. The proposed structure finally shows significant improvement over the individual phased-array of MIMO structure.

It can be shown that there will be an increase in the number of uniquely detectable targets when the transmitted signals are orthogonal [7] [59]. The identifiability analysis in [59] shows that the maximum number of targets that can be uniquely detected in one resolution cell of a collocated MIMO radar belongs to the interval $[M + N - 1, M \times N]$ where the geometrical placement of antennas in the transmitter and receiver arrays determines the exact maximum bound. For example, it was shown in [83] that the maximum bound for the bistatic MIMO radar in which the transmitter and receiver arrays are separated is $M \times N$. The above discussions confirm that compared to the monopulse phased-array radar systems [89], the MIMO radars provide more degrees of freedom in the identification and acquisition of multiple targets fallen in the same resolution cell.

There has been recently a great interest among researchers in using the collocated MIMO radars for target detection and localization. The target detection and DOA estimation problems were tackled in [81] [82]. A a number of different iterative techniques were proposed for the target DOA estimation where a collocated MIMO radar is used as the measurement tool. When the number of data snapshots is limited, another approach was proposed in [76] via an iterative approach for the sparse learning. The DOA estimation problem for multiple targets was also dealt with in [83]. By a number of simulations, it was shown that the ML estimator can identify targets more accurately when

the number of antennas increases. The detection and DOA estimation performance of the collocated MIMO radar was substantially evaluated in [7]. The probability of detection was found for the MIMO system using a Neyman-Pearson Test (NPT). Then, the MIMO detection probability was compared to the that of the phased-array radar when fully-coherent signals were transmitted. The DOA CRLB was also derived in [7] [60] for the MIMO radars with collocated antennas. It was shown in [7] that the estimation bound increases when more targets fall inside the same cell and, finally, becomes unbounded when the number of unresolved targets goes beyond a specific value, which is the maximum number of uniquely detectable targets.

Besides the DOA estimation and CRLB calculation, the optimization techniques were applied to different aspects of MIMO systems such as waveform design. The algorithms in [28] [60] find an optimal cross-correlation matrix of the transmitted signals that minimizes the DOA MSE. In [60], the DOA CRLB is suggested as the performance measure and a convex optimization algorithm is proposed for the waveform design. The proposed approach in [74] finds an expression for the transmitted signals once the optimal cross-correlation matrix is found through the related optimization techniques. The concept of the MIMO ambiguity function [68] was used in [15] to achieve an optimal waveform design for the collocated MIMO radar. While the proposed algorithm in [15] is not adaptive to the change in the location of the target, an adaptive design for orthogonal frequency-hoping signals was also formulated in [90] where the ambiguity function of a collocated MIMO radar with separate transmitter and receiver arrays is used as the cost function. Besides the above works, there are several other research on the design of optimal waveform for the unconstrained problems [2] and MIMO-Phased radars [29].

Although different issues in collocated MIMO radars were substantially explored in the literature, there are still some important topics that need more discussions. While radar systems are widely used in tracking problems, the lack of the same development for the collocated MIMO radar is felt. It was shown in [89] that bringing target motion information into the estimation algorithm can enhance the performance and mitigate the difficulty in localizing multiple unresolved targets. Although the algorithm proposed in [89] is developed for a monopulse phased-array radar, the collocated MIMO radar can be also considered as the measurement tool instead and the tracking algorithm is applied to the the MIMO structure. In addition, the antenna allocation in multiple antenna systems plays a critical rule. The question is now how the distribution of antennas affects the localization and tracking performance in collocated MIMO radars. Furthermore, there is a great interest in finding whether there is a distribution of antennas that optimizes a well-defined cost function. Therefore, developing a suitable performance metric and, then, postulating a suitable optimization algorithm for the optimal distribution of antennas in the collocated MIMO radars are the next important trends of this thesis.

1.2.2 Widely Separated MIMO Radars

While sending orthogonal waveforms provides diversity in the signal paths in collocated MIMO radars, a number of benefits can be also exploited by placing antennas widely-separated in the surveillance region [47]. A solid analysis of the widely-separated MIMO radars was first conducted in [25]. The signal model for the MIMO radar was derived in [25] where the received complex
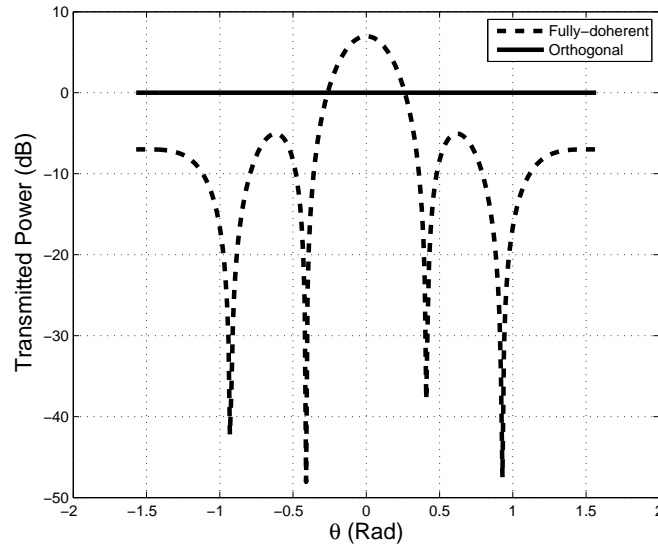
Figure 1.2: The transmit beam-pattern for a MIMO radar with $M = 5$ antennas and half-wavelength antennas.
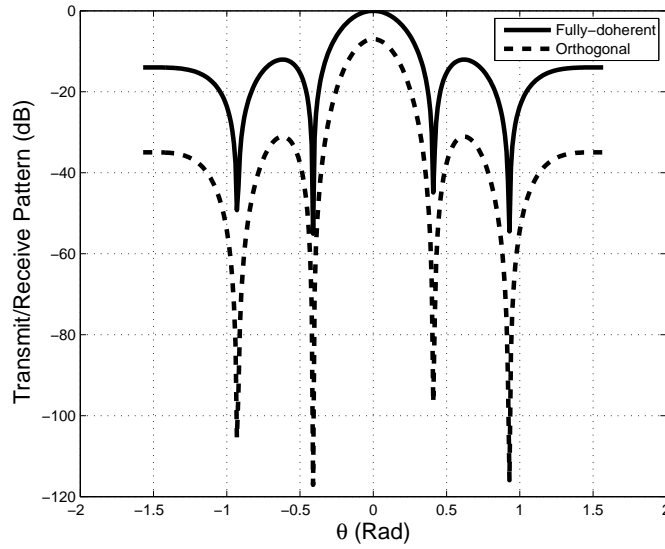
Figure 1.3: The transmit/receiv beam-pattern for a MIMO radar with $M = 5$ antennas and half-wavelength antennas.

11

signal in the receivers could be written as follows:

$$\mathbf{y}(t) = \sqrt{\frac{E}{M}} H \mathbf{s}(t - \tau) + \mathbf{n}(t) \tag{1.5}$$

with E being the total transmitted energy, H as the target scatterer matrix, τ as the reference time delay of the signal travel, and $\mathbf{n}$ being a white Gaussian complex noise term with zero mean and known variance σ_n^2. [25] also shows that under suitable conditions over the mutual distance between antennas compared to the distance of the antennas to the target, the random vector $\mathbf{h} = \begin{bmatrix} H_{11} & H_{21} & \cdots & H_{(N-1)M} & H_{NM} \end{bmatrix}'$ is Gaussian distributed with zero mean and unitary variance, $\mathbf{h} \sim \mathcal{CN}(0, I_{NM})$. Although the signal model in (1.5) looks like the one proposed for the MIMO communication systems in (1.1), there are some intrinsic differences between the two structures. First, unlike a MIMO communication system in which the transmitted signals $\mathbf{s}(t)$ are unknown to the receiver, MIMO radars known the transmitted waveforms [46]. Furthermore, the channel coefficients H_{nm} stand for the unknown reflections of the target in real scenario while the channel coefficients are known/estimated in communication systems. These evident differences make the estimation and detection problem in MIMO radars different from what offered in MIMO communication communities.

There has been a significant interest in evaluating the detection performance of widely-separated MIMO radars. It was shown in [25] that the output of the matched-filter is the sufficient statistics for detection and estimation purposes. Then, the detection probability was derived by checking the second norm of the vector of the matched-filter output. It was then demonstrated that the MIMO radar achieves higher probability of detection and lower miss-detection probability compared to the traditional phased-array, and SISO radars. It was actually indicated that the wide separation of antennas in the

MIMO radar provides diversity in the signal paths that also makes the RCS mitigation possible. In the presence of the clutter, the MIMO radar's capability in target detection was also evaluated in [1] [18] [20] [50] [87]. The gains of the MIMO radar to the phased-array one were specially quantified in [50] for a moving target in the additive colored noise with the clutter. The GRLT was extended to the MIMO radars with widely-separated antennas in [18]. The performance of the new detector was then compared to the optimum Gaussian detector and the benefits of the new approach in dealing with the non-Gaussian clutter were also quantified. In the presence of the non-homogenous clutter, the GRLT was also used to design an optimal detector for the MIMO radar in [87]. Other techniques to tackle the detection problem in the heavy clutter with different statistics are also proposed in [1] [20].

When the antennas are widely-separated, estimating the location and velocity of the target becomes essential in a widely-separated MIMO radar system. The localization problem was extensively formulated in [33] [35]. The location of a single scatterer target was estimated using the BLUE technique in [33]. Then, the location CRLB was derived in [35] and was shown that the CRLB is affected by the distribution of antennas in the surveillance region. The velocity estimation in widely-separated MIMO radars was also discussed in [49]. The results in [49] are provided for an extended target with with reflectivity varying with angle look. A ML estimator is then proposed for velocity estimation and the CRLB was also derived for optimal antenna placement. Besides the localization, the dynamic tracking problem using a widely-separated MIMO radar was also addressed in [34] [36] [40]. In [36], a novel tracking algorithm was represented in order to estimate the trajectory of a single target. Also, the PCRLB for the MIMO radar was derived in [34] and the performance of centralized and decentralized tracking configurations was compared in terms

of the MSE and the PCRLB. Another tracking approach was presented in [40] for monopulse MIMO radars to estimate parameters of each target locally at each receiver and then combine the estimates at the fusion center. Indeed, the estimated angle-of-arrival at each pair is fused with one another and a unique estimate of the target trajectory is finally obtained. A TBD algorithm was also used in [45] [85] for multitarget tracking using widely-separated MIMO radars. A simple KF based algorithm was also presented in [65] for target tracking using non-coherent MIMO radar systems. The main idea is to estimate the location of the target at each time step and then apply the Kalman filter on the noisy estimates.

Even though MIMO radars are known as a new generation of radar systems with many potential benefits, there is always a question about the difference between the MIMO radar and the traditional multistatic radar systems. In [47], joint processing was mentioned as the main benefit exploited by using the MIMO rather than the multistatic structure. Consider Figures 1.4 and 1.5 as the basic configurations of the MIMO and multistatic radars, respectively. Unlike the local processing done at each receiver of the multistatic radar, the MIMO radar enjoys the joint processing in a central unit. The detection performance of the multistatic radar was first derived in [63]. A good survey on the detection theory in multistatic radars can be also found in [21]. Although there are some efforts on the comparison between the centralized and decentralized multistatic radars in [14] [42], the difference between multistatic and MIMO structures in target detection is not still clear. Moreover, while multistatic localization and tracking were dealt with in the literature [26] [62] [71], there is no discussion on the advantages or possible disadvantages of MIMO radar to the multistatic one in localization and tracking. Therefore, a comprehensive comparison between the performance of the aforementioned structures

14
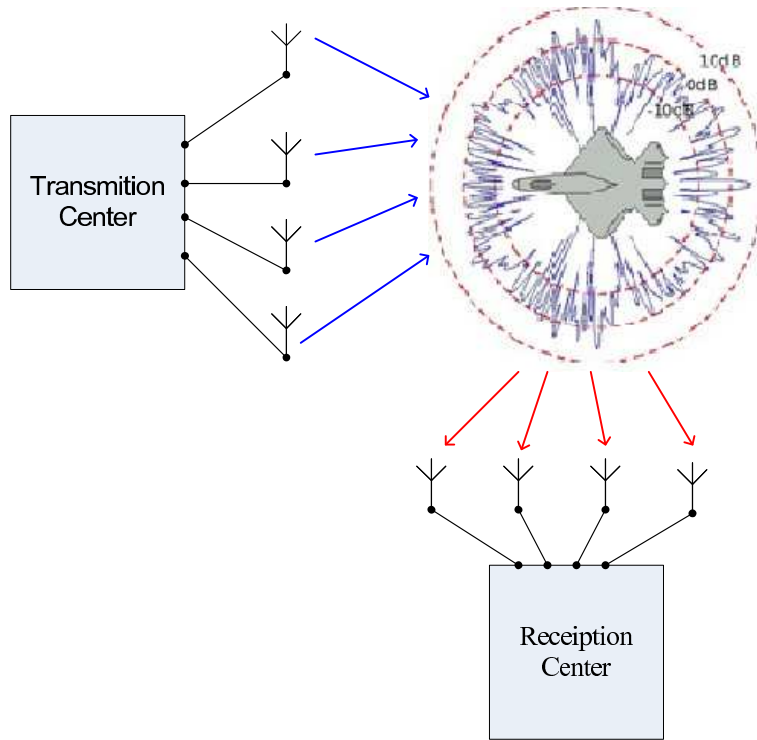
Figure 1.4: A widely-separated MIMO radar with the joint processing in the reception center.

constitutes an important trend of this thesis.

1.3   Thesis Organization And Contributions

The last two sections dealt with a review of previous works on the MIMO systems. It was shown most recent research was focused on the signal processing issued in both collocated and widely-separated MIMO radars. The main motivation for defining this thesis was to apply the tracking and sensor management concepts to the recently-proposed MIMO structures. Chapter 2 proposes a novel tracking algorithm for the collocated MIMO radars. The detection and estimation problem in widely-separated MIMO radars are discussed in Chapter 3. A new antenna allocation procedure is also formulated
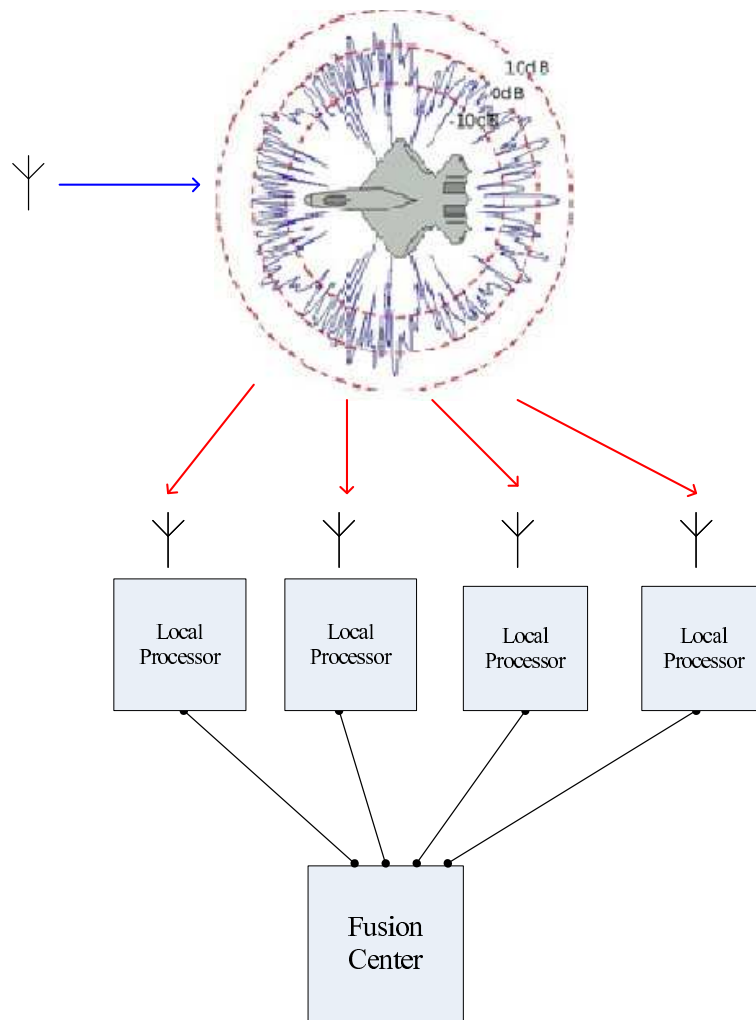
Figure 1.5: A multistatic radar configuration with the local processing being done at each receiver.

for the collocated MIMO radar in Chapter 4. Conclusions of this thesis are also provided in Chapter 5. Appendices including the proofs of theorems are attached to the end of the thesis. The main contributions of this thesis are now highlighted in the following:

1.3.1 Multiple Unresolved Target Tracking Using Collocated MIMO Radars

When multiple targets fall inside the same resolution cell of a collocated MIMO radar, it was indicated that a bounded number of targets can be uniquely detected. If more targets occupy the same cell, the localization algorithm cannot find an accurate estimate of the targets' states. This problem is dealt with by bringing the prior information on the location of targets into the estimation algorithm. The dynamic tracking is then formulated for the collocated MIMO radars in this thesis. It is observed that the conventional MIMO signal model [58] does not include any range information of targets. In this case, the signal model does not hold the observability condition and, therefore, cannot be used for tracking purposes. Based on the discussed drawbacks, the following novel contributions are made in Chapter 2 of this thesis on the collocated MIMO radar tracing and localization:

1. **A novel signal model**:

   We propose a novel signal model based on the received output of the matched filter for the collocated MIMO radar. The new model includes both DOA and range information of the target.

2. **A new localization algorithm**:

   Based on the new proposed signal model, the localization algorithm is formulated to estimate the states of targets fallen in the same cell. For

the multiple target case, the MDL criterion is utilized to estimate the number of target occupying the same cell. Then, an ML estimator is applied to the received signals to find the location of each detected target.

3. **A signal-level tracking algorithm**:

Given the output of matched-filter as the received unthresholded measurements, the tracking algorithm is formulated for the collocated MIMO radar. A MH-based algorithm [12] is chosen for the tracking purposes where a new cell-to-target association matrix is defined to handle the uncertainty in the association of targets to received measurement in different cells. Due to the nonlinearity of the signal model, the well-known UKF [55] is merged to the MH-based method to form a solid framework for tracking multiple unresolved targets using collocated MIMO radars.

4. **PCRLB Derivation**:

The tracking PCRLB is also derived for the new measurement model. The PCRLB is also formulated as a function of the number of targets occupying the same cell. It is then observed how increasing the number of targets affects the performance of localization and tracking. In addition, the impact of the antenna distribution on the estimation performance will be analyzed via the tracking PCRLB.

5. **Signal-level vs. Measurement-level Tracking**:

The main goal of the new tracking formulation is to show the capability of the new approach in estimating multiple targets where the number of target in one cell goes beyond a specific bound, which is indicated in [59]. Therefore, besides the signal-level tracking, a measurement-level framework is also constructed by considering the localization results as the received measurements and, then, applying a KF algorithm to the noisy

location estimations. Furthermore, a solid comparison is made between both tracking approaches. It will be demonstrated that the performance of the measurement-level tracking approach is affected when more targets enter the same resolution cell while the signal-level method shows much more robustness to the aforementioned case. Finally, the agreement of the tracking results with the derived PCRLB will be justified.

1.3.2   MIMO vs. Multistatic Radars For Target Localization And tracking

Chapter 3 deals with the detection, localization, and tracking in widely-separated MIMO radars. To the best of our knowledge, detection and localization techniques were developed for a single-scatterer target where the target scatterer is assumed to be the same in all pairs of transmitters and receivers. In addition, although the tracking algorithm was formulated for the widely-separated MIMO radars by considering the localization results as the measurements and, then, applying a related filtering method to the noisy measurements, there is no separate work on developing a signal-level tracking method for widely-separated MIMO radars. The above issues motivated us to offer the following contributions on the widely-separated MIMO radars:

1. **A MH-based localization algorithm**:

   A novel method is proposed in this paper to identify and localize multiple scatterer targets using a widely-separated MIMO radar. It is assumed that the target scatterer is different at different transmitter and receiver pairs. In this case, the target might become unobservable in certain pairs, which makes the recent localization techniques useless. When multiple targets are also present, the detected signals at each pair may have been

originated from an unknown permutation of multiple targets. We tackle the above problem by applying the MH-based method to the received output of matched filter. The new MH-based localization algorithm then finds the number and states of multiple targets.

2. **A signal-level tracking algorithm**:
The dynamic tracking is then extended to the widely-separated MIMO radars. Unlike the old works, we use the unthresholded received signals for the association and tracking purposed. Due to the specific form of the measurement model, it is shown that the Kalman-based methods cannot be used for the state update. Therefore, a particle filter-based technique [3] is incorporated to the proposed algorithm to update the target states.

3. **PCRLB Derivation**:
For the tracking performance evaluation, the PCRB is also derived for the widely-separated MIMO radars. The agreement of the tracking results to the derived PCRLB will be also justified via intensive simulations.

4. **Multistatic vs. MIMO Comparison**:
The detection performance of both widely-separated MIMO radar and the multistatic structure is analyzed separately. To do this, two analytical detection probability forms are derived for each structure. The MIMO and multistatic ROCs are then calculated at different target SNRs and the benefits of the MIMO to the multistatic configuration are justified. In addition, the performance of the MIMO and multistatic radars in estimating the location of multiple scattere targets is analyzed. It will be shown that the estimation improvement of the MIMO radar rather

than multistatic radar becomes more significant when the target SNR decreases.

1.3.3   Antenna Allocation For Collocated MIMO Radars

The estimation performance of a MIMO radar systems is affected by the distribution of antennas in the surveillance region. Although the antenna allocation in widely-separated MIMO radars was substantially covered in the literature [17] [35] [37] [51], no comprehensive research has been done on the same problem for the collocated MIMO systems. Chapter 4 this thesis tackles the antenna allocation problem in collocated MIMO radars. The location CRLB of the collocated MIMO radar is first derived as a function of the target states and the location of antennas. It is then shown that the distribution of antennas affects the location CRLB, which leads to poor results for the ULA structure. To find the best optimum distribution of antennas, a suitable cost function is first defined to evaluate the localization performance of the collocated MIMO radar. Then, after representing related constraints on the location of antennas, a novel optimization algorithm is formulated for the antenna allocation problem. In the presence of a single target, the optimization problem is formulated as the well-known SDP [13], which can be efficiently solved. For multiple-target case, due to the non-convexity of the cost function, a sampling-based method is suggested to capture the global optimal point. Finally, the improvement in the localization performance of the collocated MIMO radar using the new optimal structure is justified.

List of Submitted/Accpeted Publications

- A. A. Gorji, and T. Kirubarajan, "Antenna allocation for MIMO radars with collocated antennas", Submitted to *IEEE Transactions on Aerospace and Electronic Systems*, June 2012.

- A. A. Gorji, R. Tharmarasa, W. D. Blair, and T. Kirubarajan, "MIMO vs. Multistatic radars for target localization and tracking", Submitted to *IEEE Transactions on Aerospace and Electronic Systems*, November 2011.

- A. A. Gorji, R. Tharmarasa, W. D. Blair, and T. Kirubarajan, "Multiple unresolved target localization and tracking using collocated MIMO radars", Accepted For Publication, *IEEE Transactions on Aerospace and Electronic Systems*, October 2011.

- A. A. Gorji, and T. Kirubarajan, "Antenna Allocation for MIMO Radars with Collocated Antennas", In the Proceedings of the 15th IEEE International Conference on Information Fusion, Singapore, July 2012.

- A. A. Gorji, R. Tharmarasa, and T. Kirubarajan, "Widely-separated MIMO vs. multistatic radar for target localization", Proceedings of IEEE International Conference on Acoustics, Speech, and Signal Processing (ICASSP), Kyoto, Japan, March 2012.

- A. A. Gorji, R. Tharmarasa, and T. Kirubarajan, "A new co-located MIMO radar system for multi-target tracking and localization", Proceedings of the 12nd International Conference on Information Fusion, Edinburgh, Scotland, July 2010.

- A. A. Gorji, R. Tharmarasa, and T. Kirubarajan, "Tracking multiple

unresolved targets using MIMO radars", Proceedings of IEEE Aerospace Conference, Montana, USA, March 2010.

- A. A. Gorji, R. Tharmarasa and T. Kirubarajan, "An Assignment Based Algorithm for Multiple Target Localization Problems Using Widely-Separated MIMO Radars", Proceedings of SPIE Conference on Signal and Data Processing of Small Targets, San Diego, CA, April 2010.

- A. A.Gorji, R. Tharmarasa and T. Kirubarajan, "MIMO vs. Multistatic Radar for Target Localization and Tracking", Proceedings of SPIE Conference on Signal and Data Processing of Small Targets, San Diego, CA, August 2009.

Chapter 2

Multiple Unresolved Target Localization and Tracking Using Collocated MIMO Radars

2.1 Introduction

In this chapter, a new model is proposed for the output measurements of a collocated MIMO radar. The contribution of each target is observed in two neighboring cells. That is, the received output is a portion of the actual signal reflected by the target. Therefore, outputs of matched filter involve information about the range of targets in each cell as well. Nevertheless, the sampled output is the superposition of signals from multiple targets falling within the cell. To find the number of targets and the corresponding estimates in each resolution cell, the likelihood function is derived for multiple targets falling inside the same cluster. The number of targets in each cell and an estimate of states can be estimated by optimizing the derived likelihood function. The

major benefit of the localization algorithm applied to the new model is to provide an estimate of range and angle together. Also, the new model guarantees the observability of the measurements. Indeed, when targets move in time, various combinations of targets locations in one resolution cell generate diverse signals in the output of matched filter. Consequently, two configurations of targets generate different signals that may guarantee the observability of the measurement model for tracking purposes.

The other contribution of this chapter is to develop a tracking algorithm for the new developed measurement model. Two different options for the dynamic tracking of target states are considered. In the first method, tracking using localization results is done while in the second it is done using the received signals. The first method uses the estimated locations of targets as new measurements for a separate tracker that uses prior information on targets. When the number of targets exceeds the maximum bound, localization becomes inaccurate or even impossible. In addition, the localization results may become unsatisfactory even with the number of targets being below the bound. In both cases, the trackers performance is affected by the inaccuracy of localization estimates. A multiple-hypothesis based tracking method is proposed in this chapter to handle signal-level tracking for multiple unresolved targets. A cell-to-target association matrix is defined to find possible assignments between targets and cells. Due to the uncertainty in the targets state estimates, multiple associations are found according to the variance of estimation. The nonlinearity in the signal model is also dealt with by using a UKF [55]. The benefit of the proposed signal-level tracking method is to obviate the need for a separate localization step to generate measurements for tracking. This issue does not only relax the bound on the number of uniquely detectable targets,

but also reduces the computational load of the tracker. The PCRLB is derived in the final part of this chapter as a theoretical bound for performance evaluation. The derived PCRLB is, then, represented as a suitable tool for potential waveform design or sensor management for MIMO radar systems.

The rest of the chapter is organized as follows. Section 2.2 describes the collocated MIMO radar, signal model, and different structures. Target localization and maximum bound on the number of targets are discussed in section 2.3. Tracking algorithm as well as the PCRLB are also presented in section 2.4. Simulation results comparing tracking and localization techniques are given in Section 2.5.

2.2   Collocated MIMO Radars

The general structure of a collocated MIMO radar is shown in Figure 2.1, where the array of transmitters and receivers are collocated. That is, the distance between each two antennas is much shorter than the distance between antennas and targets [7]. In addition, arrays may be also collocated such that the distance between the centroid of two arrays is much shorter than the distance towards the targets. Now, assume that M and N represent the number of antennas in the array of transmitters and receivers, respectively. The following assumptions are first made for the structure used in this chapter:

- Without loss of generality, the centroid of antennas is assumed to be at the origin ($[0\ 0]'$).

- The number of targets initially present at each cell is less than the maximum bound. This is because at the initial step, existing techniques are
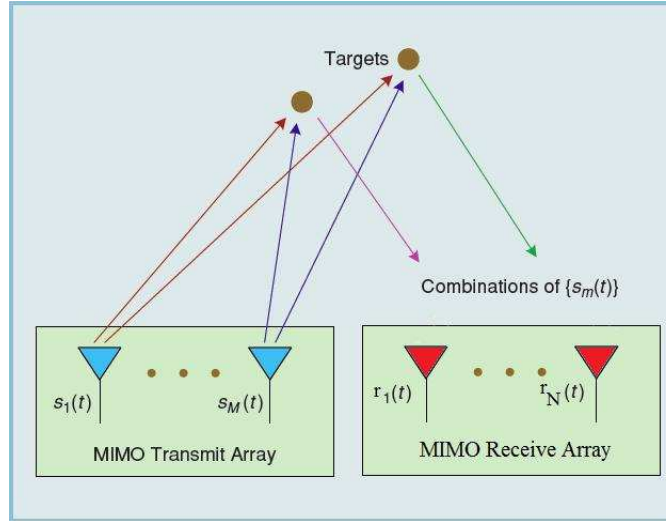
Figure 2.1: The structure of a collocated MIMO radar with M transmitters and N receivers [58]. Lines of different styles show diversity in the transmitted signals.

used for localization and they are limited by the above bound. However, in the subsequent steps when the number of target in the same cell exceeds the bound, our proposed technique works well.

- The total number of targets in the scenario is fixed. An algorithm is being developed in order to tackle time varying number of targets.

- Objects are point sources modeled as Swerling type I [75] targets. That is, target scatterers change every scan but remain constant during each scan. Explanations to include target birth and death are presented elsewhere [43].

Given signals in L snapshots, input signals are orthogonal meaning that the covariance matrix of inputs is diagonal. The covariance matrix R is defined as

$$R = \sum_{l=1}^{L} \mathbf{s}[l]\mathbf{s}^{H}[l] \tag{2.1}$$

27

where $\mathbf{s}$ is the $M \times 1$ transmitted signal vector, and $\mathbf{s}^H$ represents the complex transpose of vector $\mathbf{s}$. Assuming T targets in an arbitrary cell, the reflected signal of the t-th target can be written in the following form [7]:

$$\mathbf{z}[l] = \alpha_t A_t \mathbf{s}[l] \tag{2.2}$$

Here, $\mathbf{z}[l]$ is the reflected signal in the l-th snapshot, A_t is the system matrix, and α_t is the random scatterer of the t-th target. The random scatterer is a complex number whose real and imaginary parts are both Gaussian-distributed with mean and variance $\{\hat{\alpha}_t^R, \hat{\alpha}_t^I\}$, σ_α^2, respectively. The system matrix can be found based on the collocated antennas and far enough targets as [7]

$$
\begin{aligned}
A_t &= a_t^r a_t^t \\
(a_t^t)_i &= \exp\left(-j\frac{2\pi}{\lambda}\left(\sin(\theta_t)x_{ti} + \cos(\theta_t)y_{ti}\right)\right), i = 1, ..., M \\
(a_t^r)_l &= \exp\left(-j\frac{2\pi}{\lambda}\left(\sin(\theta_t)x_{rl} + \cos(\theta_t)y_{rl}\right)\right), l = 1, ..., N
\end{aligned}
\tag{2.3}
$$

where λ is the wavelength, M and N are the number of transmitters and receivers, respectively, a_t^t and a_t^r are transmitter and receiver steering vectors, respectively, θ_t is target DOA, and $[x_{ti}, y_{ti}]$ and $[x_{rl}, y_{rl}]$ denote the location of the i-th transmitter and l-th receiver, respectively. Now, define r_t as the t-th target range with respect to the origin. In practice, the output of matched filters is usually used instead of original signals because matched filter outputs are found based on the maximization of SNR in the output. Therefore, the output of matched filter is more suitable for detection and localization purposes. The output of matched filter is written as

$$E^c = \frac{1}{\sqrt{L}} \sum_{l=1}^{L} \mathbf{z}^c[l]\mathbf{s}^H[l] \tag{2.4}$$

where $\mathbf{z}^c$ is the received signal in the c-th cell written as

$$\mathbf{z}^c[l] = \sum_{t=1}^{T_1} \mathbf{z}_t[l] + \mathbf{w}[l] \tag{2.5}$$

with T_1 as the number of targets in the c-th cell and w as a complex additive noise that is Gaussian-distributed with zero mean and variance σ_w^2. Now, suppose there are T_2 targets in the $(c+1)$th cell. It is shown that the contribution of each target can be observed in the sampled output of matched filter in the c-th and $(c-1)$th cell [89]. Defining $\eta^c = \text{VEC}(E^c)$, it can be shown that the output of matched filter is a summation of the contribution of each target to the corresponding cell as [89]

$$\eta^c = \sum_{t=1}^{T_1} \beta_t \eta_t + \sum_{t'=1}^{T_2} (1 - \beta_{t'}) \eta_{t'} + \mathbf{w}' \tag{2.6}$$

where β_t denotes the ratio of original targets reflection observed in the c-th cell defined as

$$\beta_t = \frac{r_t + r_{bin} - r^c}{r_{bin}} \tag{2.7}$$

with r^c as the radius of the c-th cell, and r_t as the range of the t-th target. Also, η_t are the matched filter outputs when only the t-th target is available (e.g. based on the signal reflected by the t-th target only), and $\mathbf{w}'$ is the additive noise that is Gaussian with zero mean and variance $\sigma_{w'}^2$. The variance of additive noise is proportional to the transmitted power. Here, for simplicity, the transmitted power is assumed to be one. However, the more the transmitted power, the larger the variance of noise in the output of matched filter.

Remark 2.2.1 *Different configurations of targets in a resolution cell provide diverse received signals indicating that both range and angle information can be implicitly observed in signal model. It has been shown in [6] that a dynamic tracking problem including a motion model that describes the dynamic of targets, and range and bearing measurements satisfies the observability conditions of a general discrete nonlinear state space model. For the model presented in*

29

this chapter, it was shown that the localization algorithm can find an estimate of the number of targets and the target states (i.e., DOA, range and scatterer). Also, it will be shown in the next section that a unique estimate of target states can be found as long as the number of targets in each cell does not exceed the bound. In other words, the signal model can be imagined as a discrete state space tracking model that indirectly provides range and angle information. Therefore, the observability of the model can be justified using the same proof given for a general dynamic tracking problem [6]. Nonetheless, the commonly-used signal models are non-observable in the sense that the received signal is the same for different trajectories of targets that move in the same direction (i.e., the same DOAs but different ranges). While these models are suitable for detection or localization purposes, they cannot be used for target tracking problems due to the lack of observability.

2.3   Target Localization and Parameter Identifiability

The following nonlinear model can be written for η_t described in the last part [7]

$$\eta_t = \alpha_t \mathbf{d}_t \tag{2.8}$$

with the following definition for the new system matrix

$$\mathbf{d}_t = \sqrt{L} \text{VEC} \left(A_t U \Gamma^{\frac{1}{2}} \right) \tag{2.9}$$

with $\Gamma^{\frac{1}{2}}$ being the square root of matrix Γ. The set of detected cells is defined as $\Phi = \begin{bmatrix} \eta^1 & \cdots \eta^C \end{bmatrix}$ where C is the number of detected cells. A ML estimator is used to estimate parameters of targets where the parameter vector of each

target is defined as

$$\Theta_t = [\theta_t, \beta_t, \hat{\alpha}_t^R, \hat{\alpha}_t^I] \tag{2.10}$$

Here, it is assumed that all variances are known, however, it does not affect the generality of the proposed algorithm. Detected cells are classified to different clusters based on the distribution of targets in the surveillance region. Each cluster may be composed of several cells occupied by a group of targets. As an example, consider a scenario with 3 targets. Figure 2.2 shows some possible distribution of targets in 5 neighbor cells. The top-right scenario provides all three targets in C_2 leading to the formation of a cluster involving $\{C_1, C_2\}$. However, in the bottom-right graph, there are two clusters involving $\{C_1, C_2, C_3\}$ and $\{C_4, C_5\}$. Consequently, the distribution of targets determines the number of clusters as well as the number of cells in each cluster. Without loss of generality, it is assumed that there is only one cluster including $C + 1$ resolution cells. The likelihood function is written as $p(\Phi|\Theta_1, ..., \Theta_T) = \mathcal{N}(\mu, \Sigma)$ where $\mathcal{N}$ denotes a normal distribution with mean μ and covariance Σ being defined as

$$
\begin{aligned}
\mu &= [\mu_1, ..., \mu_C] \\
\Sigma &= \begin{pmatrix}
\Sigma_{11} & \Sigma_{12} & 0 & 0 & 0 & 0 \\
\Sigma_{21} & \Sigma_{22} & 0 & 0 & 0 & 0 \\
0 & 0 & . & . & . & . \\
. & . & . & . & \Sigma_{(C-1)(C-1)} & \Sigma_{(C-1)C} \\
0 & 0 & 0 & 0 & \Sigma_{C(C-1)} & \Sigma_{CC}
\end{pmatrix}
\end{aligned} \tag{2.11}
$$

Individual means are found as

$$\mu_i = \begin{cases} \sum_{t=1}^{T_1}(1 - \beta_t)\hat{\eta}_t^2 & \text{If } c = 1 \\ \sum_{t=1}^{T_C} \beta_t \hat{\eta}_t^C & \text{If } c = C \\ \sum_{t=1}^{T_c} \beta_t \hat{\eta}_t^c + \sum_{t'=1}^{T_{c+1}}(1 - \beta_{t'})\hat{\eta}_{t'}^{c+1} & \text{Otherwise} \end{cases} \tag{2.12}$$

31
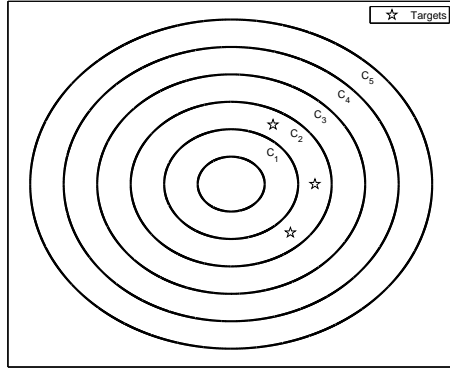
(a) one cluster with one occupied cell
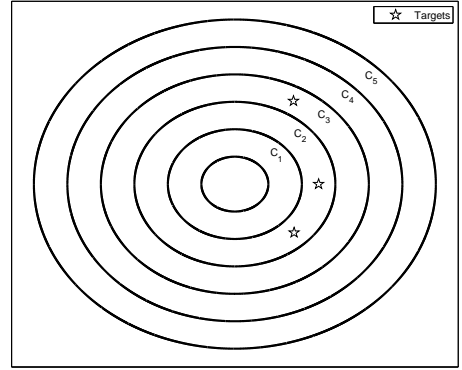
(b) one cluster with two occupied cells
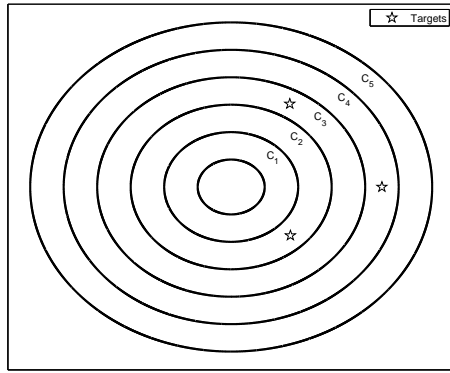
(c) one cluster with three occupied cells
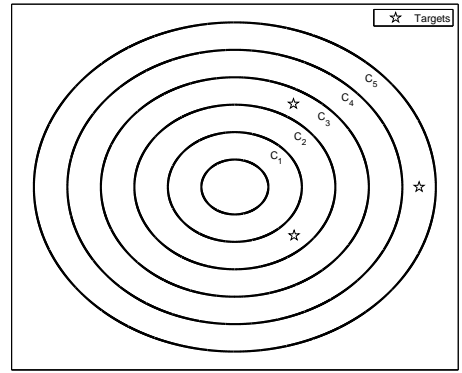
(d) two clusters with three occupied cells

Figure 2.2: Different clusters of cells based on the distribution of targets.

with $\hat{\eta}_t^c = \hat{\alpha}_t \mathbf{d}_t$ and $\mathbf{d}_t$ as the system matrix of the t-th target in the c-th cell. The same expressions can be found for the covariance knowing that $E\{(\alpha_t - \hat{\alpha}_t)(\alpha_t - \hat{\alpha}_t)'\} = 2\sigma_\alpha^2$. Because targets affect two neighboring cells, there is also a cross-correlation between adjacent cells. The diagonal terms in

the above equation can be written as

$$
\Sigma_{cc} = \begin{cases} 2\sum_{t=1}^{T_2}\sigma_\alpha^2\mathcal{D}(d_td_t')(1-\beta_t)^2 + \sigma_w^2 & \text{If } c = 1 \\ 2\sum_{t=1}^{T_{c+1}}\sigma_\alpha^2\mathcal{D}(d_td_t')(1-\beta_t)^2 + 2\sum_{t'=1}^{T_c}\sigma_\alpha^2\mathcal{D}(d_{t'}'d_{t'}')(\beta_{t'})^2 + \sigma_w^2 & \text{If } 1 < c < C \\ 2\sum_{t=1}^{T_C}\sigma_\alpha^2\mathcal{D}(d_td_t')(\beta_t)^2 & \text{If } c = C \end{cases}
$$
$$(2.13)$$

The cross-correlation terms can be similarly found as

$$
\Sigma_{c(c+1)} = 2\sum_{t=1}^{T_{c+1}}\sigma_\alpha^2\lceil\rangle\dashv\}(d_td_t')(1-\beta_t)(\beta_t) \tag{2.14}
$$

where $1 \le c \le C-1$. Note that the scatterers of different pairs are statistically independent. Therefore, the covariance matrix is written as the diagonal elements of d_td_t' in order to consider the independence of different pairs. From (2.11–2.14), it can be seen that the covariance matrix does not have any information about target scatterers. In addition, the i-th diagonal element can be written as $|d_t^i|^2$, which is independent of DOAs and, consequently, the covariance matrix is independent of target DOAs. The covariance matrix and the mean vector provide sufficient information for range, DOA, and scatterer extraction from the output of matched filter. The negative log-likelihood function can be now defined as

$$
\Gamma = \frac{1}{2}\log|\Sigma| + \frac{1}{2}(\Phi - \mu)\Sigma^{-1}(\Phi - \mu)' \tag{2.15}
$$

The goal is to find the set of parameters Θ_t and the number of targets at each cell, T_i, in order to minimize the above cost function. To do so, a MDL criterion [4] is used to find the correct number of targets in each cell. Different steps for target localization, where the number of targets in each cell is also estimated are summarized as follows:

1. Divide detected cells into separate clusters. Assume that the c-th cluster includes C cells out of which only $C-1$ cells contain a target.

2. Given T_{max} as the maximum number of targets in each cell, create a $(C-1) \times n_T$ matrix $\mathcal{I}$ whose j-th column is an arbitrary permutation of numbers between 0 and T_{max}. The j-th column is defined as follows:

$$[\mathcal{I}]_j = [I_1^j \ I_2^j \ \ldots \ I_{C-1}^j]' \tag{2.16}$$

where $0 \leq I_k^j \leq T_{max}$

3. For $n = 1$ to n_T do the following steps:

   - Construct the cost function based on the number of targets given by $[\mathcal{I}]_n$.

   - Find an estimate of targets in different cells using common optimization approaches such as Gradient based methods [13].

   - Compute the cost of the n-th hypothesis using MDL criterion as

     $$\text{MDL}_n = -L(\Theta_n) + \frac{1}{2}m_{\Theta_n}\log m_y \tag{2.17}$$

     where $L(.)$ is the likelihood of the n-th hypothesis, m_{Θ_n} is the number of independently adjusted parameters, and m_y is the dimension of observations. Here, it can be shown that $m_y = MNC$ and $m_{\Theta_n} = 4\sum_{c'=1}^{C-1} I_{c'}^n$. The likelihood can be also found from (3.30).

4. Select the best hypothesis as

   $$H^* = \min_n \text{MDL}_n \tag{2.18}$$

Note that in above algorithm the H^*-th column of $\mathcal{I}$ represents the optimal number of targets in each cell. The corresponding parameters can be also found from the optimization step.

2.3.1 Parameter Identifiability

Parameter identifiability has been discussed for MIMO radars in [59]. It is shown that the maximum number of targets that can be uniquely localized belongs to the set $[M + N - 1, M \times N - 1]$. The main idea behind the given bound is to count the maximum unique elements of system matrix A_t. Depending on the distribution of antennas, the maximum number of uniquely detectable targets changes in above given interval. However, the derived bound is based on the previous model in which the contribution of a target is only considered in its own cell. The question is whether the bound changes when the model in this chapter is taken into consideration. It can be inferred from (3.30) that Γ is a function of elements of Σ and η. In other words, the cost function can be written as $\Gamma = \Gamma_1 \left(\Sigma_{11}, ..., \Sigma_{(MNC)(MNC)} \right) + \Gamma_2 \left(\mu_1, ..., \mu_{MNC} \right) + \Gamma_3 \left(\Sigma_{11}, ..., \Sigma_{(MNC)(MNC)}, \mu_1, ..., \mu_{MNC} \right)$ where Γ_is can be found after expanding the original cost function and writing the function in terms of Σ and μ, separately. Without the loss of generality, assume that $C = 1$ indicating that all targets are located in one cell. The necessary condition for the uniqueness of optimal parameter is the full rankness of Jacobian matrix [89]. Jacobian is found with regard to covariance and mean because they are direct functions of parameters. Defining $g_1 = [\Sigma_{11}, ..., \Sigma_{(MN)(MN)}]$ as the vectorized form of covariance, the following equations are derived for Jacobian

$$G_1 = \begin{pmatrix} \frac{\partial g_1}{\partial \Theta_1^i} & \cdot & \cdot & \cdot & \frac{\partial g_1}{\partial \Theta_T^i} \\ \cdot & \cdot & \cdot & \cdot & \cdot \\ \cdot & \cdot & \cdot & \cdot & \cdot \\ \cdot & \cdot & \cdot & \cdot & \cdot \\ \frac{\partial g_{(MN)^2}}{\partial \Theta_1^i} & \cdot & \cdot & \cdot & \frac{\partial g_{(MN)^2}}{\partial \Theta_T^i} \end{pmatrix}, G_2 = \begin{pmatrix} \frac{\partial \mu_1}{\partial \Theta_1^i} & \cdot & \cdot & \cdot & \frac{\partial \mu_1}{\partial \Theta_T^i} \\ \cdot & \cdot & \cdot & \cdot & \cdot \\ \cdot & \cdot & \cdot & \cdot & \cdot \\ \cdot & \cdot & \cdot & \cdot & \cdot \\ \frac{\partial \mu_{MN}}{\partial \Theta_1^i} & \cdot & \cdot & \cdot & \frac{\partial \mu_{MN}}{\partial \Theta_T^i} \end{pmatrix} \quad (2.19)$$

where Θ_t^i denotes the i-th parameter of the t-th target. If the necessary condition is not satisfied for none of the above matrices, there will be at least two parameters Θ_1 and Θ_2 for which $G_i\Theta_1 = G_i\Theta_2$. In this case, the linear approximation of cost function gives the same optimal value for two sets of parameters, which indicated the lack of uniqueness. As discussed in the previous part, the covariance matrix does not include any information about target scatterers because it is a function of σ_α^2. Therefore, the columns of G_1 become zero when the parameter of interest is the target scatterer. In addition, the covariance matrix does not give any information about DOAs. This indicates that G_1 cannot provide any unique solution alone because it is not full-rank. Therefore, the uniqueness of solutions should be justified by exploring G_2 that is a function of all parameters. It can be shown that G_2 is a function of system matrix $\mathbf{d}$ because the mean vector is a factor of $\mathbf{d}$ or it is the summation of different targets' system matrices. Referring to (2.10) the maximum number of unique elements in the system matrix is its length $M \times N$. This leads to the conclusion that the maximum number of unique columns in G_2 cannot exceed the given bound. Consequently, the number of parameters T should be less than or equal to MN. The same analysis can be done for other parameters of every target. It is also possible to make the same conclusion for targets lying in multiple cells $C > 1$. In this case, the necessary condition is found for each cell separately.

One important point should be noted here about the bounds found above. The above bounds are the only necessary conditions for the uniqueness of solutions. The geometry of antennas and targets in the surveillance region is very important in the number of of targets that can be accurately estimated. For example, although the maximum number of unique elements in $\mathbf{d}$ is $M \times N$, the bound becomes tighter if antennas are distributed along with the x-axis.

36

In this case, in [59], it was found that the range $[M + N - 1, MN - 1]$ as the maximum bound when the distance of antennas determines the actual bound.

2.4   Tracking Algorithm

The maximum bound in target localization may be an issue in real tracking problems with MIMO radars. For example, targets may enter one resolution cell in some time steps and, therefore, get unresolved for the radar system when the total number of targets in a resolution cell exceeds the limit. Also, even when the number is less than the bound, localization algorithm may not provide good results due to the geometry of targets. To handle the limitation on the number of targets prior information of targets' movement can be used. Assume the following common near constant velocity model for the t-th target:

$$
\begin{aligned}
\mathbf{x}_t(k + 1) &= F_t \mathbf{x}_t(k) + G_t \mathbf{v}_t(k) \\
\hat{\alpha}_t(k + 1) &= \hat{\alpha}_t(k) + \delta_\alpha
\end{aligned}
\tag{2.20}
$$

where k is time step, $\mathbf{v}_t(k)$ is the additive noise that is Gaussian-distributed with zero mean and covariance matrix Q_t, F_t and G_t are motion matrices, and δ_α is the Gaussian additive noise with variance σ_α^2 modeling the uncertainty in target scatterers. Motion matrices can be defined as [5] [6]

$$
F_t =
\begin{bmatrix}
1 & T_s & 0 & 0 \\
0 & 1 & 0 & 0 \\
0 & 0 & 1 & T_s \\
0 & 0 & 0 & 1
\end{bmatrix}
, G_t =
\begin{bmatrix}
\frac{T_s^2}{2} & 0 \\
T_s & 0 \\
0 & \frac{T_s^2}{2} \\
0 & T_s
\end{bmatrix}
\tag{2.21}
$$

with T_s as the sampling time. In this chapter, the number of targets in the surveillance region is assumed to be time-invariant. Dealing with time variant number of targets happening due to new targets' birth or available targets'

death is difficult when MIMO radars are used as measurement models. This topic is discussed in [43]. Given T targets and their estimates $\mathbf{x}_t(k|k)$ at the k-th time step, a Bayesian estimator finds the posterior probability distribution of targets given measurements. Measurements are outputs of matched filters defined as $\Phi(k)$ in the previous part. The key issues in multitarget tracking using the underlying MIMO radar are:

- Grouping

- Data association

- Hypothesis generation

- Likelihood computation

- Estimates update

The first step of grouping is the classification of different targets based on their location. Group target tracking has been extensively discussed in the literature [69]. Here, targets are classified into different groups based on the associated cell. Figure 2.2 shows how different groups of targets may be constructed. The same grouping technique is done here at each time step. For simplicity, it is assumed that there is one group (cluster) at the k-th time step. In scenarios with more than one group, the superscript g is used for all parameters to clarify the category of targets and measurements.

2.4.1   Data Association

Define $\mathcal{T}_t(k)$ as the t-th track at the k-th time step. Each track is represented by its *sufficient statistics* summarizing the information content of
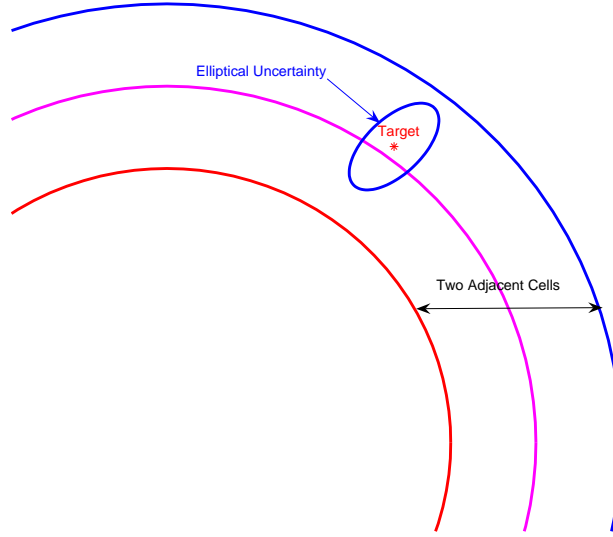
Figure 2.3: Elliptical uncertainty around the target makes it probable to be associated with each of adjacent resolution cells.

measurements [56]. As an example, the t-th track can be represented for an EKF estimator as

$$\mathcal{T}_t(k) = \{\mathbf{x}_t(k|k), P_t(k)\} \tag{2.22}$$

where $\mathbf{x}_t(k|k), P_t(k)$ are estimated mean and covariance for the t-th track, respectively. The set of all tracks at the k-th time step is written as

$$\mathcal{T}(k) = \left\{\mathcal{T}_1(k), ..., \mathcal{T}_{N(k)}(k)\right\} \tag{2.23}$$

where $N(k)$ is the number of confirmed tracks at the k-th time step. Due to the uncertainty in the estimated location of targets, a target may be assigned to different cells. Figure 2.3 shows a target with its elliptical uncertainty region. It can be observed that the target may be associated with any cell fallen in its uncertainty region. A cell-to-track association matrix is now defined as

39

$$\gamma_{tc} = \begin{cases} 1 & \text{If the } t\text{-th track is associated with the } c\text{-th cell} \\ 0 & \text{Otherwise} \end{cases} \quad (2.24)$$

A similar matrix is defined for track-to-cell association ξ_{ct}. Unlike in common tracking context in which each measurement is only associated with one track, there is no such condition here over the rows of the association matrix. In other words, an individual cell may be associated with multiple targets. Figure 2.4 shows a multi-target scenario where targets are located in one resolution cell. The uncertainty ellipses of several targets may intersect an individual cell. Consequently, this cell may be associated with multiple targets. However, the point targets are inside the cell and, therefore, the following condition is still valid:

$$0 \le \sum_{c=1}^{C} \gamma_{tf} \le 1, t = 1, ..., N(k) \quad (2.25)$$

The t-th target is assigned to the c-th cell if the following inequality is satisfied:

$$\frac{(r_t(k+1|k) - r^c)^2}{\sigma_{r,t}^2} \le \zeta \quad (2.26)$$

where $r_t(k+1|k)$ is the predicted range of the t-th target, r^c is the range of the c-th cell, and ζ is the threshold. The threshold is found such that the cell falls within the 95-percent confidence region [6]. A target may be assigned to two cells if the uncertainty region around it straddles two adjacent cells. In the above equation, $\sigma_{r,t}^2$ represents the variance of range estimation that can be found by linearizing the range model and, then, using the predicted covariance of estimation $P_t(k+1|k)$. The following equation is derived for $\sigma_{r,t}^2$

$$\begin{aligned} \sigma_{r,t}^2 &= \frac{(x_t(k+1|k))^2}{(x_t(k+1|k))^2 + (y_t(k+1|k))^2}\sigma_{x,t}^2 + \frac{(y_t(k+1|k))^2}{(x_t(k+1|k))^2 + (y_t(k+1|k))^2}\sigma_{y,t}^2 + \\ &+ \frac{x_t(k+1|k)y_t(k+1|k)}{(x_t(k+1|k))^2 + (y_t(k+1|k))^2}\sigma_{xy,t}^2 \end{aligned} \quad (2.27)$$
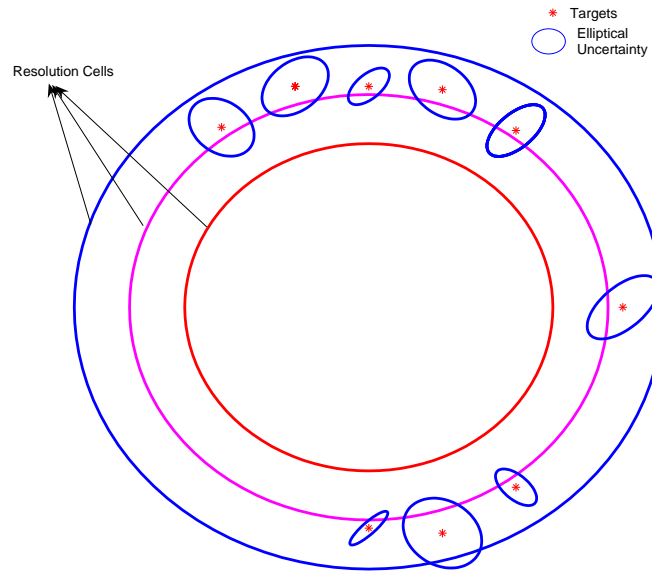
Figure 2.4: A scenario with 9 targets where targets are in the border of two cells and entering the other cell.

where $P_t(k+1|k) = \begin{bmatrix} \sigma_{x,t}^2 & \sigma_{xy,t}^2 \\ \sigma_{yx,t}^2 & \sigma_{y,t}^2 \end{bmatrix}$, and $x_t(k+1|k), y_t(k+1|k)$ denote the predicted estimates.

2.4.2   Hypothesis Generation/Evaluation

The h-th hypothesis $(\mathcal{H}_h)$ is indeed a target-to-cell association for a group of targets located in the underlying cluster. As targets may be assigned to more than one cell, different hypotheses are formed for a multi-target scenario. To evaluate each hypothesis, its likelihood is found and the one with the most value is taken as the winner. The Likelihood function for the h-th hypothesis can be written as

$$p(\Phi|\mathcal{H}_h) = p(\Phi|\gamma^h, \mathcal{T}^h(k)) \qquad (2.28)$$

where $\mathcal{T}^h(k)$ are those targets in the same cluster based on the h-th hypothesis. Note that each association involves information about the location of targets. According to Figure 2.2, targets may be grouped into different clusters because, in the new model, the effect of targets in the neighbor cell is also taken. Therefore, a target belonging to one cluster at the k-th time step may be assigned to a separate cluster in the next step. The above likelihood can be found using the expressions given in (2.13) and (3.30). The hypothesis with the lowest negative likelihood is chosen as the winner and its estimates are considered as new tracks.

2.4.3   Estimates Update

The states of targets are updated for each hypothesis separately. The update step is to find a new set of tracks $\mathcal{T}^h(k+1)$ from the previous step tracks $\mathcal{T}^h(k)$, the h-th association and measurements at the $k+1$-th time step.

The prediction step for each target can be implemented using motion models given in the previous part. Define $\mathcal{T}_t(k+1|k)$ as the predicted state for the t-th target. The same equation can be found for target scatterers using the motion model given for scatterers. The predicted DOA and range for each target can be computed as

$$\theta_t(k+1|k) = \tan^{-1}\left(\frac{y_t(k+1|k)}{x_t(k+1|k)}\right) \tag{2.29}$$

and

$$r_t(k+1|k) = \sqrt{(x_t(k+1|k))^2 + (y_t(k+1|k))^2} \tag{2.30}$$

respectively. The predicted range coefficients $\beta_t(k+1|k)$ can be easily found with the above predicted range and (3.2). Therefore, the predicted parameter vector can be written as $\Theta_t(k+1|k) = [\theta_t(k+1|k), \beta_t(k+1|k), \hat{\alpha}_t^r(k+1|k), \hat{\alpha}_t^I(k+1|k)]$ and the parameter vector for all targets is indicated by $\Theta(k+1|k)$. Define $\Theta^h(k+1|k) \subset \Theta(k+1|k)$ as those targets falling in the same cluster based on the h-th hypothesis. The posterior probability distribution of states given measurements for the h-th hypothesis can be written as

$$
\begin{aligned}
p\left(\mathcal{T}_t^h(k+1), \alpha_t^h(k+1)|Y(1:k+1)\right) &\propto\ p\left(\mathcal{T}_t^h(k+1), \alpha_t^h(k+1)|Y(1:k)\right) \times \\
&\times\ p\left(Y(k+1)|\mathcal{T}_t^h(k+1), \alpha_t^h(k+1), Y(1:k)\right)
\end{aligned}
\tag{2.31}
$$

The first term in the right hand side characterizes prediction stage that can be written as

$$
\begin{aligned}
p\left(\mathcal{T}_t^h(k+1), \alpha_t^h(k+1)|Y(1:k)\right) &=\ \int p\left(\mathcal{T}_t^h(k+1), \alpha_t^h(k+1)|\mathcal{T}_t(k), \alpha_t(k)\right) \times \\
&\times\ p\left(\mathcal{T}_t^h(k+1), \alpha_t^h(k+1)|\mathcal{T}_t(k), \alpha_t(k)\right) d\mathcal{T}_t(k)d\alpha_t(k)
\end{aligned}
\tag{2.32}
$$

In (2.31–2.32), $\mathcal{T}_t^h(k+1)$ and $\alpha_t^h(k+1)$ denote new estimates according to the h-th association. Also, $\mathcal{T}_t(k+1)$ and $\alpha_t(k)$ represent the elements of the

best hypothesis in the previous time step. The above steps are usually called tracking recursion in the literature (or the Chapman-Kolmogorov equations) [80]. The tracking recursion rarely yields a closed-form solution [80] when the measurement model is nonlinear. Due to nonlinearity in the measurement model, traditional KF or EKF [6] provide poor results. In this chapter, a UKF is used for states update. Due to the dimension of states that may be considerably large when multiple targets fall in different cells, UKF is a computationally feasible choice because other nonlinear filtering methods such as particle filtering [3] suffer from the curse of dimensionality.

The measurement is the output of the matched filter from all cells. To reduce the computational cost those cells that are far from the cluster of targets can be discarded. The various steps of the UKF can be summarized as follows where, for simplicity, superscript h has been removed:

- **Sampling**

  Sampling in the UKF is deterministic and the number of samples is fixed to $2 \times (n_x) + 1$ where n_x is the dimension of states. Those targets falling in the same cluster are updated together. Because the targets are moving, the number of clusters is also changing over time. If there are T_c targets in the c-th cluster, the number of samples will be $6T_c + 1$ where each target has 6 states consisting of its motion states, and the real and imaginary parts of scatterer. For simplicity, assume that all targets are now in the the same cell c. Each sample is generated using the following procedure:

$$
\mathbf{X}_c^i(k+1|k) =
\begin{cases}
\mathbf{X}_c(k|k) & \text{if } i = 0 \\
\mathbf{X}_c(k|k) + \xi\sqrt{P_c(k|k)}_i & \text{if } 1 \leq i \leq n_x \\
\mathbf{X}_c(k|k) - \xi\sqrt{P_c(k|k)}_{i-n_x} & \text{if } n_x + 1 \leq i \leq 2n_x
\end{cases}
\tag{2.33}
$$

44

where $\mathbf{X}_c(k|k)$ and $P_c(k|k)$ are state vector and covariance matrix of estimated targets, respectively, falling inside the c-th cluster. Note that above new states can be created by stacking states and covariances of individual targets in the c-th cluster. Also, $\xi = \sqrt{n_x + \lambda}$ [1], and $\sqrt{P_{c_i}}$ denotes the i-th column of the square-root of matrix $\sqrt{P_c}$.

- **Time Prediction**

  Time prediction of states and corresponding covariances can be found using the drawn samples as

  $$
  \begin{aligned}
  \mathbf{X}_c(k+1|k) &= \sum_{i=0}^{2n_x} w_i^m \mathbf{X}_c^i(k+1|k) \\
  P_c(k+1|k) &= \sum_{i=0}^{2n_x} w_i^c \left(\mathbf{X}_c^i(k+1|k) - \mathbf{X}_c(k+1|k) \right) \times \left(\mathbf{X}_c^i(k+1|k) - \mathbf{X}_c(k+1|k) \right)'
  \end{aligned}
  $$
  (2.34)

  with w^m, w^c as sampling weights defined as

  $$
  \begin{aligned}
  w_0^c &= w_0^m + (1 - \kappa^2 + \omega), w_0^m = \frac{\lambda}{\lambda + n_x} \\
  w_i^c &= w_i^m = \frac{1}{2(n_x + \lambda)}
  \end{aligned}
  $$
  (2.35)

  Here, $0 < \kappa \le 1$ is the primary scaling factor determining the extent of the spread of the sigma-points around the mean [55]. Also, it is shown that for Gaussian priors of states, $\omega = 2$ is a good design.

- **Measurement Update**

  It is probable that the generated sigma points fall inside the resolution cells beyond of the current cluster of targets. This happens when there is no prior information about the velocity of targets and, therefore, the

---

[1] λ is a parameter adjusting the spread of samples drawn around the mean. More details about different possibilities for the aforementioned parameter can be found in [55].

initial velocity is set to zero. In this case, the predicted covariance $P_c(k+ 1|k)$ is so large that some sigma points are located in other cells. This is the reason that the output of all cells are used as the measurement. The sampled output of matched filter can be found as

$$\mu_c^i(k + 1|k) = h\left(\mathbf{X}_c^i(k + 1|k)\right) \tag{2.36}$$

Here, $h(.)$ is the nonlinear function of the matched filter output. According to (2.8) and (2.10), h is a function of the target DOA, scatterer, and range coefficients. Therefore, the predicted output of the matched filter is computed based on the predicted DOA, scatterer and range coefficients given by (2.34). Now, define $\hat{Y}(k+1|k)$ as the predicted output of matched filter. This vector holds the outputs for all resolution cells in the surveillance region[2]. Each generated sigma point may provide the outputs for different cells in the region. The range of each sigma-point can be found using (2.30). Define $Y^i(k + 1|k)$ as the ith predicted measurement and assume $\mu_c^i(k + 1|k)$ falls in C_i cells belonging to the set $C_i = \{c_1^i, ..., c_{n_i}^i\}$. Then, the ith predicted measurement for different cells can be defined as follows:

$$Y_{c'}^i(k + 1|k) = \begin{cases} 0_{MN} & \text{If } c' \text{ does not belong to } C_i \\ \{\mu_c^i(k + 1|k)\}_{c'} & \text{Otherwise} \end{cases} \tag{2.37}$$

Where 0_{MN} is an $M \times N$ vector, and $\{\mu_c^i(k+1|k)\}_{c'}$ denotes the generated sigma-point in the c'th resolution cell of the c-th cluster.[3] The predicted output can be now found as

$$\hat{Y}(k + 1|k) = \sum_{i=0}^{2n_x} w_i^m Y^i(k + 1|k) \tag{2.38}$$

---

[2]It is more efficient to discard those cells that are very far from the cluster of targets.
[3]Note that every cluster may be comprised of several resolution cells.

The same can be also computed for the cross-correlation and covariance matrices as

$$
\begin{aligned}
P_{YY}(k+1|k) &= \sum_{i=0}^{2n_x} w_i^c \left(Y^i(k+1|k) - \hat{Y}(k+1|k) \right) \left(Y^i(k+1|k) - \hat{Y}(k+1|k) \right)' \\
P_{\mathbf{X}Y} &= \sum_{i=0}^{2n_x} w_i^c \left(\mathbf{X}_c^i(k+1|k) - \mathbf{X}_c(k+1|k) \right) \left(Y^i(k+1|k) - \hat{Y}(k+1|k) \right)'
\end{aligned}
$$

$$(2.39)$$

The Kalman gain can be also computed using covariance matrices found above

$$K(k+1) = P_{\mathbf{X}Y} P_Y \tag{2.40}$$

Finally, the updated estimates of mean and covariances are given as

$$\mathbf{X}_c(k+1|k+1) = \mathbf{X}_c(k+1|k) + K(k+1)\left(Y(k+1) - \hat{Y}(k+1|k) \right) \tag{2.41}$$

$$P_c(k+1) = P_c(k+1|k) - K(k+1)P_{YY}K(k+1)' \tag{2.42}$$

Note that $Y(k+1)$ is more general than Φ defined in the localization part and involves outputs of detected cells. Here, outputs of other cells should be also taken into consideration because the sigma points may fall in undetected cells. The above steps can be done for each hypothesis separately. For different hypotheses, different clusters may be constructed and, therefore, different resolution cells may be assigned to targets. In this case, the likelihood of the h-th hypothesis can be found by (2.31) where $\mathcal{T}^h$ is the set of estimated states based on the h-th hypothesis. Final estimates can be found based on the following model-selection strategy:

$$\mathcal{T}(k+1) = \max_h p\left(Y(k+1)|\gamma^h, \mathcal{T}^h(k+1) \right) \tag{2.43}$$

2.4.4 PCRLB Derivation

The PCRLB defines the best MMSE for any unbiased estimator when the estimator is the state of a moving target [**?**]. The PCRLB for a multitarget tracking problem was suggested in [79] in terms of Riccati-like recursions as

$$J(k) = D^{22}(k-1) - D^{21}(k-1)\left(J(k-1) + D^{11}(k-1)\right)^{-1} D^{12}(k-1) \quad (2.44)$$

with the following definitions for the unknown terms

$$
\begin{aligned}
D^{11}(k-1) &= E\left[-\nabla_{X(k-1)}^{X(k-1)} \log p(X(k)|X(k-1))\right] &&(2.45)\\
D^{12}(k-1) &= E\left[-\nabla_{X(k)}^{X(k-1)} \log p(X(k)|X(k-1))\right] = [D^{21}(k-1)]'\\
D^{22}(k-1) &= D^{33}(k-1) + J_y(k) &&(2.46)\\
D^{33}(k-1) &= E\left[-\nabla_{X(k)}^{X(k)} \log p(X(k)|X(k-1))\right] &&(2.47)
\end{aligned}
$$

where $J_y(k)$ is measurement information defined as

$$J_y(k) = E\left[\frac{\partial \log p(\mathbf{Y}(k)|\mathbf{X}(k))}{\partial \mathbf{X}(k)} \left(\frac{\partial \log p(\mathbf{Y}(k)|\mathbf{X}(k))}{\partial \mathbf{X}(k)}\right)'\right] \quad (2.48)$$

Here, $\mathbf{Y}(k)$ are the output of the matched filter and the expectation is also taken with respect to outputs and target states. For simplicity, assume that all T targets in the surveillance region are in the same cluster at the kth time step. Therefore, $\mathbf{X}(k)$ is the stacked vector of all individual targets' states as

$$\mathbf{X}(k) = [(\mathbf{X}_1(k))' \ldots (\mathbf{X}_T(k))']' \quad (2.49)$$

With the following definition for individual target's states

$$\mathbf{X}_i(k) = [(\mathbf{x}_i(k))' \ \hat{\alpha}_i^R(k) \ \hat{\alpha}_i^I(k)]' \quad (2.50)$$

The distribution $p(\mathbf{Y}(k)|\mathbf{X}(k))$ is Gaussian with mean μ and covariance Σ given by (2.11). It is also clear that both mean and covariance are functions

of parameters of targets Θ_t defined by (2.10). It can be shown that the $[a, b]$th element of the FIM is calculated as [89]

$$
\begin{aligned}
J_y^p &= E\left[\frac{\partial \log p(\mathbf{Y}(k)|\mathbf{X}(k))}{\partial \Theta^a}\left(\frac{\partial \log p(\mathbf{Y}(k)|\mathbf{X}(k))}{\partial \Theta^b}\right)'\right] = \\
&= \left(\frac{\partial \mu}{\partial \Theta^a}\right)'\Sigma^{-1}\frac{\partial \mu}{\partial \Theta^b} + \frac{1}{2}\mathcal{T}\left(\Sigma^{-1}\frac{\partial \Sigma}{\partial \Theta^a}\Sigma^{-1}\frac{\partial \Sigma}{\partial \Theta^b}\right)
\end{aligned}
\tag{2.51}
$$

where $\Theta = [(\Theta_1)' \ \ldots \ (\Theta_T)']'$ is the stacked parameter vector, and Θ^a is the a-th element of the vector. Derivatives of the mean and covariance matrix with respect to parameters of the target can be found in the Appendix I. Now, define the following matrix:

$$
\Omega = \begin{pmatrix}
\omega_1 & 0 & . & . & . & 0 \\
0 & \omega_2 & 0 & . & . & 0 \\
. & . & . & . & . & . \\
. & . & . & . & . & . \\
. & . & . & . & . & . \\
0 & . & . & . & 0 & \omega_T
\end{pmatrix}
\tag{2.52}
$$

Here, ω_t is the Jacobian matrix of nonlinear function $F : \{\theta_t, r_t, \hat{\alpha}_t^r, \hat{\alpha}_t^I\} \rightarrow \{x_t, y_t, \hat{\alpha}_t^r, \hat{\alpha}_t^I\}$ defined as

$$
\omega_t = \begin{pmatrix}
\frac{\partial \theta_t}{\partial x_t} & \frac{\partial r_t}{\partial x_t} & 0 & 0 \\
\frac{\partial \theta_t}{\partial y_t} & \frac{\partial r_t}{\partial y_t} & 0 & 0 \\
0 & 0 & 1 & 0 \\
0 & 0 & 0 & 1
\end{pmatrix}
\tag{2.53}
$$

where the derivatives are as defined in the Appendix 6.1. Based on above matrices, a measurement's contribution to the FIM is found as

$$
J_y = \Omega J_y^p \Omega'
\tag{2.54}
$$

The following simplified recursive equation is usually used in the literature to update overall FIM [79]:

$$J(k) = \left(\Gamma_* + F_*(J(k-1))^{-1}F_*'\right)^{-1} + J_y \tag{2.55}$$

where F_* and Γ_* are augmented motion matrix and noise covariance, respectively. Each matrix can be created as $F_* = \text{diag}(\{F_*^1, ..., F_*'\}), \Gamma_* = \text{diag}(\{\Gamma_*^1, ..., \Gamma_*'\})$ where $\text{diag}(\{.\})$ is the diagonalized form of all matrices in the set. Each individual matrix is also written as

$$F_*^t = \begin{pmatrix} F_t & 0 & 0 \\ 0 & 1 & 0 \\ 0 & 0 & 1 \end{pmatrix}, \Gamma_*^t = \begin{pmatrix} G_t Q_t G_t' & 0 & 0 \\ 0 & \sigma_\alpha^2 & 0 \\ 0 & 0 & \sigma_\alpha^2 \end{pmatrix} \tag{2.56}$$

The Fisher matrix $J(k)$ can be initialized using the FIM of localization (J_y) at $k = 0$. Having $J(k)$ at each time step, the PCRLB can be immediately found by taking an inverse of FIM as $\text{PC}(k) = (J(k))^{-1}$.

2.5 Simulation Results

A MIMO radar system with 2 transmitters and 2 receivers is designed for simulations. The distribution of antennas is shown in Figure 2.5. The parameters of the surveillance region and the radar system are listed in Table 2.1. In the following, the performance of localization and tracking are evaluated based on the given structure.

2.5.1 Localization

The maximum number of uniquely detectable targets is 3 for the given structure because the system matrix $\mathbf{d}$ has 3 unique elements. First, the

performance of localization is evaluated for a single target case with parameters being $\{820, \frac{\pi}{4}, 3, 3\}$. The target SNR can be also found by

$$\text{SNR} = \frac{MN|\alpha|^2}{\sigma_w^2} \tag{2.57}$$

The optimization algorithm is implemented on the given scenario. Figure 2.6 shows the RMSE of estimation and the CRLB for different target SNRs. Results show that the RMSE values match CRLB, especially when the target SNR is high enough.

The algorithm is now tested for different numbers of targets in the same cell. The target SNR is fixed to be 15dB for each target. Three targets are added to the scenario with parameters presented in Table 2.2. In addition, target scatterers are assumed to be the same for all targets (i.e., 15dB for other three targets). Table 2.3 presents the RMSE of each target estimation in different scenarios where each scenario involves different numbers of targets with parameters of targets summarized in Table 2.2. For the 2-target scenario, the RMSE is less than the range bin size (30m). However, the RMSE of target 1 has increased about 50% compared to the single target case. When the 3-target scenario is considered, the RMSE is still lower than the range bin size but the RMSE values for the first two targets show about 80% increase compared to the 2-target case. The results in the 4-target scenario are not acceptable at all because the RMSE exceeds the range bin size for all targets. For the first target, a 600% increase is observed in the RMSE in comparison with the single target case. The same behavior can be observed for other targets when the number of targets in the cell varies. In other words, simulation results show that the RMSE of localization increases when the number of targets in one cell approaches the limit.

For multiple targets in the same cell, the geometry of targets also affects

Table 2.1: Parameters of the radar system and surveillance region

	$R_{\mathbf{max}}$	σ_w^2	σ_α^2	$r_{\mathbf{bin}}$	$p_{\mathbf{fa}}$	L	δ_α
Value	2000m	3	10^{-4}	30m	10^{-4}	128	10^{-4}

the accuracy of estimation. Assume that for the 2-target case the first target is fixed with the DOA shown in Table 2.3 but the DOA of the second target varies. The RMSE of localization for every situation is presented in Table 2.4. It can be observed that for DOAs around $\frac{\pi}{3}$ the localization error is higher than the localization error for other DOAs. However, when targets become well-separated in $\theta_2 = 0$, the localization RMSE gets about 50% smaller than the previous case with $\theta_2 = \frac{\pi}{3}$.

The target RMSE may be more affected for scenarios with targets being closely-spaced in the state space. In general, it can be concluded that even with the number of targets in one cell below the maximum bound, the RMSE may be affected by the poor geometry of targets in the cell. The number of antennas plays an important role in the accuracy of target localization. Consider the 3-target scenario where the MIMO radar discussed before leads to poor results according to Table 2.3. The average RMSE of all targets is shown in Figure 2.7 for the different numbers of transmitters varying between 2 and 10. It is clear from the graph that by increasing the number of antennas, localization RMSE can be improved significantly. That is, changing the number of antennas has improved the maximum bound discussed before that indicates that there is a relationship between the maximum bound and the accuracy of target localization. The same improvement can be observed by distributing antennas differently. In this case, the maximum number of unique elements in the system matrix is increased that leads to an improvement in the maximum bound.
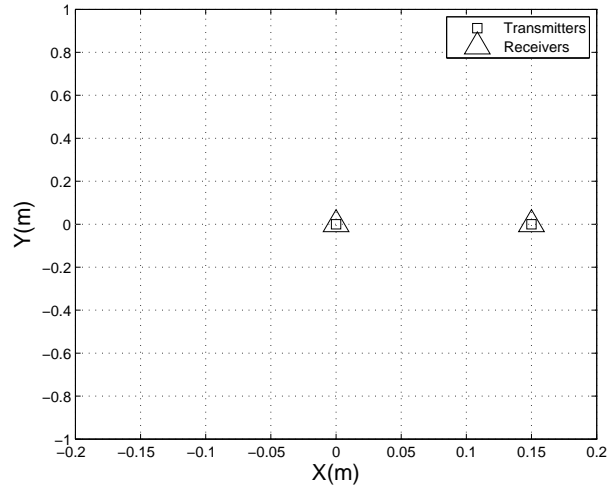
Figure 2.5: Distribution of transmitters and receivers in the surveillance region.
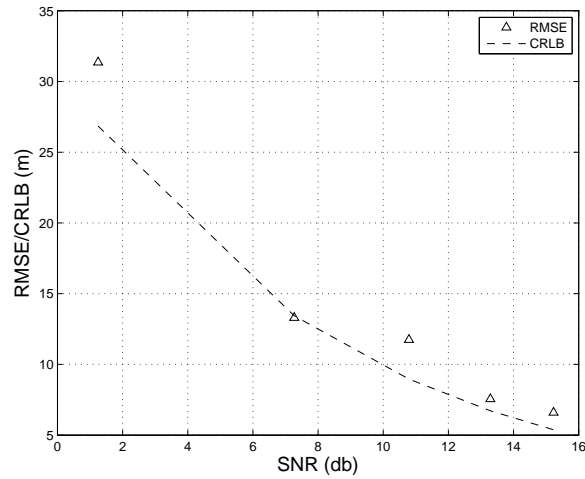
Figure 2.6: CRLB and RMSE of localization for a single target case.

Table 2.2: Parameters of 3 extra targets added to the multiple-target scenario

	DOA	Range
Target 2	$-\frac{\pi}{6}$	830
Target 3	0	825
Target 4	$\frac{\pi}{5}$	820

Table 2.3: RMSE results in meters for different numbers of targets in the same cell

	Single target	2-target	3-target	4-target
Target 1	6.6	10.32	27.1	42.83
Target 2	-	7.08	19.65	67.61
Target 3	-	-	24	98.2
Target 4	-	-	-	98.1

Table 2.4: RMSE results for different geometry of targets $(\theta_1 = \frac{\pi}{4})$

	Target 1	Target2
$\theta_2 = -\frac{\pi}{4}$	8.48	7.68
$\theta_2 = -\frac{\pi}{6}$	10.32	7.08
$\theta_2 = 0$	7.83	5.63
$\theta_2 = \frac{2\pi}{9}$	16.84	16.07
$\theta_2 = \frac{\pi}{3}$	14.38	24.35
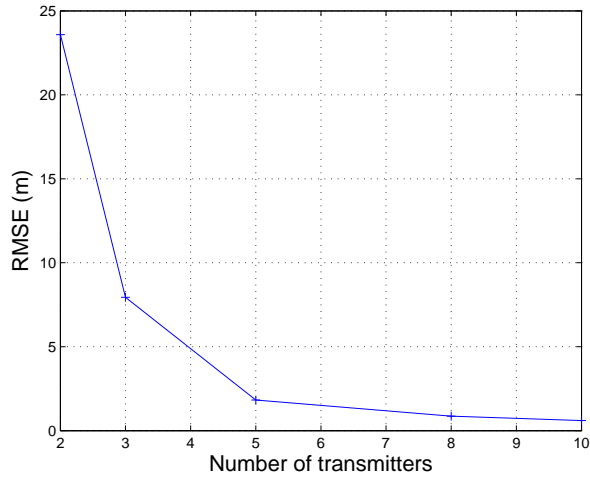
Figure 2.7: Average CRLB of localization for different number of transmitters.

54

2.5.2   Tracking

The same structure used in the last part is taken for the MIMO radar and surveillance region. Two different methods are used here for tracking. First, localization algorithm is done at each time step in order to estimate the location of available targets and corresponding scatterers. Localization results are used as measurements for the tracking algorithm that is a simple KF. This approach is called *localization-level* tracking. The second method is what was discussed in this chapter where the outputs of the matched filter are directly used for tracking purposes. This approach is called *signal-level* tracking.

A 2-target scenario is first considered. Simulation is done in 100 scans where targets are first in different cells but enter the same cell after some time. Figure 2.8 shows the generated trajectory for the 2-target scenario. Signal and localization level tracking algorithms are applied to the generated measurements. The RMSE and the PCRLB for both targets are shown in Figure 2.9 after 100 Monte Carlo runs. It can be seen that there is a jump in the localization-level tracking results around the time in which both targets are in the same cell. It was discussed in the last part that the geometry of targets plays an important role in the accuracy of the estimated RMSE of target localization. In this scenario, when targets enter the same cell, RMSE of localization is so large that a jump occurs in the tracking results. However, this phenomenon is not observed in signal-level tracking because localization results are not used in this approach.

Now, consider another scenario with three targets when all targets enter the same cell after some time steps. Also, two targets are closely-spaced in the state space making it harder to have good estimates of targets' location. Figure 2.10 shows the generated trajectories for the 3-target scenario. Results of localization and signal level tracking as well as the PCRLB can be observed
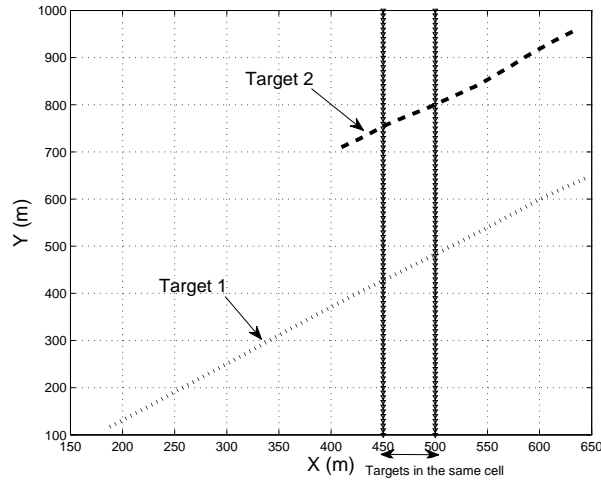
Figure 2.8: The generated 2-target scenario. Targets enter the same cell as shown in the graph.

in Figure 2.11. It can be observed that at the beginning and the end of simulation, results are the same because targets are located in the different cells. However, localization-level tracking results are much worse during the intervals with the targets being unresolved or closely-spaced in the state space. The reason is the inaccuracy of localization results used as the measurements for the tracking algorithm.

The simulation can be done for scenarios with more number of targets in one resolution cell where localization cannot provide any reasonable results due to exceeding the bound. Consider a scenario with 4 targets with generated trajectories shown in Figure 2.12. The number of targets in three consecutive cells is also given in Figure 2.13. It can be observed that there are four targets available in cell c_2, which indicates that the maximum bound is violated. The PCRLB as well as the CRLB for the designed scenario are plotted in Figures 2.14 and 2.15, respectively. Figure 2.15 shows that CRLB suddenly increases after $t = 20$ when all targets become unresolved. For the next time steps,

(a)Target 1   (b)Target 2
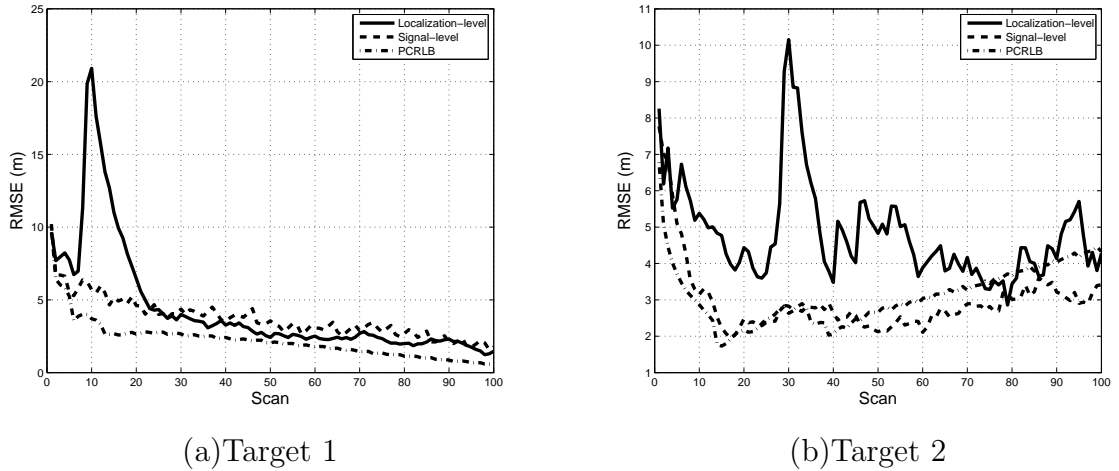
Figure 2.9: RMSE and the PCRLB for the 2-target scenario.

CRLB goes to infinity as long as targets occupy the same cell. Nevertheless, Figure 2.14 shows that the PCRLB still remains bounded in the period of time that the number of targets exceeds the bound.

To see the performance of tracking using the method proposed in this chapter, the signal-level tracking algorithm is applied to the generated data. The RMSE results are presented in Figure 2.16 for all targets. Compared to Figure 2.14, it can be observed that the RMSE follows the PCRLB. Also, it can be inferred that the signal-level tracking has been able to provide an estimate of target states in the time interval that all targets become unresolved.

From the simulations, the superiority of the proposed signal-level tracking over the localization-level tracking can be observed. It is also possible to compare the computational cost of both algorithms. Although the computational complexity of the algorithm needs to be carefully analyzed in a separate work, the goal here is to show how the signal-level approach can be operated faster than the localization-level algorithm. Simulations have been done on a $3GHz$ Intel-Core2 Duo processor with $2GB$ memory. The average simulation time for

57
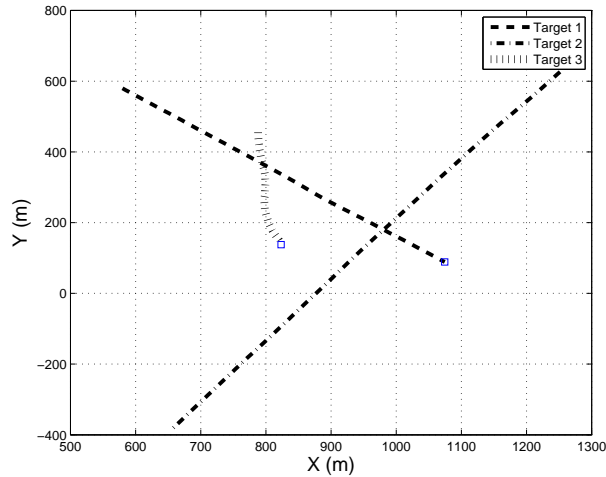
Figure 2.10: The generated 3-target scenario. Targets enter the same cell where two of them are also closely spaced.

two tracking algorithms applied to the 3-target scenario is found separately. The average simulation time for the signal-level tracking approach is 85.7 seconds while the value for the localization-level approach becomes around 3773 seconds. In other words, the signal-level tracking method is about 45 times faster than the localization-level method. The bottleneck in the simulation is the localization step due to the time needed for nonlinear optimization. The optimization procedure is done for the localization-level method at each time step while it is only done once in the signal-level tracking in order to initialize possible targets. Therefore, besides the better performance, the signal-level tracking is much more computationally efficient than localization-level tracking is. This issue can be critical in scenarios with a large number of targets in the same cluster.
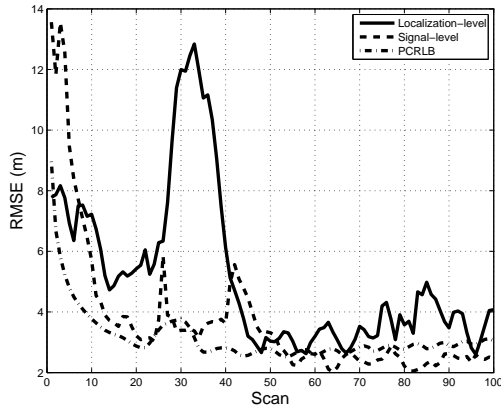
(a)Target 1
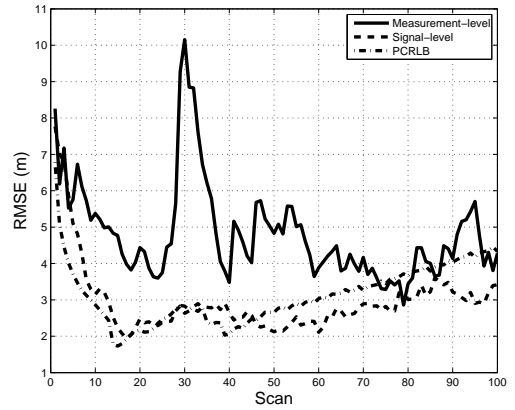
(b)Target 2
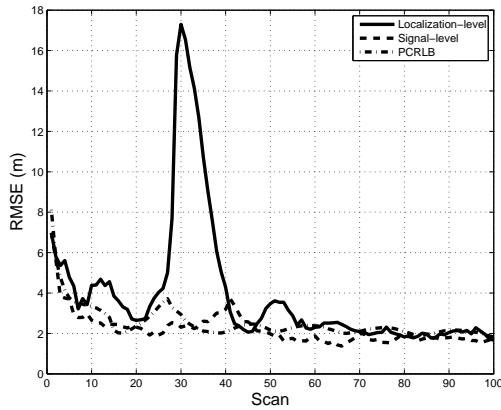
(c)Target 3

Figure 2.11: RMSE and the PCRLB for the 3-target scenario.

2.5.3 Impact of MIMO Parameters

It was shown in the last part that when the number of transmitters increases, localization results are improved. With the fixed number of antennas, the geometry of transmitters and receivers is also very influential on the PCRLB. For example, the target structure may not be observable for some geometries.

Consider the antenna distribution discussed in this chapter. Assume there

59
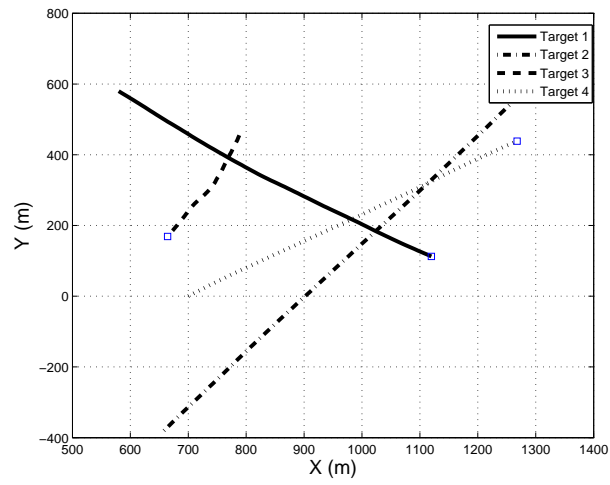
Figure 2.12: The 4-target scenario where all targets enter the same cell for a period of time.
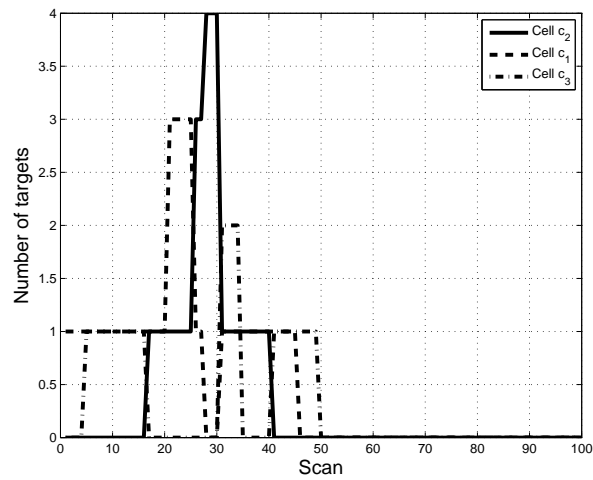
Figure 2.13: The number of targets in three consecutive cells for the 4-target scenario.
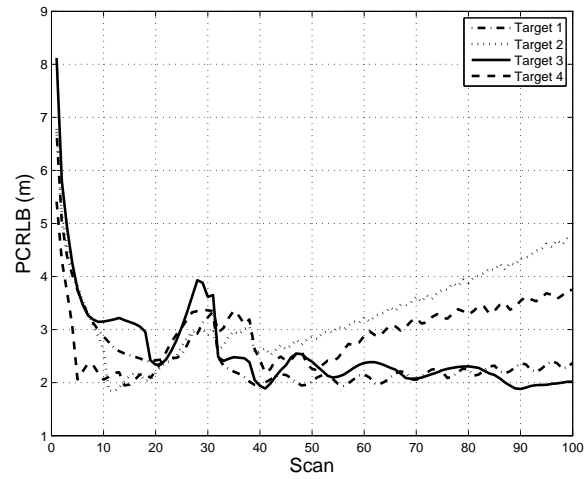
Figure 2.14: The PCRLB for the 4-target scenario.
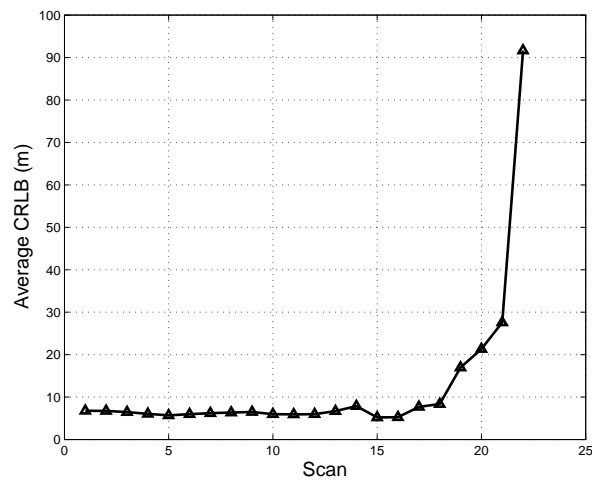
Figure 2.15: Localization CRLB for the 4-target scenario. CRLB begins to diverge when targets become unresolved.
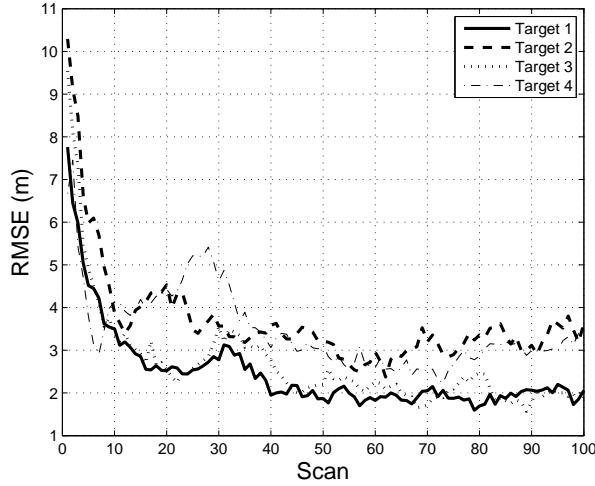
Figure 2.16: RMSE of signal-level tracking for the 4-target scenario after 100 Monte Carlo runs.

are 2 targets in the surveillance region located at $\frac{\pi}{6}$ and $\frac{2\pi}{3}$, respectively. Other parameters of targets such as range and scatterer are the same as in Table 2.2. Since $\sin(\frac{\pi}{6}) = \sin(\frac{2\pi}{3})$, the same matrix is found for each target. Now, if only one of these two parameters are available, the localization algorithm cannot distinguish above DOAs from one another and, hence, the targets are not observable. The same can be found for other structures when the system matrix is periodic. The system matrix is periodic with period θ_d if $\mathbf{d}(\theta + \theta_d)$ has the same elements as $\mathbf{d}(\theta)$. For the structure used in the last part, the period is $\frac{\pi}{2}$ because elements of the system matrix are the same for $\theta_1 = \theta, \theta_2 = \theta + \frac{\pi}{2}$. A similar thing may happen for other structures if for every $1 \leq i \leq MN$, there is one $1 \leq j \leq MN, j \neq i$ for which $\mathbf{d}_i(\theta + \theta_d) = \mathbf{d}_j(\theta)$. In this case, the elements of the new system matrix are the same as the last one.

Besides the above problem, the distribution of antennas influences the tracking performance. Define another geometry for antennas as shown in Figure 2.17. The average PCRLB for the 3-target case is shown in Figure 2.18
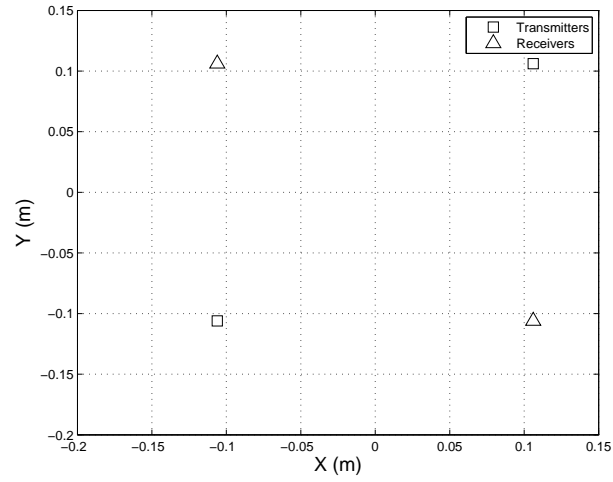
Figure 2.17: The distribution of antennas in the new structure.

for the new MIMO structure and the one used for simulations. It can be seen that the new structure has yield a lower PCRLB than the old one.
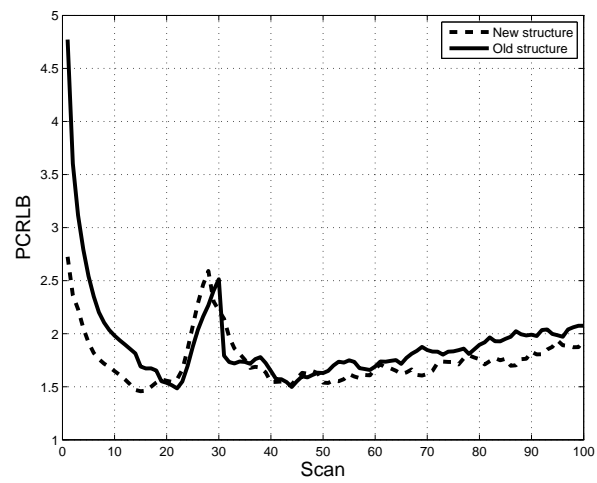
Figure 2.18: The PCRLB for the new and old structure of MIMO radar.

Chapter 3

Widely-Separated MIMO vs. Multistatic Radars for Target Localization and Tracking

3.1   Introduction

In this chapter, detection, localization, and tracking performance of widely-separated MIMO radars is addressed. In particular, the contributions of this chapter can be characterized as follows:

- **A comparative study of detection performance**:
  The first contribution of this chapter is to present a comparison between the detection performance of MIMO and multistatic radars. To do this, the probability of detection is derived separately for each structure in the presence of multiple-scatterer targets. It is observed that, for the same target SNR, MIMO radars enjoy a higher probability of detection in comparison with multistatic radars.

- **A new MH-based localization algorithm**:

  A new localization algorithm is developed specifically for multiple-scatterer targets. While previous methods were proposed for the case where the target amplitude is the same in all directions [33] [35] [34] [65], it is shown that the performance of target localization is adversely affected if targets become unobservable in certain transmitter-receiver pairs. This chapter presents a MH-based algorithm to associate signals in different transmitter-receiver pairs. The MH-based algorithm provides an estimate of the number and the states of corresponding targets. Unlike the previous works, the new MH-based algorithm can be also applied to multitarget scenarios where targets become unobservable in an arbitrary number or permutation of transmitter-receiver pairs. The MH-based algorithm is also applied to the multistatic radar and its localization performance is compared to MIMO radar results.

- **A signal-level tracking algorithm**:

  A novel signal-level tracking algorithm is also proposed in this chapter. It is shown that, although the received signals are Gaussian-distributed, the states of the target appear in the covariance of the Gaussian function, which makes the estimation problem nonlinear and non-convex. As a result, standard filtering techniques such as EKF and UKF cannot be used. A particle filter algorithm is then proposed as an alternative to deal with the dynamic target tracking. Finally, the PCRLB is derived for the MIMO radar system to justify the accuracy of tracking and localization.

The rest of this chapter is organized as follows: Section 3.1 presents the general structure of a well-separated MIMO radar. The signal model is described

66

in this section along with matched filtering and measurement generation. Target detection for MIMO and multistatic radars is discussed in this section as well. An MH-based algorithm for multitarget localization is proposed in Section 3.2. In addition, a particle filter-based method is presented for multitarget tracking problems. After the PCRLB derivation in Section 3.3, Section 3.4 presents simulation results for the MIMO and multistatic configurations. Using several simulations, the performances of both structures in terms of detecting, localizing, and tracking multiple-scatterer targets are evaluated.

MIMO Radars with Widely-separated Antennas

Consider a MIMO radar system comprising M transmitters and N receivers where the positions of the i-th transmitter and the j-th receiver are denoted by $\mathbf{x}_{ti}$ and $\mathbf{x}_{rj}$, respectively, with $\mathbf{x} = [x\ y]'$. The l-th target follows the classical Swerling type I model [75] extended for the multiple sensor case in [25]. Each target is modeled by an infinite number of random scatterers with the reflectivity factor being denoted by ζ_p^l [25]. It is assumed that the target and reflectivity factors remain constant during each scan time while they could change from one scan to another. The narrowband waveforms transmitted by the i-th antenna, $s_i(t)$, is assumed to be a complex signal with $\frac{1}{T} \int_T |s_i(t)|^2 dt = 1$, where T denotes the duration of the emitted pulse. Note that each pulse may consist of several sub-pulses in order to capture the statistical properties of the target properly. Given N_s as the number of snapshots (sub-pulses), T can be written as $T = N_s \times T_s$ where T_s denotes the duration of every sub-pulse. Defining τ as the pulse-width, T_s can be defined as $T_s = C \times \tau$. Here, C

corresponds to the number of resolution cells. It is assumed that transmitters send orthogonal signals with the following condition:

$$\int_T s_i(t)s_j^*(t)dt = \delta(i - j); \ \forall i, j \tag{3.1}$$

where $()^*$ is the complex conjugate operator and $\delta(.)$ is the Dirac delta function. The received signal in the n-th antenna can be written as the superposition of the reflected signals from all scatterers. The effect of the infinite number of scatterers was explored in [25] by integrating over all reflectivity factors. The non-coherent baseband equivalent received signal in the n-th antenna for a single target can be written as

$$y_n(t) = \sum_{m=1}^{M} h_{nm}s_m(t - \tau_{nm}) + w_n(t) \tag{3.2}$$

where τ_{nm} denotes the time delay of the signal emitted by the m-th transmitter, reflected by the target, and received by the n-th antenna. Also, $w_n(t)$ corresponds to a complex white Gaussian additive noise with zero mean and variance σ_w^2. The time delay in the above equation can be written as

$$\tau_{nm} = \frac{1}{c}(\sqrt{(x(t) - x_{tm})^2 + (y(t) - y_{tm})^2} + \sqrt{(x(t) - x_{rn})^2 + (y(t) - y_{rn})^2}) \tag{3.3}$$

with $[x(t); y(t)]'$ being the location of the target. The unknown term h_{nm} in (3.2) corresponds to the target scatterer for the (n, m)-th pair of transmitters and receivers. It is shown in [25] that the output signal in (3.2) is Gaussian-distributed with zero mean and unity variance. It also assumes that the variance is the same in all pairs. This assumption might be violated if different pairs of transmitters and receivers capture different aspects of the target. In general, it is assumed that $h_{nm} \sim \mathcal{CN}(0, \alpha_{nm}^2)$ where α_{nm}^2 denotes the reflection power in the direction of the (n, m)-th pair. Now, define $\bar{H} = [h_{11} \ldots h_{N1} \ldots h_{NM}]$. It is also shown in [25] that if transmitters and

68

receivers are widely separated in the surveillance region, $\bar{H} \sim \mathcal{CN}(0, \bar{\alpha})$ with $\bar{\alpha} = \text{diag}\left([\alpha_{11}^2 \; \alpha_{21}^2 \; ... \; \alpha_{NM}^2]'\right)$. In other words, distributing antennas widely enough in the surveillance region provides $M \times N$ independent paths.

3.1.1   Matched-Filtering and Measurement Model

It is shown in [25] that the output of the matched filter is the sufficient statistics for target detection provided that the additive noise level is known. The output of the matched filter can be obtained for each snapshot in the (n, m)-th pair as

$$\eta_{nm}^s(t) = \frac{1}{\tau} \int_{T_s} y_n(\lambda) s_m^*(t + \lambda) d\lambda \tag{3.4}$$

Assuming that each transmitted signal is a unit-power pulse with width τ and substituting y_n from (3.2) in (3.4), the following equation can be obtained for the output of the matched filter [89]:

$$\eta_{nm}^s(t) = h_{nm}^s \Lambda_{\tau_{nm}}(\tau) + \hat{w}_{nm}(t) \tag{3.5}$$

where h_{nm}^s is a realization of the target scatterer at the s-th snapshot, and $\Lambda_{\tau_{nm}}(\tau)$ denotes a triangular function defined by [89]

$$\Lambda_{\tau_{nm}}(\tau) = \begin{cases} \frac{t - \tau_{nm} + \tau}{\tau} & \tau_{nm} - \tau \leq t \leq \tau_{nm} \\ -\frac{t - \tau_{nm} - \tau}{\tau} & \tau_{nm} \leq t \leq \tau_{nm} + \tau \\ 0 & \text{otherwise} \end{cases}$$

Also, $\hat{w}_{nm}(t)$ is a complex white Gaussian noise with zero mean and variance σ_w^2. Sampling the output of the matched filter every τ seconds, the sampled output is now defined as $\eta_{nm}(c)$ by taking an average over all received signals in different snapshots as

$$\eta_{nm}(c) = \frac{1}{N_s} \sum_{s=1}^{S} [\eta_{nm}^s(c\tau)] \tag{3.6}$$

69

Here, $\eta_{nm}^s(c\tau)$ is obtained as

$$\eta_{nm}^s(c\tau) = \begin{cases} \beta_{nm} h_{nm}^s & c = c_{nm} \\ (1 - \beta_{nm}) h_{nm}^s & c = c_{nm} - 1 \quad + \hat{w}_{nm} \\ 0 & \text{otherwise} \end{cases} \tag{3.7}$$

where c_{nm} denotes the index of the resolution cell within which the target falls. In addition, β_{nm} is the ratio of the target complex amplitude that can be found using the triangular similarity as

$$\beta_{nm}^l = \frac{\tau_{nm} + \tau - \tau_{c_{nm}}}{\tau} \tag{3.8}$$

with $\tau_{c_{nm}} = c_{nm} \times \tau$. Signals are normally received and processed in several snapshots in order to smoothen the output of the matched filter, which reflects the statistics of the target more accurately. Defining $\eta^* = [\eta_{nm}(c_{mn}); \eta_{nm}(c_{nm} - 1)]$, it can be shown that η^* is a complex Gaussian random variable with $\eta^* \sim \mathcal{CN}(0, \sigma_w^2 I_{2\times2} + \Sigma_{nm})$ where $I_{2\times2}$ is an identity matrix, and Σ_{nm} is defined as

$$\Sigma_{nm} = \begin{bmatrix} \beta_{nm}^2 \alpha_{nm}^2 & \beta_{nm}(1 - \beta_{nm})\alpha_{nm}^2 \\ \beta_{nm}(1 - \beta_{nm})\alpha_{nm}^2 & (1 - \beta_{nm})^2 \alpha_{nm}^2 \end{bmatrix} \tag{3.9}$$

For other cells that are not occupied by any target, $\eta_{nm}(c) \sim \mathcal{CN}(0, \sigma_w^2)$. In the multitarget case, the distribution of η becomes more complicated. For a scenario with L targets occupying C_{nm}^* consecutive resolution cells, those cells belonging to the set $\{c_1, ..., c_{C_{nm}^*}\}$ with N_{c_i} being the number of targets in the (c_i)-th cell. The stacked vector η^* is now defined as

$$\eta^* = [\eta_{nm}(c_1 - 1) \; . \; . \; . \; \eta_{nm}(c_{C_{nm}^*})]$$

Again, η^* is Gaussian-distributed with zero mean and covariance matrix $\sigma_w^2 I_{C_{nm}^*+1} + \Sigma_{nm}$. The covariance matrix Σ_{nm} can now be written as

$$\Sigma_{nm} = [O_1 \; O_2 \; . \; . \; . \; O_{C_{nm}^*+1}]' \tag{3.10}$$

70

where each O_i term is defined as

$$
O_i = \begin{cases} \begin{bmatrix} 0 & . & \Sigma^{ii} & \Sigma^{i(i+1)} & 0 & . & 0 \end{bmatrix}' & i \neq C^*_{nm}+1 \\ \begin{bmatrix} 0 & 0 & . & . & . & \Sigma^{(C^*_{nm}+1)(C^*_{nm}+1)} \end{bmatrix}' & \text{otherwise} \end{cases} \tag{3.11}
$$

with Σ_{ii} and $\Sigma_{i(i+1)}$ being given by

$$
\Sigma^{ii} = \begin{cases} \sum_{l=1}^{N_{c_1}} (1 - \beta^l_{nm})^2 \alpha^2_{nm}(l) & i = 1 \\ \sum_{l=1}^{N_{c_{C^*_{nm}}}} (\beta^l_{nm})^2 \alpha^2_{nm}(l) & i = C^*_{nm}+1 \\ \sum_{l=1}^{N_{c_i}} (\beta^l_{nm})^2 \alpha^2_{nm}(l) + \sum_{l'=1}^{N_{c_{i-1}}} (1 - \beta^{l'}_{nm})^2 \alpha^2_{nm}(l') & \text{otherwise} \end{cases} \tag{3.12}
$$

$$
\Sigma^{i(i+1)} = \sum_{l=1}^{N_{c_{i+1}}} (1 - \beta^l_{nm}) \beta^l_{nm} \alpha^2_{nm}(l) \tag{3.13}
$$

Several clusters of consecutive cells that are occupied by multitargets may be found. In this case, $\eta^*_{c'}$ is defined for each (c')-th cluster separately and the covariance matrix is similarly defined according to the presence of targets in resolution cells.

3.1.2 Target Detection

Define the signal vector as $\mathbf{y} = [y_1 \; y_2 \; \ldots \; y_N]^H$ with H being the Hermition transpose. Hypotheses H_0 and H_1 are also defined as events corresponding to the absence and presence of the target, respectively. The optimal likelihood ratio test is provided for target detection as [25]

$$
\gamma = \frac{\log p(\mathbf{y}|H_1)}{\log p(\mathbf{y}|H_0)} \gtrless_{H_0}^{H_1} \delta \tag{3.14}
$$

where δ denotes the threshold and γ is the Neyman-Pearson likelihood ratio. It can be shown that the above likelihood ratio test is equivalent to

$$
\gamma = ||\eta||^2 \gtrless_{H_0}^{H_1} \delta \tag{3.15}
$$

where $\eta = [\eta_{11} \; \eta_{21} \; \ldots \; \eta_{NM}]^H$. Here, δ is set to ensure a certain probability of false alarm (P_{fa}). The complex output of matched filter can be described by the following distribution:

$$\eta_{nm} \sim \begin{cases} \hat{w}_{nm} & H = H_0 \\ h_{nm} + \hat{w}_{nm} & H = H_1 \end{cases} \tag{3.16}$$

Therefore, for $H = H_1$, $\eta_{nm} \sim \mathcal{CN}(0, \sigma_w^2 + \alpha_{nm}^2)$. It can be shown that the distribution of $|\eta_{nm}|^2$ is χ_2^2 (Chi-square) with two degrees of freedom [66]. The distribution of the test statistics γ was found in [25] with the variance of target scatterers being the same in all directions. In this case, $\gamma \sim (\sigma_w^2 + \alpha^2)\chi_{2MN}^2$ with α^2 being the assumed variance. However, for the multiple scatterer case, the distribution cannot be calculated using the procedure in [25]. Here we derive the expressions for the distributions of the test statistics for the multiple scatterer case. Assume the set of variances is classified into G groups where N_g corresponds to the number of repeated variances in the g-th group. Also, assume that α_g^2 is the variance assigned to the g-th group. The test statistics can be now written as

$$\gamma = \sum_{g=1}^{G} ||\eta_g||^2$$

with η_g being the test statistics corresponding to the g-th group. According to the derived distribution for the equal-variance case, each $||\eta_g||^2 \sim (\sigma_w^2 + \alpha_g^2)\chi_{2N_G}^2$ and, therefore, the distribution of the test statistics under the above assumptions is obtained as

$$Q(\gamma) = \sum_{g=1}^{G} (\sigma_w^2 + \alpha_g^2)\chi_{2N_g}^2 \tag{3.17}$$

The analytical form of Q was found in [11] for MIMO communication systems. It has been shown that Q can be written as

$$Q(\gamma; G, \alpha_1^2, ..., \alpha_G^2) = \prod_{g=1}^{G} \frac{1}{\alpha_g^{2N_g}} \sum_{g=1}^{G} \sum_{l=1}^{N_g} \frac{\Gamma_{l,g,G}}{(N_g - l)!}(-\gamma)^{N_g-l} e^{-\frac{\gamma}{\alpha_g^2}} \qquad (3.18)$$

with the following definition for $\Gamma_{l,g,G}$

$$\Gamma_{l,g,G} = (-1)^{N_g-1} \sum_{v \in \Xi_{l,g}} \prod_{j \neq g} \binom{v_j + N_g - 1}{v_j} \left(\frac{1}{\alpha_j^2} - \frac{1}{\alpha_g^2}\right)^{-(N_g+v_j)} \qquad (3.19)$$

Here, $v = [v_1 \ v_2 \ \ldots \ v_G]'$ and the new $\Xi_{l,g}$ can be defined as the set of all partitions of $(l-1)$ members as

$$\Xi_{l,g} = \left\{ [v_1 \ v_2 \ \ldots \ v_G] \in \mathcal{Z}^G | \sum_{j=1}^{G} v_j = l-1, v_g = 0, v_j \geq 0 \forall j \right\}$$

Given the above set, Γ can be found for every combination of l, g based on the vector $G = [N_1 \ N_2 \ \ldots \ N_G]'$. The general distribution of (3.18) can be simplified into

$$Q(\gamma; G, \alpha_1^2, ..., \alpha_G^2) = \prod_{g=1}^{G} \frac{1}{\alpha_g^{2N_g}} \sum_{g=1}^{G} \sum_{l=1}^{N_g} (-1)^{N_g-l} \Gamma_{l,g,G} \alpha^{2(N_g-l+1)} \mathcal{E}(\gamma; N_g-l+1, \frac{1}{\alpha_g^2})$$

$$(3.20)$$

where $\mathcal{E}(\gamma; N_g-l+1, \frac{1}{\alpha_g^2})$ denotes the well-known Erlang distribution [24] with parameters $k = N_g - l + 1$ and $\lambda = \frac{1}{\alpha_g^2}$. Now, back to the original detection problem, the probability of detection can be defined as

$$P_d^{MIMO} = \text{prob}\,(\gamma \geq \zeta | H_1) \qquad (3.21)$$

where the threshold ζ can be found with respect to the assigned probability of false alarm as

$$P_{fa}^{MIMO} = \text{prob}\,(\gamma \geq \zeta | H_0) \qquad (3.22)$$

Simplifying (3.21), the following expression for the threshold is derived [25]:

$$\zeta = \sigma_w^2 F_{2MN}^{-1}(1 - P_{fa}) \tag{3.23}$$

where F_{2MN}^{-1} denotes the inverse cumulative χ^2 distribution with $2MN$ degrees of freedom. The probability of detection can be now written as

$$
\begin{aligned}
P_d^{MIMO} &= 1 - prob\left(\gamma \leq \zeta | H_1\right) = \\
&= 1 - \prod_{g=1}^{G} \frac{1}{\alpha_g^{2N_g}} \sum_{g=1}^{G} \sum_{l=1}^{N_g} (-1)^{N_g-l} \Gamma_{l,g,G} \alpha^{2(N_g-l+1)} C_{\mathcal{E}}(\zeta; N_g - l + 1, \frac{1}{\alpha_g^2})
\end{aligned}
\tag{3.24}
$$

Here, $C_{\mathcal{E}}(\zeta; N_g - l + 1, \frac{1}{\alpha_g^2})$ is the cumulative function of Erlang distribution that can be simply written as [24]

$$C_{\mathcal{E}}(\zeta; N_g - l + 1, \frac{1}{\alpha_g^2}) = 1 - \sum_{n=0}^{N_g-l} e^{-\frac{\zeta}{\alpha_g^2}} \frac{\left(\frac{\zeta}{\alpha_g^2}\right)^n}{n!} \tag{3.25}$$

Note that the expression given by (3.25) is a generalization of the detection probability derived in [25]. Our new derived detection probability can be used for a multiple scatterer target scenario.

3.1.3   Probability of Detection for Multistatic Radars

The local probability of false alarm and the probability of detection for every pair can be computed using the Swerling equations as [75]

$$
\begin{aligned}
P_{fa}^p &= \exp\left(-\frac{\zeta^2}{2}\right) \\
P_d^p &= \exp\left(-\frac{\zeta^2}{2(1 + d_p)}\right)
\end{aligned}
\tag{3.26}
$$

with d_p being the target SNR in the p-th pair of transmitters and receivers. Now, a probability vector $P_d = \begin{bmatrix} P_d^1 \ P_d^2 \ \dots \ P_d^{MN} \end{bmatrix}'$ is defined to characterize

the local detection information for each pair. The m/n logic can be used to calculate the total probability of detection. The following m/n logic can be applied to the detection problem [32]:

$$P_d^{tot} = \sum_{n=n^*}^{MN} \left\{ \left[\sum_{p=0}^{n-n^*} (-1)^p \begin{pmatrix} p \\ n \end{pmatrix} \right] \left(\sum_{v \in \Theta_{n,MN,0}} \left[\prod_v P_d^v \right] \right) \right\} \qquad (3.27)$$

Here, $\Theta_{n,MN,0}$ denotes all possible v permutations of the set $[1\ 2\ \ldots\ MN]'$. A recursive algorithm was proposed in [30] to facilitate the computing of the above permutations. The recursive algorithm can be summarized as

$$\sum_{v \in \Theta_{n,MN,0}} \left[\prod_v P_d^v \right] = \sum_{a_1=0}^{MN-v+1} P_d^{a_1} \left(\sum_{a_2=a_1}^{MN-v+2} P_d^{a_2} \left(\ldots \sum_{a_v=a_{v-1}}^{MN} P_d^{a_v} \right) \right) \qquad (3.28)$$

3.2 Target Localization and Tracking

For a multitarget scenario, the state of the l-th target at the k-th time step is defined by $\mathbf{x}^l(k) = [x^l(k)\ \dot{x}^l(k)\ y^l(k)\ \dot{y}^l(k)]'$ with positions and velocities in the x and y direction, respectively. The parameter vector of the l-th target can be also defined as

$$\theta^l = [\beta_{11}^l\ \ldots\ \beta_{MN}^l\ (\alpha_{11}^l)^*\ \ldots\ (\alpha_{MN}^l)^*]^H \qquad (3.29)$$

where β_{ij}^l denotes the signal ratio of the l-th target (according to (3.8)) in the (i,j)-th transmitter-receiver pair. The main problem in target localization using MIMO radars is that targets might become unobservable in certain pairs of transmitters and receivers. Also, there is no information available about the index of observable pairs or variance of scattering a priori. To handle the above problems, a multiple hypothesis algorithm is proposed here to take all possible cell combinations in different pairs into consideration. The main feature of the new MH-based algorithm is its capability to deal with multitarget scenarios

with multiple-scatterers where there might be no signal from targets in certain transmitter-receiver pairs.

3.2.1   An MH-based Algorithm for Target Localization

In a multiple hypothesis-based algorithm [12], a hypothesis can be defined as an event showing the potential presence of a target in the f-th resolution cell. The implementation of the MH-based algorithm can be fundamentally divided into four steps as described below:

- Hypothesis Initialization:

  Without loss of generality, the first two pairs are used for hypothesis initialization.[1] Define $\eta_p(f)$ as the matched filter signal received in the p-th pair and f-th resolution cell. There are two possible approaches to extract the necessary measurements for localization. The first approach is to use the received signals directly. Note that the received signal is Gaussian-distributed with zero mean and covariance matrix given by (3.10). However, targets' information is embedded in the covariance matrix, which is also nonlinear with respect to the target parameters. Therefore, the traditional EKF or UKF algorithms [55] cannot be applied here. Although nonlinear filtering methods such as particle filtering can be applied to the localization problem, the huge computational load of the particle filter algorithm combined with the MH-based method can be prohibitive. Therefore, an alternative approach where scatterer and ratio measurements are first extracted from the received signals is proposed.

  Now, define $\tilde{\beta}_p(f)$ and $\tilde{\alpha}_p(f)$ as the estimates of a potential target's signal ratio and scatter standard deviation in the f-th cell, respectively.

---

[1]It is possible to use more initial pairs for hypothesis generation. However, there is a trade-off between the number of initial pairs and the computational cost.

The above estimates can be found by optimizing the likelihood function given by

$$\mathcal{L}_p(f) = -\log \prod_s^S \left(\frac{p(\phi_p^s(f)|H_1)}{p(\phi_p^s(f)|H_0)} \right) \tag{3.30}$$

where S is the number of snapshots, $\phi_p^s(f) = \left[(\eta_p^s(f-1))^* \ (\eta_p^s(f))^* \right]^H$, and two unknown probability density functions are defined as

$$p(\phi_p^s(f)|H_1) = \mathcal{CN}(\phi_p^s(f); 0, \Sigma_p(\beta_p(f), \alpha_p(f))) \tag{3.31}$$

$$p(\phi_p^s(f)|H_0) = \mathcal{CN}(\phi_p^s(f); 0, \sigma_w^2 I_2) \tag{3.32}$$

Here, $\Sigma_p(\beta_p(f), \alpha_p(f))$ denotes the covariance matrix of the received signal given in (3.9) where the ratio and standard deviation of the target scatterer are provided as input parameters for the covariance matrix. The log-likelihood given by (3.31) is a function of target parameters. Therefore, a nonlinear optimization problem can be defined in order to find an estimate of defined parameters as follows:

$$(\tilde{\beta}_p(f), \tilde{\alpha}_p(f)) = arg \min_{\beta, \alpha} \mathcal{L}_p(f), \ \ 0 \le \beta \le 1, \ 0 \le \alpha \le \alpha_{max} \tag{3.33}$$

A suitable gradient-based nonlinear optimization technique [13] may be used to solve the above problem. The estimated results can be represented by two vectors $\Phi_p = [\tilde{\beta}_p(1) \ \tilde{\beta}_p(2) \ . \ . \ . \ \tilde{\beta}_p(F)]'$ and $\Psi_p = [\tilde{\alpha}_p(1) \ \tilde{\alpha}_p(2) \ . \ . \ . \ \tilde{\alpha}_p(F)]'$, respectively. Now, to initialize the hypotheses, define $\mathcal{C}_{f_1 f_2}$ as a potential combination of cells in the first two pairs where f_1 and f_2 correspond to the f_1-th and f_2-th resolution cells in the first and second pair, respectively. The range measurement for each of the above represented cells can be written as

$$r_i(f_i) = R(f_i - 1) + \tilde{\beta}_i(f_i) r_{bin} + n_i(f_i), \ i = 1, 2 \tag{3.34}$$

77

where $R(f_i - 1) = (f_i - 1)r_{bin}$ and $n_i(f_i)$ denotes the range measurement additive noise that is Gaussian-distributed with zero mean and variance σ_r^2. The range measurement variance can be found as

$$\sigma_r^2 = (r_{bin})^2 \sigma_\beta^2$$

Here, the variance σ_β^2 of the ratio estimate can be assumed to be equal to the CRLB of estimation errors. The CRLB of localization will be derived in the next section. We assume that the CRLB is now available and, therefore, the range variance can be obtained analytically. Given $r_1(f_1)$ and $r_2(f_2)$ as the range measurements, the (f_1, f_2) combination is accepted as a potential target estimate if the ellipsoids constructed by the geometrical placement of $r_1(f_1)$ and $r_2(f_2)$ intersect. Referring to Figure 3.1, it can be observed that there is no intersection for the combination on the right side while ellipsoids on the left intersect. The h-th hypothesis is now created if a combination of cells is validated using the above intersection-finding procedure. The h-th hypothesis can be defined as

$$\mathcal{H}_0(h) = \{r_{p_1}(f_{p_1}), r_{p_2}(f_{p_2}), C_0(f_1, f_2)\} \tag{3.35}$$

where $C_0(f_1, f_2)$ denotes the cost of the hypothesis. Here, the cost of each hypothesis is equal to the likelihood given by (3.30). Note that indices p_1 and p_2 in (3.35) indicate that any arbitrary pairs might be chosen for the initialization stage.

- Estimate Initialization:

  Without loss of generality, three pairs of transmitters and receivers are chosen to initialize target estimates although any other number of initial pairs can be also considered with more computation. The h-th hypothesis is created by assigning the h'-th initial hypothesis to the f_h-th cell
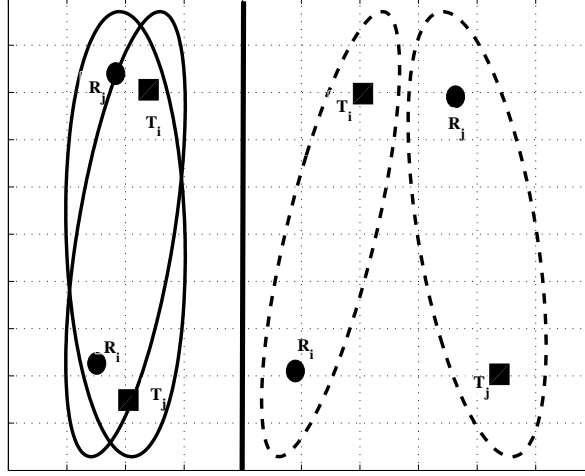
Figure 3.1: Geometrical placement of target location constructed from the range measurements of the first two pairs of transmitter-receiver.

of the current pair provided that the f_h-th cell intersects the ellipsoids created by the cells belonging to the h'-th hypothesis. In this case, the new hypothesis can be written as

$$\mathcal{H}_p(h) = \left\{ \mathbf{x}_p^h, \Sigma_p^h, r_p(f_h), C_p(f_h), \mathcal{H}_0(h') \right\} \tag{3.36}$$

where $\mathbf{x}_p^h$ and Σ_p^h are the estimated state and the corresponding covariance of the hypothesized target, respectively. The new cost can be also found as

$$C_p^h(f_h) = p^* \left(\phi_p(f_h) \right) \times C_0^{h'}(f_{h'_1}, f_{h'_2}) \tag{3.37}$$

where

$$p^* \left(\phi_p(f_h) \right) = \frac{p \left(\phi_p(f_h) | H_1 \right)}{p \left(\phi_p(f_h) | H_0 \right)} \tag{3.38}$$

with likelihoods being found using (3.31). In order to estimate the state of the target, the range measurement vector of the new hypothesis is first

79

written as $\mathbf{r}_p^h = [r_p(f_h)\; r_{p_2}(f_{h'_2})\; r_{p_1}(f_{h'_1})]'$. The Least Square (LS) method [6] can be used to find an estimate of the target state $\mathbf{x}_p^h = [x^h\; y^h]'$ and the associated covariance. The new h-th hypothesis, hence, includes the information of a potential initialized target. The set of initialized estimates are updated in the subsequent pairs in order to provide the final estimates of available targets.

- Update Step:

Given $\mathcal{H}_p(h')$ as the h'-th initialized hypothesis, the first step is to find those measurements in the $(p+1)$-th pair that can be associated with the h'-th hypothesis. The f_h-th cell is assigned to the h'-th hypothesis if the following inequality holds:

$$\frac{(r_{p+1}(f_h) - \tilde{r}_{p+1}^{h'})^2}{\sigma_r^2(h')} \leq \lambda \tag{3.39}$$

Here, $\tilde{r}_{p+1}^{h'}$ denotes the predicted range of the h'-th hypothesis that can be found by the range equation of (3.3) with $\mathbf{x}_p^h$ being used as the estimated state. The range variance $\sigma_r^2(h')$ can be also found by linearizing the range equation around the estimate of the target as

$$\sigma_r^2(h') = \zeta_1 \Sigma_p^{h'}(xx) + \zeta_2 \Sigma_p^{h'}(yy) + \zeta_3 \Sigma_p^{h'}(xy) + \frac{r_{bin}^2}{12} \tag{3.40}$$

with

$$\zeta_1 = \frac{(x_p^{h'})^2}{(x_p^{h'})^2 + (y_p^{h'})^2} \tag{3.41}$$

$$\zeta_2 = \frac{(y_p^{h'})^2}{(x_p^{h'})^2 + (y_p^{h'})^2} \tag{3.42}$$

$$\zeta_3 = \frac{x_p^{h'} y_p^{h'}}{(x_p^{h'})^2 + (y_p^{h'})^2} \tag{3.43}$$

Assuming that the f_h-th cell falls inside the gate of the h'-th hypothesis,

the new hypothesis is created as

$$\mathcal{H}_{p+1}(h) = \left\{ \mathbf{x}_{p+1}^h, \Sigma_{p+1}^h, r_{p+1}(f_h), C_{p+1}(f_h), \mathcal{H}_p(h') \right\} \qquad (3.44)$$

The new state $\mathbf{x}_{p+1}^h$ and the associated covariance Σ_{p+1}^h can be obtained using an Extended Kalman Filter (EKF) with $r_{p+1}(f_h)$ and $\tilde{r}_{p+1}^{h'}$ being the received and predicted measurements, respectively, and $\alpha_{p+1}^2(f_h)$ as the scatterer measurement. Defining $\bar{\mathbf{x}}_p^{h'} = [(\mathbf{x}_p^{h'})' \; \alpha_p^{h'}]'$ as the new extended state and $\bar{\Sigma}_{p+1}^h = \begin{bmatrix} \Sigma_{p+1}^h & 0 \\ 0 & \sigma\alpha_{p+1}^h \end{bmatrix}$ as the associated covariance (with $\sigma\alpha$ being the variance of scatterer estimate), the updated state and covariance can be obtained using the standard Extended Kalman equations [6] with the range equation of (3.3) as the nonlinear measurement model. Finally, the cost of the new hypothesis can be found as

$$C_{p+1}^{h'}(f_h) = C_p^h(f_{h'})p^* \left(\phi_{p+1}(f_h) \right) \qquad (3.45)$$

where $p^* \left(\phi_{p+1}(f_h) \right)$ is found from (3.38).

- Pruning:

  Once all hypotheses are initialized for the p-th pair, a pruning step can be followed in order to remove those hypotheses that are less probable to have originated from a potential target. Hypotheses may be pruned based on the quality (cost) or the m/n association logic [5] [12]. The first approach is based on the normalized cost of each hypothesis. This method is not robust, especially for multiple-scatterer targets when the target is not observable in certain transmitter-receiver pairs. In this case, the normalized cost declines significantly and the associated hypothesis is removed. To avoid the removal of valid hypotheses, an (m/n) logic is combined with the quality based method. Defining a binary variable H

to determine the status of the h-th hypothesis, the following logic can be presented:

$$\begin{cases} H^h = 1 & C_p^h(f_h) \geq \omega \bigwedge \frac{n_p^h}{p} \geq \zeta \\ H^h = 0 & \text{otherwise} \end{cases} \tag{3.46}$$

where n_p^h denotes the number of pairs in which the h-th hypothesis is assigned to a measurement, and ω and ζ are the quality and the logic thresholds, respectively. Note that the selection of ζ depends on the chosen m/n logic.

- Global Hypothesis Selection:

All hypotheses must be compatible in a general MH-based algorithm [12]. For our application, the compatibility of hypotheses is checked when the data from all pairs are processed. Assuming $\mathcal{H}_{MN}$ as the set of all survived hypotheses, compatible hypotheses that do not have any common associated measurement are drawn. Defining $\mathcal{C}_{MN}^h$ as the set of all cells assigned to the h-th hypothesis, two hypotheses h_1 and h_2 are compatible if

$$\mathcal{C}_{MN}^{h_1} \cap \mathcal{C}_{MN}^{h_2} = \{\emptyset\} \tag{3.47}$$

If there are some common cells shared by two hypotheses, the one with the highest likelihood is selected. Finally, the remaining hypotheses $\mathcal{H}_{MN}^*$ are considered as the set of global hypotheses with no common associated cell. The number of global hypotheses represents the number of detected targets in the surveillance region.

Given $\mathcal{G}$ as the number of global hypothesis, the g-th hypothesis representing the presence of a real target is defined by

$$\mathcal{H}^g(h) = \left\{ \mathbf{x}_g^h, \Sigma_g^h, \mathcal{C}_g^h \right\} \tag{3.48}$$

with C_g^h as the final cost assigned to the g-th hypothesis.

3.2.2   Tracking Algorithm

The state of the l-th target is defined as $\mathbf{x}^l(k) = [x^l(k)\ \dot{x}^l(k)\ y^l(k)\ \dot{y}^l(k)\ \alpha_{11}^l(k) \ldots \alpha_{MN}^l(k)]'$
. The dynamical model to characterize the motion of the l-th target can be
represented as

$$\mathbf{x}^l(k) = \bar{F}\mathbf{x}^l(k-1) + \begin{bmatrix} \Gamma\mathbf{w}(k) \\ \mathbf{w}_\alpha(k) \end{bmatrix} \tag{3.49}$$

with $\bar{F} = \begin{bmatrix} F & 0 \\ 0 & I_{MN} \end{bmatrix}$, $\mathbf{w}$ and $\mathbf{w}_\alpha$ being Gaussian noises with zero mean

and covariance matrices $\begin{bmatrix} \sigma_1^2 & 0 \\ 0 & \sigma_2^2 \end{bmatrix}$ and $\sigma_\alpha^2 I_{MN}$, respectively. The standard
parameters of the motion model (i.e., F, Γ) can be also determined according to
the type of the motion assumed for each target (e.g., nearly constant velocity,
nearly constant acceleration, or constant turn models [6]). The measurements
are the outputs of matched filter that can be re-written as

$$\eta_{nm}(k) \sim \mathcal{CN}(0, \sigma_w^2 I_{C_{nm}^*} + \Sigma_{nm}) \tag{3.50}$$

with Σ_{nm} being defined by (3.10). Also, C_{nm}^* denotes the number of adjacent
resolution cells occupied by targets. Although it is possible to extract ratio
and scatterer measurements for the tracking step again using the optimization
technique given by (3.33), the direct approach with the output of matched
filter being used as the output signals is preferred. Potential advantages of
direct method compared to the measurement-level (indirect) method were also
discussed in Chapter 2.

Nonlinear filtering using Particle Filter (PF) [3] has been recently applied to
several tracking and estimation problems [80]. Assume that an initial estimate
of targets can be obtained using the localization algorithm. Initial estimates
are represented by $\mathbf{x}^l(0)$ with the associated covariance $\Sigma^l(0)$. Initial particles

and associated weights can be generated using

$$\mathbf{x}_i^l(0) \sim \mathcal{N}(\mathbf{x}^l(0), \Sigma^l(0)), \ \tilde{w}_i^l(0) = \frac{1}{N_p} \tag{3.51}$$

with N_p being the number of particles and $\tilde{w}$ the normalized particle weight. It has to be also noted that, in multitarget cases, two targets may be separated in the state space while they fall in the same or adjacent cells for certain transmitter-receiver pairs. In this case, the covariance matrix in (3.10) has to be found by considering the effect of multiple targets that fall in the same cluster of cells. Therefore, states of those targets in the same cluster have to be augmented into one state vector for particle generation. Defining $\mathbf{x}_i^l(k)$ and $\tilde{w}_i^l$ as the i-th generated particle and the associated weight of the l-th target in the k-th time step, respectively, different steps of the proposed PF algorithm for widely-separated MIMO radar systems are discussed in Algorithm I.

 Remark: Each class of cells is constructed according to the number of adjacent cells potentially occupied by a number of targets. For example, given three generated particles occupying resolution cells $c_1 = 20$, $c_2 = 30$, and $c_3 = 29$, respectively, there are two classes with targets $\{1\}$ and $\{2, 3\}$ located in each class, respectively. Referring to (3.52), the number of classes can be found based on the given states $\left\{ \mathbf{x}_{i_1}^1, ..., \mathbf{x}_i^l, ..., \mathbf{x}_{i_L}^L \right\}$.

3.3   Posterior Cramer-Rao Lower Bound

The PCRLB on the state estimation accuracy can be written in terms of Ricatti-like recursions [79] as

$$J(k) = D^{22}(k-1) - D^{21}(k-1) \left(J(k-1) + D^{11}(k-1) \right)^{-1} D^{12}(k-1) \tag{3.56}$$

Algorithm 1 The Tracking Algorithm for MIMO Radars

Initial States: $\left\{\mathbf{x}_i^l(k), \tilde{w}_i^l(k)\right\}$

Measurements: $\eta_{1:NM}(k+1)$

for $p = 1$ to MN **do**

    Particle Generation: $\mathbf{x}_i^l(k+1|k) \sim \mathcal{N}(\bar{F}\mathbf{x}_i^l(k), \bar{\Gamma})$ with $\bar{\Gamma} = \left[\begin{array}{c} \Gamma Q \Gamma' \\ \sigma_\alpha^2 \end{array} \right]$.

    for $l = 1$ to L **do**

      for $i = 1$ to N_p **do**

      Find the likelihood as

$$
\begin{aligned}
p\left(\eta_p(k+1)|\mathbf{x}_i^l(k+1|k)\right) &= \sum_{i_1=1}^{N_p} \cdots \sum_{i_{l-1}=1}^{N_p} \sum_{i_{l+1}}^{N_p} \cdots \sum_{i_L=1}^{N_p} \tilde{w}_{i_1}^1 \ldots \tilde{w}_{i_L}^L \times \\
&\times \quad p\left(\eta_p(k+1)|\mathbf{x}_{i_1}^1(k+1|k), \ldots, \mathbf{x}_i^l, \ldots, \mathbf{x}_{i_L}^L\right)
\end{aligned}
$$

$$(3.52)$$

      where the likelihood on the right-hand side of the above equation can be written as

$$
p\left(\eta_p(k+1)|\mathbf{x}_{i_1}^1(k+1|k), \ldots, \mathbf{x}_i^l, \ldots, \mathbf{x}_{i_L}^L\right) = \mathcal{N}(0, \Sigma_p(\mathbf{x}_{i_{j_1}}^{j_1}, \ldots, \mathbf{x}_i^l, \ldots, \mathbf{x}_{i_{j_l}}^{j_l}))
$$

$$(3.53)$$

      Here, j_n, $n \neq l$ denotes the index of the n-th member of the set of targets for which $\mathbf{x}^{j_n}$ falls in the cell which is occupied by the l-th target.

      Calculate the weight as

$$
w_i^l(k+1) = p\left(\eta_p(k+1)|\mathbf{x}_i^l(k+1|k)\right)
$$

    end for

    Normalize the particle weights as $\tilde{w}_i^l(k+1) = \frac{w_i^l(k+1)}{\sum_{i=1}^{N_p} w_i^l(k+1)}$

    Find the variance of particle weights as

$$
\sigma_P^l(k+1) = \frac{1}{\sum_{i=1}^{N_p} (\tilde{w}_i^l(k+1))^2}
$$

$$(3.54)$$

    if $\sigma_P^l(k+1) < \epsilon$ **then**

      Do the resampling to multiply/suppress particles with high/low wights. The resampling step can be described as

$$
\left\{\tilde{w}_{1:N_p}^l(k+1), \mathbf{x}_{1:N_p}^l(k+1)\right\} \leftarrow \left\{\frac{1}{N_p}, \mathbf{x}_{N(1:N_p)(k+1|k)}^l\right\}
$$

$$(3.55)$$

      with $N(1 : N_p)$ being a selection of N_p indices from the set $\{1, 2, \ldots, N_p\}$.

    end if

    Report $\mathbf{x}_{1:N_p}^l(k+1)$ as the estimated states and $\tilde{w}_{1:N_p}^l(k+1)$ as the associated weight.

    end for

end for

---

where D^{ij}s are defined as

$$D^{11}(k-1) = E\left[-\nabla_{X(k-1)}^{X(k-1)} \log p\left(X(k)|X(k-1)\right)\right] \tag{3.57}$$

$$D^{12}(k-1) = E\left[-\nabla_{X(k)}^{X(k-1)} \log p\left(X(k)|X(k-1)\right)\right] = \left(D^{12}(k-1)\right)' \tag{3.58}$$

$$D^{22}(k-1) = D^{33}(k-1) + J_y(k) \tag{3.59}$$

$$D^{33}(k-1) = E\left[-\nabla_{X(k)}^{X(k)} \log p\left(X(k)|X(k-1)\right)\right] \tag{3.60}$$

Here, the expectation is taken over the target states. The state and parameter vector of the l-th target can be defined as

$$X^l(k) = [(\mathbf{x}^l(k))' \alpha_{11}^l \ldots \alpha_{NM}^l]' \tag{3.61}$$

$$\Theta^l(k) = [\beta_{11}^l \ldots \beta_{NM}^l \ \alpha_{11}^l \ldots \alpha_{NM}^l]' \tag{3.62}$$

The measurement information matrix $J_y(k)$ can be now written as

$$J_y(k) = E\left[\frac{\partial \log p\left(Y(k)|X(k)\right)}{\partial X(k)} \left(\frac{\partial \log p\left(Y(k)|X(k)\right)}{\partial X(k)}\right)'\right] \tag{3.63}$$

with the expectation being taken over received signals, and $Y(k)$ being the received signal vector defined as $Y(k) = [(\eta_{11}(k))^* \ldots (\eta_{MN})^*]^H$. Given the independence of signals generated in different transmitter-receiver pairs, the FIM [6] due to the measurements can be written as $J_y(k) = \sum_{p=1}^{MN} J_y^p(k)$ with the following form for $J_y^p(k)$:

$$J_y^p(k) = \Omega J_y^{p,\theta} \Omega' \tag{3.64}$$

Here, $\Omega = diag\left(\Omega^1, ..., \Omega^L\right)$ and $J_y^{p,\theta}$ denotes the FIM with respect to the parameter vector of targets. The individual terms Ω^l can be written as

$$[\Omega^l]_{ij} = \frac{\partial \Theta_i^l}{\partial X_j^l} \tag{3.65}$$

The above term can be found as follows:

$$
\Omega^l = \begin{bmatrix}
\frac{\partial \beta_{11}^l}{\partial x^l} & . & . & . & \frac{\partial \beta_{NM}^l}{\partial x^l} & 0_{NM \times NM} \\
0 & 0 & . & . & . & 0 \\
\frac{\partial \beta_{11}^l}{\partial y^l} & . & . & . & \frac{\partial \beta_{NM}^l}{\partial y^l} & 0_{NM \times NM} \\
0 & 0 & . & . & . & 0 \\
0_{NM \times 1} & 0_{NM \times 1} & . & . & . & I_{NM}
\end{bmatrix}
\tag{3.66}
$$

The necessary derivatives can be also found as

$$
\frac{\partial \beta_{nm}^l}{\partial x^l} = \frac{1}{r_{bin}} \left(\cos(\zeta_m) + \cos(\eta_n) \right)
\tag{3.67}
$$

$$
\frac{\partial \beta_{nm}^l}{\partial y^l} = \frac{1}{r_{bin}} \left(\sin(\zeta_m) + \sin(\eta_n) \right)
\tag{3.68}
$$

with the following definitions for ζ_m and η_n:

$$
\zeta_m = \tan^{-1} \left(\frac{y^l - y_{tm}}{x^l - x_{tm}} \right)
\tag{3.69}
$$

$$
\eta_n = \tan^{-1} \left(\frac{y^l - y_{rn}}{x^l - x_{rn}} \right)
\tag{3.70}
$$

Substituting the above terms in (4.20), the system matrix can be fully determined.

Given the location of targets, c_l^p is defined as the resolution cell assigned to the l-th target in the p-th pair. Resolution cells can be divided into different classes according to their distribution. Adjacent cells normally fall in the same group. Now, assume N_C^p as the total number of classes in the p-th pair. Also, define $I_c^p = \{i_1^p, .., i_c^p\}$ as the indices of cells in the c-th class. The FIM can be now written for the p-th pair as

$$
J_y^{p,\theta} = \sum_{c=1}^{N_C^p} J_y^{p,\theta,c}(k)
\tag{3.71}
$$

It was shown in Section II that the received signal is Gaussian-distributed with the covariance matrix provided by (3.10). The FIM for the $[a, b]$th element of

87

a multivariate Gaussian distribution with zero mean and covariance Σ_p^c can be obtained as [89]

$$[J_y^{p,\theta,c}]_{ab}(k) = \frac{1}{2}\mathcal{T}((\Sigma_p^c)^{-1}\frac{\partial\Sigma_p^c}{\partial\Theta_a(k)}(\Sigma_p^c)^{-1}\frac{\partial\Sigma_p^c}{\partial\Theta_b(k)}) \tag{3.72}$$

with Tr(.) being the trace, and $\Theta_a(k)$ being the a-th member of the parameter vector $\Theta_a(k)$. Substituting (3.72) in (3.71), the following form can be found for FIM

$$[J_y]_{ab}(k) = \frac{1}{2}\sum_{p=1}^{MN}\sum_{c=1}^{N_C^p}\Omega_p^c\left(\mathcal{T}\left((\Sigma_p^c)^{-1}\frac{\partial\Sigma_p^c}{\partial X_a(k)}(\Sigma_p^c)^{-1}\frac{\partial\Sigma_p^c}{\partial X_b(k)}\right)\right)(\Omega_p^c)' \tag{3.73}$$

where Ω_p^c corresponds to the matrix Ω calculated for the c-th cluster in the p-th pair. To find the derivatives given in (3.72) and (4.19), consider the c-th cluster with L_p^c targets. Assume that the l-th target is located in the $f_p^c(l)$-th cell with $f_p^c(1:L_p^c)$ as the set of all cells occupied by the L_p^c targets. The occupied cells are numbered from 1 to $N_c^p + 1$ with N_c^p being the number of occupied cells. Note that $N_c^p \leq L_p^c$. Given $v_p^c(l)$ as the index of the cell corresponding to the l-th target, the derivative can be written based on (3.10) as

$$\frac{\partial[\Sigma_p^c]_{ij}}{\partial\theta_p^l} = \begin{cases} [D_\theta^l\Sigma_p^c]_{k_ik_j} & (i,j)\in\{v_p^c(l), v_p^c(l)-1\} \\ 0 & \text{otherwise} \end{cases} \tag{3.74}$$

with $k_i = 1$ if $i = v_p^c(1)$ and $k_i = 2$ otherwise. Also, $[D_\theta^l\Sigma_p^c]$ is defined as the derivative of the covariance matrix due to the l-th target with respect to the ratio and scatter parameters. The derivative can be calculated as

$$[D_\beta^l\Sigma_p^c] = 2\begin{bmatrix} \beta_p\alpha_p^2 & (\frac{1}{2}-\beta_p)\alpha_p^2 \\ (\frac{1}{2}-\beta_p)\alpha_p^2 & (\beta_p-1)\alpha_p^2 \end{bmatrix} \tag{3.75}$$

$$[D_\alpha^l\Sigma_p^c] = 2\begin{bmatrix} \beta_p^2\alpha_p & (1-\beta_p)\beta_p\alpha_p \\ (1-\beta_p)\beta_p\alpha_p & (1-\beta_p)^2\alpha_p \end{bmatrix} \tag{3.76}$$

The term $\frac{\partial [\Sigma_p^c]_{ij}}{\partial \theta_p^l}$ can be now computed for all values of θ. The resulting deriva-

tive is then used to calculate the FIM.

The CRLB of target localization can be now obtained by taking the inverse of the above FIM as $\text{CRLB} = J_y^{-1}$. It was shown in [79] that the general form of (3.56) can be simplified to

$$J(k) = \left(\Gamma_* + F_* \left(J(k-1) \right)^{-1} F_*' \right)^{-1} + J_y(k) \qquad (3.77)$$

where Γ_* and F_* are the generalized motion covariance and the state dynamic matrix, respectively. In addition, $\Gamma_* = \text{diag} \left\{ \Gamma^1, ..., \Gamma^L \right\}$ and $F_* = \text{diag} \left\{ F^1, ..., F^L \right\}$. Here, F^i and Γ^j denote the motion matrices of the j-th target. The PCRLB for the tracking accuracy can be now found by inverting the FIM as $J^{-1}(k)$.

3.4   Numerical Results

Consider a MIMO system with three transmitters and three receivers (i.e., $M = 3$, $N = 3$). Two targets are in the surveillance region. Antennas are placed in the surveillance region symmetrically such that the location of each antenna can be calculated as $\mathbf{x}_i = [R\cos(\theta_i) \ R\sin(\theta_i)]'$ with R and θ_i being the range and bearing of the i-th antenna, respectively. Note that transmitters and receivers can be placed in any arbitrary configuration. Analytical approaches for optimal antenna allocation in MIMO radars can be also found in [35] [51]. With $R = 500$ and $\theta_0 = \frac{\pi}{18}$, Figure 3.2 shows the geometry of antennas and targets in the surveillance region. All results are obtained over 50 Monte Carlo runs.

Table 3.5: Key Parameters of the Widely-separated MIMO Radar System

Variable	R_{max}	r_{bin}	N_s	σ_α^2	f_c	v_{max}	P_{fa}
Value	10 km	50 m	128	10^{-3}	4 GHz	15 m/s	10^{-4}

3.4.1   Target Detection and Localization

Figure 3.3 shows ROC curve for two different SNRs for both MIMO and multistatic radars. For a low SNR ($SNR = 5$dB), there is a significant gap between the ROC curves of MIMO and multistatic radars. In addition, the MIMO radar's probability of detection converges much faster than that of the multistatic radar. The performance gap for the MIMO radar is also tighter than that of the multistatic radar for the scenario with $SNR = 10$dB. In this case, both radars achieve a high probability of detection even at low false alarm probabilities. The probability of detection versus different target SNRs
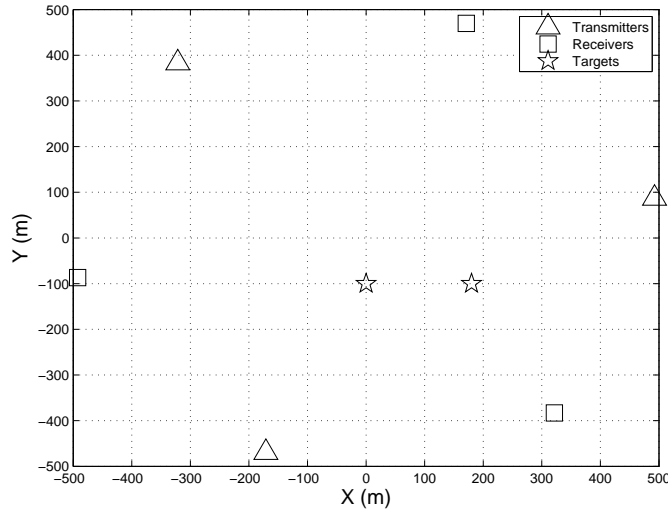
Figure 3.2: The distribution of antennas and targets in the surveillance region.

for both MIMO and multistatic radar processing can be also found in Figure

90
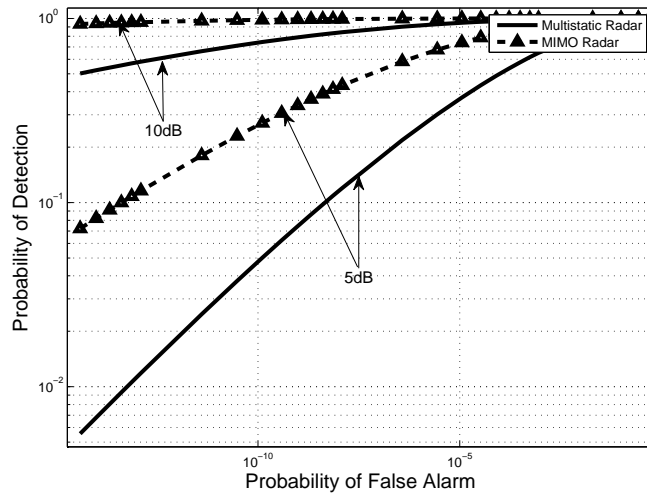
Figure 3.3: ROC of MIMO and multistatic radars at two different SNRs.

3.4. It can be observed that the MIMO radar outperforms the multistatic radar, especially at low target SNRs.

A single-target scenario, where it is first assumed that the target is observable in all pairs (i.e., target SNR is the same in all pairs), is now considered. The proposed MH-based algorithm is applied on the data generated by both MIMO and multistatic structures. The empirical probability of detection is calculated for each structure by enumerating the number of scans in which an estimate of the target location is obtained. Figure 3.4 presents the empirical and optimal probability of detection for each structure. While the MIMO radar detects the target with a probability close to the optimal one, the multistatic radar provides poor results, especially at low SNRs. When the SNR increases, the detection probabilities of both structures converge to the optimal value. Now, the RMSE of estimation is calculated and presented in Figure 3.5 for different target SNRs. Although the target is detected by the MIMO radar

91

at SNRs less than 10dB, the multistaic radar fails to find an estimate of the target at low SNRs. At higher SNRs, the RMSE of target estimation using the MIMO radar is significantly reduced, and then approaches the CRLB bound at medium SNRs. While MIMO radar shows lower RMSE compared to the multistatic radar at medium SNRs, both structures achieve desired RMSEs at higher SNRs. In summary, the performances of both MIMO and multistatic radars are close to the CRLB at high SNRs. However, it can be observed that MIMO radar outperforms the multistatic one at low SNR cases.
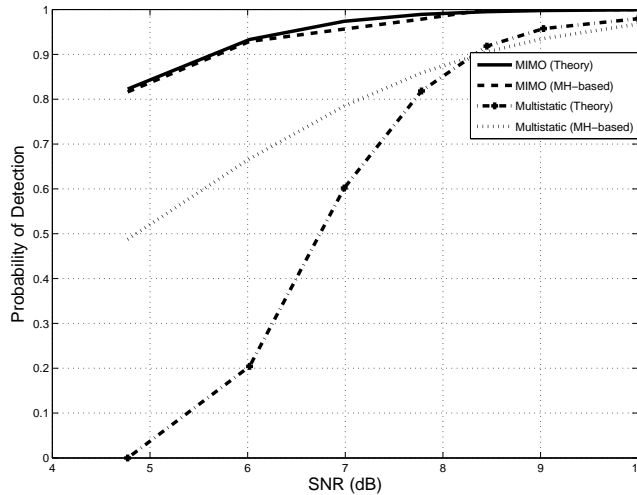
Figure 3.4: Probability of detection versus target SNR for MIMO and multi-static radars ($P_{fa} = 10^{-4}$).

To see the effect of multiple-scatterer targets in the localization perfor-mance, we define the observability rate as $\frac{N_o}{MN}$ with N_o being the number of observable pairs. The p-th pair is observable if $P_d^p \geq \epsilon$. For this part, $\epsilon = .01$ is chosen. The RMSE of estimation is now found at two different SNRs (7dB
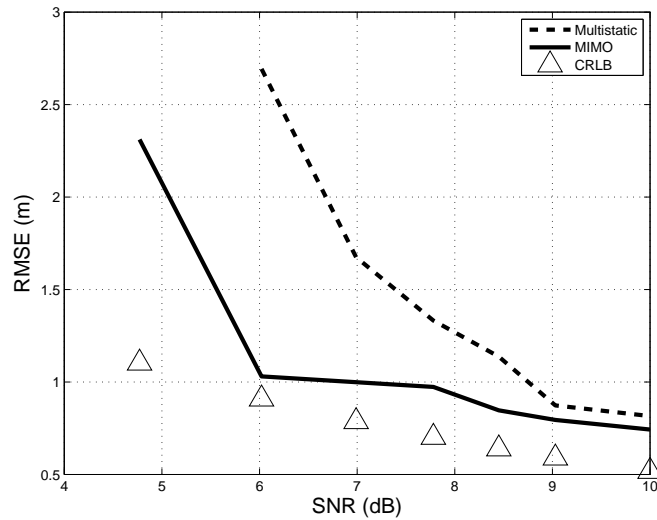
Figure 3.5: RMSE of localization for different target SNRs.

and 10dB). Figure 3.6 shows the RMSE results for different percentages of observability. It can be seen that the MIMO radar outperforms the multistatic radar at low percentages with, at least, 20% lower RMSE for $SNR = 10$dB. With an increase in the percentage of observability, the RMSE values of both structures become closer. Also, CRLB and RMSEs match when the target becomes observable in more transmitter-receiver pairs. The other important note on Figure 3.6 is that the gap in the localization RMSE becomes more significant at lower SNRs. Indeed, for $SNR = 7$dB, MIMO achieves a 40% lower RMSE than the multistatic radar at low observability percentages. Although the gap is reduced at higher observability percentages, the rate of improvement is still much slower than at $SNR = 10$dB. This experiment shows that the effect of the number of observable pairs becomes more significant at lower SNRs. In other words, MIMO radar provides superior RMSE results than the

multistatic radar at low SNR and low percentages of observability.
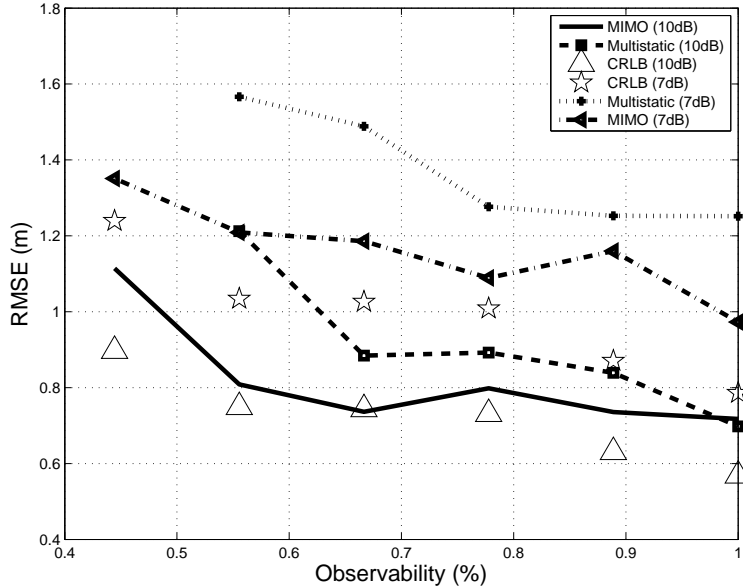
Figure 3.6: RMSE of target localization versus the percentage of observability for two different SNRs.

In order to analyze the performance of the proposed algorithm in multitarget localization, a two-target scenario is considered with the locations being shown in Figure 3.2. Although the targets are well-separated in the state space, they become closely-spaced in certain pairs of transmitters and receivers. RMSE of target estimation using the MH-based algorithm is provided in Figure 3.7. At low SNRs ($SNR = 6$dB), the multistatic radar misses both targets. Although the targets are successfully detected by both structures at medium SNRs, the MIMO radar yields 100% lower RMSE of position estimation than the multistatic radar for the first target. The RMSE results approach to each other when the SNR of targets is $10dB$. In this case, RMSE also reaches the CRLB. The other important note on the two-target scenario

is that the RMSE does not reach the CRLB at the low SNRs. However, when the SNR goes up, not only does the RMSE of targets approach the CRLB, but also RMSE of both targets become closer. In other words, for the two-target scenario, a significant improvement is observed in the performance of the MH-based algorithm once the SNR is high enough.
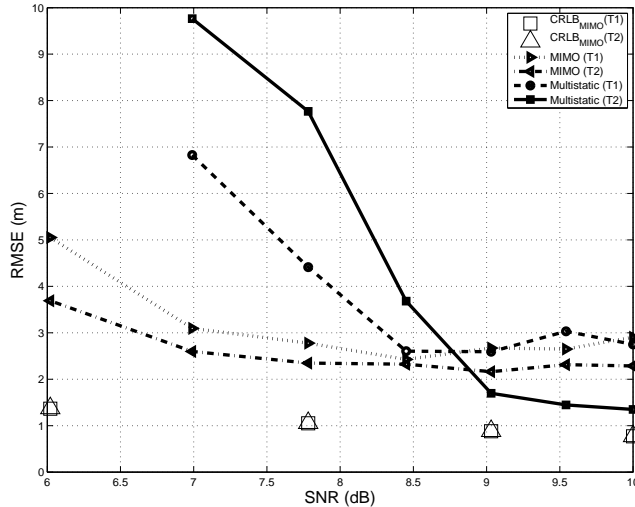
Figure 3.7: RMSE of target localization for the two-target scenario.

3.4.2 Target Tracking

Consider the two-target scenario with the initial locations being shown in Figure 3.2. It is also assumed that the rate of observability is equal to 60% for both targets. In order to evaluate the performance of the tracking algorithm, the targets are assumed to become closely-spaced at subsequent time steps. Trajectories of targets are generated in 50 scans. While targets are well-separated initially, they approach each other in the subsequent scans. In

this case, targets also fall in the same cells of all pairs in the period that they become closely-spaced. Figure 3.8 presents the number of common cells occupied by two targets in different scans. It can be observed that, initially, targets are well-separated in most cells. However, in the subsequent scans, the number of common cells increases. The tracking algorithm is now applied to the generated data in order to estimate the states of targets. The parameters of the tracking algorithm and targets are presented in Table 3.5. Figure 3.9 presents the actual and estimated trajectories of targets as well as the ellipsoidal uncertainty regions. The graph confirms the capability of the tracking approach in estimating the states of targets, even when targets become closely-spaced in the sate space. The RMSE of target tracking is also depicted in Figure 3.10. For performance evaluation, the PCRLB of tracking is also included in Figure 3.10. It can be seen that there is a jump in the RMSE of tracking during the period when targets become closely-spaced. This jump is also observed in the PCRLB of tracking.

Finally, the tracking scenario is re-constructed with only the trajectory of the first target being shown in Figure 3.9. The particle-based algorithm is now applied to the generated data with the same parameters given in Table 3.6. Figure 3.11 shows the RMSE and PCRLB results for the single target case. It can be observed that there is no jump in the RMSE of localization due to the absence of the other target, which is also confirmed by the PCRLB.

Even though the above analysis was done for a MIMO radar, the same simulations can be also obtained for a multistatic radar. Because the localization performance of MIMO and multistatic radars has been already compared, the same performance is also expected for the tracking. In addition, while the tracking algorithm was applied to a simple two-target scenario, it can be also

used for scenarios with any number of observable pairs and targets. Time-varying number of targets and observable pairs can be handled within the same work. This will require the handling of target birth/death an online calculation of the variance of scatterers.

3.4.3   Computational Complexity vs. Performance

Given F as the number of resolution cells, the computational complexity of the initialization step of the MH-based algorithm applied to the MIMO radar is of order $O(F^3)$. Once the hypotheses are initialized, the data association step is of order $O(F^2)$. Therefore, the MIMO processing suffers from high computational load when a large number of cells are considered. Unlike the MIMO radar, the multistatic radar provides a more computationally efficient solution, where the number of initial hypotheses determines the computational complexity. The higher the threshold over the received signals, the more computationally efficient the estimation algorithm. However, the accuracy of the results is significantly affected when the threshold is increased. In other words, there is a trade-off between the computational complexity and the accuracy of estimation using a multistatic radar. It can be observed that a MIMO radar provides higher probability of detection with more accurate estimation than multistatic radars. In high SNR scenarios, it was shown that both multistatic and MIMO radars provide satisfactory results. However, in low SNR scenarios, multistatic radar achieves the same performance as the MIMO accomplishes provided that a sufficiently-low threshold is applied on the received signals. In this case, the computational complexity of multistatic radars will be the same as that of MIMO radars because detections are declared in most resolution cells. In high SNRs, the multistatic radar is preferred over the MIMO radar due to computational considerations.
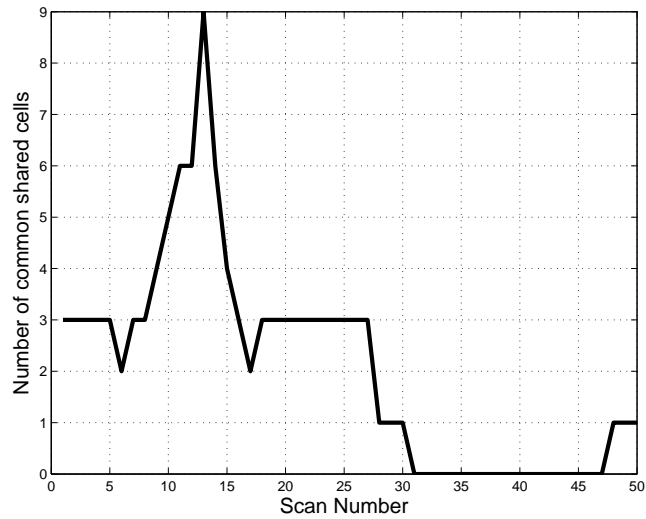
Figure 3.8: The number of common (shared) cells in different scans for the two-target scenario.

Table 3.6: Widely-separated MIMO Tracking Parameters

Variable	Value	Description
N_p	1000	# of particles
m/n	3/4	m/n logic
T_s	1	Sampling time
N_{MCMC}	50	# of Monte Carlo runs
SNR	$7dB$	Target SNR
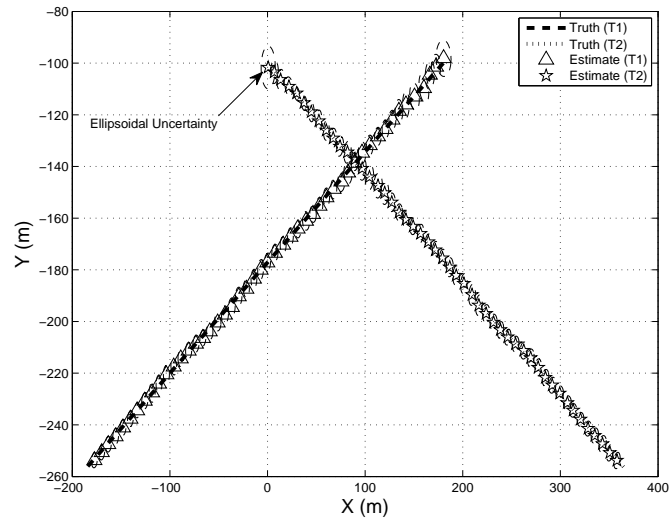
Figure 3.9: Estimated trajectories and the ellipsoidal uncertainty regions for the two-target scenario.
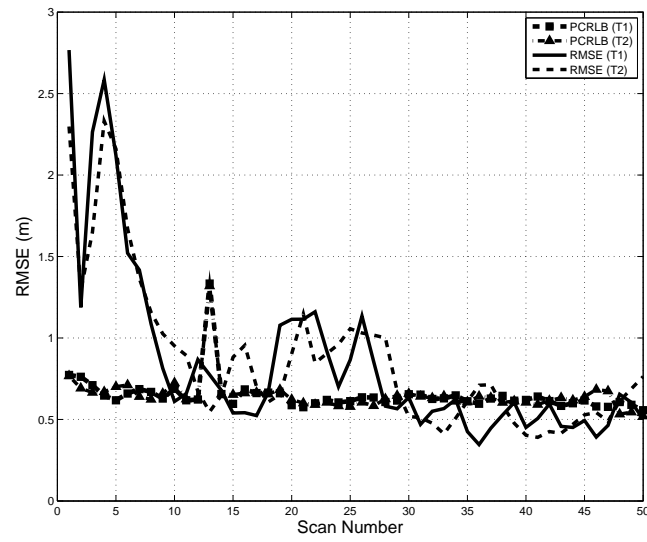
Figure 3.10: RMSE and PCRLB recursion of position estimations for the two-target scenario.
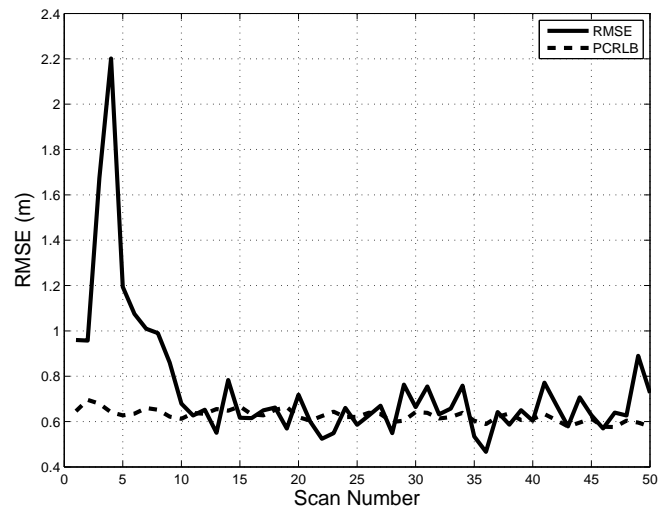
Figure 3.11: RMSE and PCRLB recursion of position estimations for the single-target scenario.

Chapter 4

Antenna Allocation For Collocated MIMO Radars

4.1   Introduction

In this chapter, the antenna allocation problem is developed for collocated MIMO radar systems. To the best of our knowledge, there is no comprehensive work on the design and analysis of an optimal antenna placement framework for collocated MIMO radars. The main contributions of this chapter are as follows:

- A novel CRLB derivation for MIMO radars with collocated antennas: Although the CRLB was derived in the literature for the collocated MIMO radars, the effect of the range information was not considered in the CRLB derivation. In addition, there is no compact CRLB derivation in terms of the location of antennas. In this chapter, the CRLB is first derived for a collocated MIMO radar where both DOA and range information are embedded in the signal model, and the impact of the

situation in which multiple targets fall inside the same resolution cell is also taken into consideration. Then, it will be shown how the location of antennas affects the CRLB and the localization performance.

- A convex optimization approach for the single-target case:
  It is shown that the antenna allocation problem can be dealt with by optimizing the location CRLB. To do this, the cost function is defined by applying suitable operators (e.g. determinant, trace, or maximum eigenvalue) to the CRLB. When a single target is located inside the resolution cell, the optimization algorithm is simplified to the well-known SDP using the related convex relaxation techniques.

- An optimization algorithm for cases with multiple unresolved targets:
  When multiple targets fall inside the same resolution cell, it is observed that the cost function is not convex anymore. In this case, due to the presence of sinusoid terms in each entry of the FIM, the cost function cannot be also simplified into a convex form. Therefore, a sampling-based approach is proposed where initial conditions of the optimization algorithm are generated in a way that the algorithm moves towards the global minimum. Simulation results also confirm the efficacy of the proposed method in finding the optimum antenna allocation when multiple targets lie in the same or consecutive resolution cells.

The rest of this chapter is organized as follows. Section 4.2 presents a brief overview of MIMO radars with collocated antennas. CRLB is derived for the MIMO system in Section . Section 4.4 deals with the antenna allocation problem where the convex optimization framework for the single-target case is also described. Simulation results that are the main part of this chapter are given in section 4.5.

103

4.2 MIMO Radars with collocated Antennas

Consider an array of antennas with M transmitters and N receivers.

Definition 4.2.1 *Define $s_{ti} = [x_{ti} \; y_{ti}]'$ and $s_{rj} = [x_{rj} \; y_{rj}]'$ as the location of the i-th transmitter and the j-th receiver in a 2-dimensional surveillance region, respectively.*

Assumption 4.2.1 *There are T targets available in the region where $x_t = [x_t \; y_t]'$ denotes the location of the t-th target. Also, the reflection of each target is modeled by a complex random variable $\alpha_t = \xi_t + j\zeta_t$ with ξ and ζ being the real and imaginary parts of α, respectively.*

Assumption 4.2.2 *It is assumed that the target's reflection obeys a Swerling type I model [75] where $\{\xi_t \sim \mathcal{N}(\bar{\xi}_t, \sigma_\alpha^2)\}$ and $\{\zeta_t \sim \mathcal{N}(\bar{\zeta}_t, \sigma_\alpha^2)\}$.*

Assumption 4.2.3 *It is assumed that the distance between each two antennas is much smaller than the distance of the array to each target. It is also assumed that the arrays of transmitters and receivers are both collocated with the origin as the center of the mass of the array.*

Definition 4.2.2 *Define $h[k] = [h_1[k] \; \cdots \; h_M[k]]^H$ as the transmitted waveform in the k-th snapshot with K being the number of total snapshots.*

4.2.1 Signal Model

Considering a collocated structure, resolution cells can be defined as a set of cocentric circles where the radios of the c-th circle equals cr_{bin} with r_{bin} denoting the resolution width. Figure 4.1 shows a simple configuration of resolution cells as well as the antennas that are distributed uniformly. It is observed that the target is located inside the c-th cell.

104
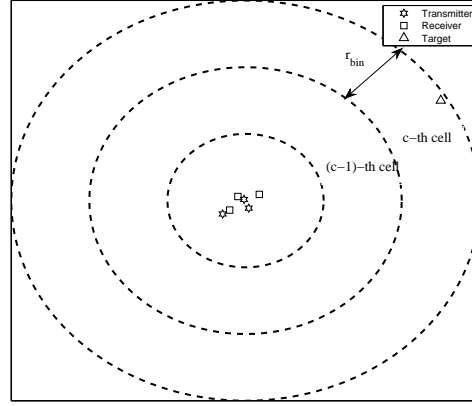
Figure 4.1: A simple collocated MIMO radar with three transmitters and three receivers. The target is located inside the c-th cell. The resolution cells are shown as cocentric circles with cr_{bin} being the radius of the c-th cell.

Assumption 4.2.4 *It is assumed that all T targets are distributed in C consecutive cells (e.g. $(c^* + 1)$ to $(c^* + C)$)where n_c denotes the number of targets available inside the c-th cell. Without loss of generality, it is assumed that $c^* = 0$.*

Assumption 4.2.5 *Transmitters send orthogonal signals with a diagonal cross-correlation matrix being defined as*

$$R = \frac{1}{K} \sum_{k=1}^{K} \boldsymbol{h}[k]\boldsymbol{h}^H[k] = \mathcal{D}\left([P_1 \ \cdots \ P_M]'\right) \tag{4.1}$$

where P_m denotes the total transmitted power by the m-th antenna.

Definition 4.2.3 *Defining $r_t^c = ||\boldsymbol{x}_t^c||_2$ as the Euclidean distance of the t-th target in the c-th cell to the origin, the ratio parameter β_t^c is defined as follows:*

$$\beta_t^c = \frac{r_t^c + (1 - c)r_{bin}}{r_{bin}} \tag{4.2}$$

105

Now, given all assumptions, the received output of the matched filter in the c-th resolution cell can be written as follows [43]:

$$
\eta_c = \begin{cases} \sum_{t=1}^{n_{c+1}}(1-\beta_t^{c+1})\phi_t^{c+1} & c=0 \\ \sum_{t=1}^{n_c}\beta_t^c\phi_t^c & c=C \\ \sum_{t_1=1}^{n_c}\beta_{t_1}^c\phi_{t_1}^c + \sum_{t_2=1}^{n_{c+1}}(1-\beta_{t_2}^{c+1})\phi_{t_2}^{c+1} & \text{otherwise} \end{cases} + w \qquad (4.3)
$$

where w denotes a complex Gaussian noise with independent real and imaginary parts being distributed as $\{\Re(w), \Im(w)\} \sim \mathcal{N}(0, \sigma_w^2)$, and ϕ_t^c is the contribution of the t-th target in the signal received in the c-th cell, which is written as $\phi_t^c = \alpha_t^c\psi_t^c$ with the following form for the unknown term in the right-hand side of the equality [43]:

$$
\psi_t^c = \sqrt{K}\mathrm{VEC}(A_t^c R^{\frac{1}{2}}) \qquad (4.4)
$$

Here, $\mathrm{VEC}(A)$ stands for the matrix vectorization operator, and A_t^c denotes the well-known steering matrix of the t-th target defined as follows [60]:

$$
\begin{aligned}
A_t^c &= \mathbf{b}_t^c(\mathbf{a}_t^c)^H & (4.5) \\
\mathbf{a}_t^c &= \exp\left(-j\frac{2\pi}{\lambda}[\sin(\theta_t^c) \; \cos(\theta_t^c)]S_t\right) & (4.6) \\
\mathbf{b}_t^c &= \exp\left(-j\frac{2\pi}{\lambda}[\sin(\theta_t^c) \; \cos(\theta_t^c)]S_r\right) & (4.7)
\end{aligned}
$$

where λ is the wavelength, θ_t^c denotes the DOA of the t-th target with respect to the origin, and the matrices S_t and S_r are defined as

$$
\begin{aligned}
S_t &= [\mathbf{s}_{t1} \; \cdots \; \mathbf{s}_{tM}] & (4.8) \\
S_r &= [\mathbf{s}_{r1} \; \cdots \; \mathbf{s}_{rN}] & (4.9)
\end{aligned}
$$

Definition 4.2.4 *Given the vector of the output of the matched-filter as* $\eta = [\eta_1^* \; \cdots \; \eta_C^*]^H$*, define* $\rho = [\Re(\eta_1) \; \Im(\eta_1) \; \cdots \; \Re(\eta_C) \; \Im(\eta_C)]'$*.*

Now, the mean received output of the matched filter is defined as $\bar{\rho} = [\Re(\bar{\eta}_1)\ \Im(\bar{\eta}_2)\ \cdots\ \Re(\bar{\eta}_C)\ \Im(\bar{\eta}_C)]'$. The unknown terms $\Re(\bar{\eta}_c)$ and $\Im(\bar{\eta}_c)$ can be found by calculating $\Re(\bar{\phi}_t^c)$ and $\Im(\bar{\phi}_t^c)$ as follows and then replacing in (4.3), respectively:

$$
\begin{aligned}
\Re(\bar{\phi}_t^c) &= \bar{\xi}_t^c\Re(\psi_t^c) - \bar{\zeta}_t^c\Im(\psi_t^c) \\
\Im(\bar{\phi}_t^c) &= \bar{\xi}_t^c\Re(\psi_t^c) + \bar{\zeta}_t^c\Im(\psi_t^c)
\end{aligned}
\tag{4.10}
$$

where the unknown terms in the right-hand side of the above equation can be written as follows:

$$
\begin{aligned}
\Re(\psi_t^c) &= \sqrt{K}\cos\left(\frac{2\pi}{\lambda}[\sin(\theta_t^c)\ \cos(\theta_t^c)]\Omega(S_t, S_r, R)\right) \\
\Im(\psi_t^c) &= \sqrt{K}\sin\left(\frac{2\pi}{\lambda}[\sin(\theta_t^c)\ \cos(\theta_t^c)]\Omega(S_t, S_r, R)\right)
\end{aligned}
\tag{4.11}
$$

with Ω being defined as

$$
\Omega(S_t, S_r, R) = (1_{1\times M}\odot S_r - S_t\odot 1_{1\times N})\left(R^{\frac{1}{2}}\odot 1_{1\times N}\right)
\tag{4.12}
$$

where $\odot$ is the Kronicker product, and $1_{a\times b}$ stands for a $a\times b$ matrix with all entries equal to one.

Given the signal model in (4.3) and the mean output of the matched-filter in (4.10), the following proposition provides the distribution of the output of the matched-filter [43]:

Proposition 4.2.1 *In a scenario with T targets located in C neighboring cells, the output of the matched-filter received by a collocated MIMO radar with M transmitters and N receivers (e.g. ρ) is Gaussian distributed with mean $\bar{\rho}$ and*

107

covariance Σ *defined as follows:*

$$\Sigma = \begin{pmatrix} \Sigma_{11} & \Sigma_{12} & 0 & \cdots & & 0 \\ \Sigma_{21} & \Sigma_{22} & 0 & \cdots & & 0 \\ 0 & 0 & \ddots & \cdots & & 0 \\ 0 & 0 & \cdots & \Sigma_{(C-1)(C-1)} & \Sigma_{(C-1)C} \\ 0 & 0 & \cdots & \Sigma_{C(C-1)} & \Sigma_{CC} \end{pmatrix} \qquad (4.13)$$

with the following definitions for Σ_{cc} *and* $\Sigma_{c(c-1)}$ *terms:*

$$\Sigma_{cc} = \begin{cases} K\sigma_\alpha^2 \left(\sum_{t=1}^{n_1}(1-\beta_t^1)^2 + \sigma_w^2 \right) I_{2MN} & c = 0 \\ K\sigma_\alpha^2 \left(\sum_{t=1}^{n_C}(\beta_t^C)^2 + \sigma_w^2 \right) I_{2MN} & c = C \\ K\sigma_\alpha^2 (\sum_{t_1=1}^{n_c}(\beta_{t_1}^c)^2 + & otherwize \\ \sum_{t_2=1}^{n_{c+1}}(1-\beta_{t_2}^c)^2 + \sigma_w^2) I_{2MN} & \end{cases}$$

$$\Sigma_{c(c-1)} = K\sigma_\alpha^2 \sum_{t=1}^{n_c}(1-\beta_t^c)\beta_t^c I_{2MN} \qquad (4.14)$$

4.3   Cramer-Rao Lower Bound

CRLB provides the best Minimum Mean Squared Error (MMSE) bound for any unbiased estimator [6]. The CRLB provides a good offline metric to evaluate the performance of every unbiased estimator. In this section, the CRLB is derived for a collocated MIMO radar. It is shown that the CRLB is a function of the mutual distances between any two antennas. Also, a scenario is considered with T targets distributed in C consecutive cells where different number of targets might be located inside each cell.

Definition 4.3.1 *For the t-th target located in the c-th resolution cell, define the state and parameter vector X_t^c and Θ_t^c, respectively, as follows:*

$$X_t^c = [x_t^c \ y_t^c \ \bar{\xi}_t^c \ \bar{\zeta}_t^c]' \qquad (4.15)$$

$$\Theta_t^c = [\theta_t^c \ \beta_t^c \ \bar{\xi}_t^c \ \bar{\zeta}_t^c]' \qquad (4.16)$$

The CRLB is the inverse of the well-known FIM defined as follows [6]:

Definition 4.3.2 *Assuming $\boldsymbol{y}$ as the received noisy measurements and θ as the parameters of the measurement model, define the following matrix operator:*

$$J_{\theta\theta'} = E_{\boldsymbol{y}} \left[\frac{\partial \log p(\boldsymbol{y}|\theta)}{\partial \theta} \left(\frac{\partial \log p(\boldsymbol{y}|\theta)}{\partial \theta} \right)' \right] \tag{4.17}$$

Refer to the definition of ρ and its distribution provided by Proposition 4.2.1 and define the stacked state and parameter vector of all targets as $X = \left[(X_1^1)' \; \cdots \; (X_{n_1}^1)' \; (X_1^2)' \; \cdots \; (X_{n_C}^C)' \right]'$ and $\Theta = \left[(\Theta_1^1)' \; \cdots \; (\Theta_{n_1}^1)' \; (\Theta_1^2)' \; \cdots \; (\Theta_{n_C}^C)' \right]'$, respectively. In this case, the FIM can be shown by $J_{XX'}$. The defined FIM can be now written in the following form:

$$J_{XX'} = E_{\rho} \left[\frac{\partial \log p(\rho|X)}{\partial X} \left(\frac{\partial \log p(\rho|X)}{\partial X} \right)' \right] \tag{4.18}$$

Using the chain-rule for partial derivatives, the above FIM can be more simplified to the following form [43]:

$$J_{XX'} = \Gamma J_{\Theta\Theta'} \Gamma' \tag{4.19}$$

Here, Γ is called the system matrix and is written as

$$\Gamma = \begin{bmatrix} \gamma_1^1 & 0_{4\times4} & \cdots & 0_{4\times4} \\ 0_{4\times4} & \gamma_2^1 & \cdots & 0_{4\times4} \\ \vdots & \vdots & \ddots & \vdots \\ 0_{4\times4} & \cdots & 0_{4\times4} & \gamma_{n_C}^C \end{bmatrix} \tag{4.20}$$

with $0_{4\times4}$ as a 4×4 zero-matrix, and individual γ_t^c terms being defined as

$$\gamma_t^c = \begin{bmatrix} \frac{\partial \theta_t^c}{\partial x_t^c} & \frac{\partial \beta_t^c}{\partial x_t^c} & 0 & 0 \\ \frac{\partial \theta_t^c}{\partial y_t^c} & \frac{\partial \beta_t^c}{\partial y_t^c} & 0 & 0 \\ 0 & 0 & 1 & 0 \\ 0 & 0 & 0 & 1 \end{bmatrix} \tag{4.21}$$

where the unknown partial derivatives can be derived by using the definition of the ratio in (4.2) and the following equation for the target DOA:

$$\theta_t^c = \tan^{-1}\left(\frac{y_t^c}{x_t^c}\right) \tag{4.22}$$

Now, the FIM derivation comes to finding the unknown term $J_{\Theta\Theta'}$ in (4.19). The new $J_{\Theta\Theta'}$ can be broken into the following sub-matrices:

$$J_{\Theta\Theta'} = \begin{bmatrix} J_{(\Theta^1)(\Theta^1)'} & J_{(\Theta^1)(\Theta^2)'} & 0 & 0 & \cdots & 0 \\ J_{(\Theta^2)(\Theta^1)'} & J_{(\Theta^2)(\Theta^2)'} & J_{(\Theta^2)(\Theta^3)'} & 0 & \cdots & 0 \\ 0 & J_{(\Theta^3)(\Theta^2)'} & J_{(\Theta^3)(\Theta^3)'} & J_{(\Theta^3)(\Theta^4)'} & \cdots & 0 \\ \vdots & \vdots & \vdots & \ddots & \ddots & \vdots \\ 0 & 0 & \cdots & J_{(\Theta^{C-1})(\Theta^{C-2})'} & J_{(\Theta^{C-1})(\Theta^{C-1})'} & J_{(\Theta^{C-1})(\Theta^C)'} \\ 0 & 0 & \cdots & 0 & J_{(\Theta^C)(\Theta^{C-1})'} & J_{(\Theta^C)(\Theta^C)'} \end{bmatrix} \tag{4.23}$$

Here, Θ^c denotes a $4 \times n_c$ vector formed by stacking the parameters of those targets falling inside the c-th cell. The following equation can be written for Θ^c:

$$\Theta^c = [(\Theta_1^c)' \cdots (\Theta_{n_c}^c)']' \tag{4.24}$$

Each individual entry in (4.23) can be also written as follows:

$$J_{(\Theta^{c_1})(\Theta^{c_2})'} = \begin{bmatrix} J_{(\Theta_1^{c_1})(\Theta_1^{c_2})'} & \cdots & J_{(\Theta_1^{c_1})(\Theta_{n_{c_2}}^{c_2})'} \\ \vdots & \ddots & \vdots \\ J_{(\Theta_{n_{c_1}}^{c_1})(\Theta_{n_{c_2}}^{c_2})'} & \cdots & J_{(\Theta_{n_{c_1}}^{c_1})(\Theta_{n_{c_2}}^{c_2})'} \end{bmatrix},$$
$$c_1 \in \{c_2, c_2 + 1\} \tag{4.25}$$

Finally, each entry of the FIM in (4.25) can be simplified into the following form:

$$
J_{(\Theta_n^{c_1})(\Theta_m^{c_2})'} = \begin{bmatrix}
J_{\theta_n^{c_1}\theta_m^{c_2}} & J_{\theta_n^{c_1}\beta_m^{c_2}} & J_{\theta_n^{c_1}\bar{\xi}_m^{c_2}} & J_{\theta_n^{c_1}\bar{\zeta}_m^{c_2}} \\
J_{\beta_n^{c_1}\theta_m^{c_2}} & J_{\beta_n^{c_1}\beta_m^{c_2}} & J_{\beta_n^{c_1}\bar{\xi}_m^{c_2}} & J_{\beta_n^{c_1}\bar{\zeta}_m^{c_2}} \\
J_{\bar{\xi}_n^{c_1}\theta_m^{c_2}} & J_{\bar{\xi}_n^{c_1}\beta_m^{c_2}} & J_{\bar{\xi}_n^{c_1}\bar{\xi}_m^{c_2}} & J_{\bar{\xi}_n^{c_1}\bar{\zeta}_m^{c_2}} \\
J_{\bar{\zeta}_n^{c_1}\theta_m^{c_2}} & J_{\bar{\zeta}_n^{c_1}\beta_m^{c_2}} & J_{\bar{\zeta}_n^{c_1}\bar{\xi}_m^{c_2}} & J_{\bar{\zeta}_n^{c_1}\bar{\xi}_m^{c_2}}
\end{bmatrix}
\tag{4.26}
$$

Note that the matrix given by (4.26) is a 4×4 FIM sub-matrix that includes the information correlation between the parameters of the n-th target in the c_1-th cell and the m-th target in the c_2-th cell. Before presenting the algebraic expressions for each entry of the FIM given in (4.26), the following new notations are defined:

Definition 4.3.3 *Assuming the n-th target located in the c_1-th cell, define the following new notations:*

$$
\omega_n^{c_1}(l) = \frac{2\pi}{\lambda} \left[\sin(\theta_n^{c_1}) \; \cos(\theta_n^{c_1})\right] \Omega(:,l)
\tag{4.27}
$$

$$
\boldsymbol{p}_n^{c_1} = \left[\cos(\theta_n^{c_1}) \; -\sin(\theta_n^{c_1})\right]'
\tag{4.28}
$$

$$
\breve{\beta}_n^{c_1} = \left[(1 - \beta_n^{c_1}) \; \beta_n^{c_1}\right]'
\tag{4.29}
$$

where $\Omega(:,l)$ denotes the l-th column of matrix Ω with $\Omega(S_t, S_r, R)$ being written as Ω for the sake of brevity.

Definition 4.3.4 *For each two targets falling inside cells c_1 and c_2, respectively, the following notations are defined:*

$$
\kappa_{c_1 c_2}^{nm} = \bar{\xi}_n^{c_1}\bar{\xi}_m^{c_2} + \bar{\zeta}_n^{c_1}\bar{\zeta}_m^{c_2}
\tag{4.30}
$$

$$
\iota_{c_1 c_2}^{nm} = \bar{\xi}_n^{c_1}\bar{\zeta}_m^{c_2} - \bar{\zeta}_n^{c_1}\bar{\xi}_m^{c_2}
\tag{4.31}
$$

The covariance matrix Σ found in (4.13) can be now rewritten for cells $\{c_1 - 1, c_1, c_2\}$ with $c_1 \in \{c_2, c_2 - 1\}$. Using the general form given by (4.13) and

expressions provided by (4.14), the new covariance matrix can be written as

$$\Sigma_* = \begin{bmatrix} c_1 & c_4 & 0 \\ c_4 & c_2 & c_5 \\ 0 & c_5 & c_3 \end{bmatrix} \odot I_{2MN} \tag{4.32}$$

where c_i terms are found using (4.14). Similarly, the new notation $\bar{\rho}_*$ is defined as

$$\bar{\rho}_* = [\Re(\bar{\eta}_{c_1-1})\ \Im(\bar{\eta}_{c_1-1})\ \Re(\bar{\eta}_{c_1})\ \Im(\bar{\eta}_{c_1})\ \Re(\bar{\eta}_{c_2})\ \Im(\bar{\eta}_{c_2})]' \tag{4.33}$$

Now, it is straightforward to show that the inverse of Σ_* can be written in the following form:

$$\Sigma_*^{-1} = \begin{bmatrix} k_1 & k_4 & k_5 \\ k_4 & k_2 & k_6 \\ k_5 & k_6 & k_3 \end{bmatrix} \odot I_{2MN} \tag{4.34}$$

The following proposition provides algebraic expressions for each entry of the FIM in (4.26):

Proposition 4.3.1 *Assume a scenario with T targets falling inside C consecutive resolution cells. Each entry of the FIM defined by (4.26) can be calculated*

as follows:

$$J_{\theta_n^{c_1}\theta_m^{c_2}} = K\left(\frac{2\pi}{\lambda}\right)^2 \times$$

$$\times \left[\sum_{l=1}^{MN}(\boldsymbol{p}_n^{c_1})'\Omega(:,l)\Omega'(:,l)\boldsymbol{p}_m^{c_2}\left(\kappa_{c_1c_2}^{nm}\cos(\omega_m^{c_2}(l)-\omega_n^{c_1}(l))+\iota_{c_1c_2}^{nm}\sin(\omega_m^{c_2}(l)-\omega_n^{c_1}(l))\right)\right]\times$$

$$\times C_{\theta_n^{c_1}\theta_m^{c_2}} \tag{4.35}$$

$$J_{\beta_n^{c_1}\beta_m^{c_2}} = \frac{K}{r_{bin}^2}\left[\sum_{l=1}^{MN}\kappa_{c_1c_2}^{nm}\cos(\omega_m^{c_2}(l)-\omega_n^{c_1}(l))+\iota_{c_1c_2}^{nm}\sin(\omega_m^{c_2}(l)-\omega_n^{c_1}(l))\right]C_{\beta_n^{c_1}\beta_m^{c_2}} +$$

$$+ F(\beta_n^{c_1},\beta_m^{c_2}) \tag{4.36}$$

$$J_{\bar{\xi}_n^{c_1}\bar{\xi}_m^{c_2}} = J_{\bar{\zeta}_n^{c_1}\bar{\zeta}_m^{c_2}} = K\left[\sum_{l=1}^{MN}\cos\left(\omega_n^{c_1}(l)-\omega_m^{c_2}(l)\right)\right]C_{\theta_n^{c_1}\theta_m^{c_2}} \tag{4.37}$$

$$J_{\theta_n^{c_1}\beta_m^{c_2}} = \frac{K}{r_{bin}}\frac{2\pi}{\lambda}\left[\sum_{l=1}^{MN}(\boldsymbol{p}_n^{c_1})'\Omega(:,l)\left\{\kappa_{c_1c_2}^{nm}\cos(\omega_m^{c_2}(l)-\omega_n^{c_1}(l))+\iota_{c_1c_2}^{nm}\sin(\omega_m^{c_2}(l)-\omega_n^{c_1}(l))\right\}\right]\times$$

$$\times C_{\theta_n^{c_1}\beta_m^{c_2}} \tag{4.38}$$

$$J_{\theta_n^{c_1}\bar{\xi}_m^{c_2}} = K\frac{2\pi}{\lambda}\left[\sum_{l=1}^{MN}(\boldsymbol{p}_n^{c_1})'\Omega(:,l)\left\{-\bar{\zeta}_n^{c_1}\cos(\omega_m^{c_2}(l)-\omega_n^{c_1}(l))+\bar{\xi}_n^{c_1}\sin(\omega_m^{c_2}(l)-\omega_n^{c_1}(l))\right\}\right]\times$$

$$\times C_{\theta_n^{c_1}\theta_m^{c_2}} \tag{4.39}$$

$$J_{\theta_n^{c_1}\bar{\zeta}_m^{c_2}} = K\frac{2\pi}{\lambda}\left[\sum_{l=1}^{MN}(\boldsymbol{p}_n^{c_1})'\Omega(:,l)\left\{\bar{\xi}_n^{c_1}\cos(\omega_m^{c_2}(l)-\omega_n^{c_1}(l))+\bar{\zeta}_n^{c_1}\sin(\omega_m^{c_2}(l)-\omega_n^{c_1}(l))\right\}\right]\times$$

$$\times C_{\theta_n^{c_1}\theta_m^{c_2}} \tag{4.40}$$

$$J_{\beta_n^{c_1}\bar{\xi}_m^{c_2}} = \frac{K}{r_{bin}}\left[\sum_{l=1}^{MN}\left\{\bar{\xi}_n^{c_1}\cos(\omega_m^{c_2}(l)-\omega_n^{c_1}(l))+\bar{\zeta}_n^{c_1}\sin(\omega_m^{c_2}(l)-\omega_n^{c_1}(l))\right\}\right]C_{\beta_n^{c_1}\theta_m^{c_2}} \tag{4.41}$$

$$J_{\beta_n^{c_1}\bar{\zeta}_m^{c_2}} = \frac{K}{r_{bin}}\left[\sum_{l=1}^{MN}\left\{\bar{\zeta}_n^{c_1}\cos(\omega_m^{c_2}(l)-\omega_n^{c_1}(l))-\bar{\xi}_n^{c_1}\sin(\omega_m^{c_2}(l)-\omega_n^{c_1}(l))\right\}\right]C_{\beta_n^{c_1}\theta_m^{c_2}} \tag{4.42}$$

$$J_{\bar{\xi}_n^{c_1}\bar{\zeta}_m^{c_2}} = K\left[\sum_{l=1}^{MN}\sin(\omega_n^{c_1}(l)-\omega_m^{c_2}(l))\right]C_{\theta_n^{c_1}\theta_m^{c_2}} \tag{4.43}$$

with $F(\beta_n^{c_1},\beta_m^{c_2})$ being a known function of ratios, and the following expression being given for unknown coefficients in the right-hand side of the above

equations:

$$C_{\theta_n^{c_1}\theta_m^{c_2}} = \begin{cases} \left[(\breve{\beta}_n^{c_1})' \ 0\right] \Sigma_*^{-1} \left[0 \ (\breve{\beta}_m^{c_2})'\right]' & c_1 = c_2 - 1 \\ \left[0 \ (\breve{\beta}_n^{c_1})'\right] \Sigma_*^{-1} \left[0 \ (\breve{\beta}_m^{c_2})'\right]' & otherwise \end{cases} \tag{4.44}$$

$$C_{\beta_n^{c_1}\beta_m^{c_2}} = \begin{cases} [-1 \ 1 \ 0] \, \Sigma_*^{-1} \, [0 \ -1 \ 1]' & c_1 = c_2 - 1 \\ [0 \ -1 \ 1] \, \Sigma_*^{-1} \, [0 \ -1 \ 1]' & otherwise \end{cases} \tag{4.45}$$

$$C_{\theta_n^{c_1}\beta_m^{c_n}} = \frac{\partial C_{\theta_n^{c_1}\theta_m^{c_2}}}{\partial \beta_m^{c_2}}, \ \ C_{\beta_n^{c_1}\theta_m^{c_2}} = \frac{\partial C_{\theta_n^{c_1}\theta_m^{c_2}}}{\partial \beta_n^{c_1}} \tag{4.46}$$

Proof See Appendix 6.2.

Note that the above proposition can be used to find the FIM for every tuple $\{\Theta_n^{c_1}, \Theta_m^{c_2}\}$ where $1 \leq \{c_1, c_2\} \leq C$ and $1 \leq n \leq n_{c_1}$ and $1 \leq m \leq n_{c_2}$. The calculated FIMs in (4.26) are then inserted in (4.25) and (4.23), respectively, to obtain $J_{\Theta\Theta'}$. The CRLB is finally found by inverting the FIM as

$$C_{XX'} = (\Gamma^{-1})' C_{\Theta\Theta'} \Gamma^{-1} \tag{4.47}$$

with $C_{\Theta\Theta'} = (J_{\Theta\Theta'})^{-1}$.

4.4 Optimal Antenna Allocation

It can be shown that the localization performance of the collocated MIMO radar is affected by the distribution of antennas in the surveillance region. Consider a scenario with two antennas ($N = 2, M = 2$), where each antenna can both transmit and receive signals. We take a single target scenario into consideration with parameters $[30^o \ .33 \ 1 \ 1]'$, which is located in $\{r, \theta\} = [825\text{m} \ 30^o]'$. The variance of DOA estimates (C_{θ^2}) is now shown in Figure 4.2 in terms of different inter-antenna distances for the designed scenario. It can be observed that the geometry of sensors (inter-sensor distances) affects the performance

114
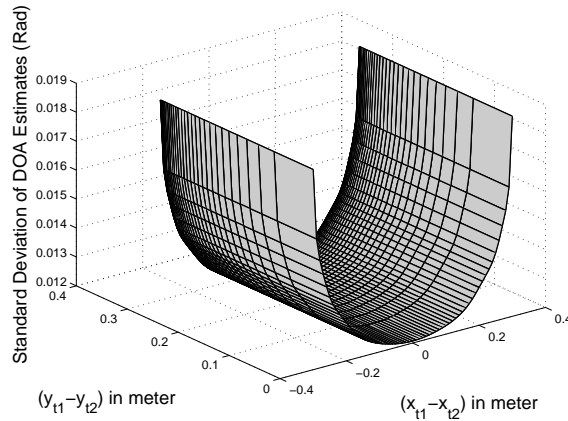
Figure 4.2: The variance of the DOA estimation for different inter-sensor distances. The designed scenario includes a single-emitter and a collocated MIMO radar with two transmitters and two receivers.

bound of DOA estimation, where the estimation variance at the minimum point is 33% lower than the maximum variance. Unfortunately, the graphical tool cannot be developed for cases with more antennas. Therefore, this section concerns with designing a systematic algorithm for the antenna allocation problem in collocated MIMO radars. First, the case with a single target available in the surveillance region is considered. It is shown that considering suitable geometric constraints, the antenna allocation problem can be formulated as a well-known SDP procedure [13]. Then, the problem is extended to the case with multiple targets available in the same or consecutive resolution cells. It is shown that the derived cost function is non-convex and a sampling-based approach is proposed to capture the global minimum of the cost function.

4.4.1 Single Target Case

When a single target is placed in an arbitrary resolution cell, all $\cos(.)$ and $\sin(.)$ terms in the individual entries of the FIM defined by (4.26) vanish. Let us assume $\Theta = \left[\theta^c \ \beta^c \ \bar{\xi}^c \ \bar{\zeta}^c\right]'$ as the parameter vector of the single target fallen in the c-th cell. Using the results given in Proposition 4.3.1, it can be observed that only terms $J_{\theta^c \nu^c}$ are a function of the antenna locations where $\nu^c \in \{\theta^c, \beta^c, \bar{\xi}^c, \bar{\zeta}^c\}$. On the other hand, according to the definition of the matrix Ω in (4.12), it can be shown that:

$$\sum_{l=1}^{MN} \Omega(:,l) = 0 \tag{4.48}$$

It can be observed that only the term $J_{(\theta^c)^2}$ can be considered as a function of the antenna locations.

Definition 4.4.1 *Define the difference between the m-th transmitter and the n-th receiver as follows:*

$$\Delta \boldsymbol{s}_{nm} = \boldsymbol{s}_{tm} - \boldsymbol{s}_{rn} \tag{4.49}$$

Corollary 4.4.1 *In a collocated MIMO radar with M transmitters and N receivers, where a single target is located in the c-th resolution cell, the FIM is a function of inter-antenna differences. In addition, all entries of the FIM are independent of the inter-sensor differences except $J_{(\theta^c)^2}$, which is also a convex function of the unknown differences.*

Proof It was shown that only $J_{(\theta^c)^2}$ is a function of the sensor locations. Now, it is demonstrated that it is a convex function of the parameters (difference vectors). Using the algebraic terms given by Proposition 4.3.1, the entry $J_{(\theta^c)^2}$ can be simplified into the following form:

$$J_{(\theta^c)^2} = K \left(\frac{2\pi}{\lambda}\right)^2 |\alpha^c|^2 \left[\sum_{l=1}^{nm} (\mathbf{p}^c)'\Omega(:,l)\Omega'(:,l)\mathbf{p}^c\right] C_{(\theta^c)^2} \tag{4.50}$$

116

Consider the definition of Ω in (4.12). It can be then observed that $\Omega(:,l)$ is a linear function of the corresponding difference vector $\Delta \mathbf{s}_{nm}$. It is also known that $J_{(\theta^c)^2}$ is a convex function of $\Omega(:,l)$ terms due to the appearance of quadratic terms in (4.50) [13]. Therefore, $J_{(\theta^c)^2}$ is also a convex function of the difference vectors.

The antenna allocation problem can be now dealt with by minimizing the trace of CRLB, maximizing the determinant of FIM, or minimizing the maximum eigenvalue of CRLB [60]. The following lemma proposes the convex optimization formulation for the antenna allocation problem in a collocated MIMO radar system where a single-target scenario is considered:

Lemma 4.4.1 *Consider a collocated MIMO radar with M transmitters and N receivers. In addition, assume that there is a single target located in the c-th resolution cell. Then, a convex optimization algorithm that finds an optimal placement of antennas is given as follows:*

$$\max_{\{\Delta s_{11}, \cdots, \Delta s_{nm}\}} \quad J_{(\theta^c)^2} \tag{4.51}$$

Proof The optimization problem can be formulated as minimizing the determinant of the CRLB, which is equivalent to maximizing $|J_{XX'}|$. In addition, the system matrix Γ defined in (4.20) is independent of the location of the antennas. Therefore, the final goal is to maximize $|J_{\Theta^c(\Theta^c)'}|$. Now, the FIM in (4.26) can be written in the following new form:

$$J_{\Theta^c(\Theta^c)'} = \begin{bmatrix} J_{(\theta^c)^2} & \mathbf{b}' \\ \mathbf{b} & B \end{bmatrix} \tag{4.52}$$

where $\mathbf{b}$ and B are the blocked vector and matrix formed by remaining entries of $J_{\Theta^c\Theta^c}$ in (4.26), respectively. The determinant term can be written as

$$|J_{\Theta^c\Theta^c}| = |B||J_{(\theta^c)^2} - \mathbf{b}'B\mathbf{b}| \tag{4.53}$$

117

It is known that both B and $\mathbf{b}$ are independent of the antenna placement. Therefore, the determinant maximization can be achieved by maximizing $J_{(\theta^c)^2}$ with respect to Ω. However, it is also known that Ω is a linear function of $\Delta\mathbf{s}_{nm}$ terms. The optimization problem can be finally simplified to maximizing $J_{(\theta^c)^2}$ with respect to $\Delta\mathbf{s}_{nm}$ terms, which is the final form given in (4.51).

The final optimization problem can be now constructed by imposing the following constraints on the inter-antenna distances:

The inter-antenna distance:

In practice, antennas need to be well-separated enough to ensure maintenance and safety considerations. In addition, the inter-antenna distance should be small enough to have the far-field assumption still valid. Based on the given targets, the following constraints can be considered:

$$||\Delta\mathbf{s}_{nm||_2} \geq d_{nm} \tag{4.54}$$

$$||\Delta\mathbf{s}_{nm}||_2 \leq e_{nm}, \forall\ m = 1, ..., M,\ n = 1, ..., N \tag{4.55}$$

where e_{nm} and d_{nm} are design parameters.

The center of the mass constraint:

It was mentioned in Assumption 4.2.3 that the center of the mass of the array is located in the origin. Therefore, the following new constraints are formed on the location of antennas:

$$\sum_{m=1}^{M} \mathbf{s}_{tm} + \sum_{n=1}^{N} \mathbf{s}_{rn} = 0 \tag{4.56}$$

Note that the FIM is a function of inter-antenna distances and therefore, a set of optimal difference vectors might correspond to an infinite number of sensor locations. The constraint given by (4.56) ensures that the mass center of the obtained geometry is in the origin. The uniqueness of optimal solution is further discussed in this section.

Considering the above defined constraints, the new optimization problem can be written as follows:

$$\max_{\{\Delta \mathbf{s}_{11}, \cdots, \Delta \mathbf{s}_{nm}\}} \sum_{m=1}^{M} \sum_{n=1}^{N} (\mathbf{p}^c)' \Delta \mathbf{s}_{nm} \Delta \mathbf{s}'_{nm} \mathbf{p}^c$$

$$\text{S.T} \qquad ||\Delta \mathbf{s}_{nm}||_2 \geq d_{nm}$$

$$||\Delta \mathbf{s}_{nm}||_2 \leq e_{nm}$$

$$\sum_{m=1}^{M} \mathbf{s}_{tm} + \sum_{n=1}^{N} \mathbf{s}_{rn} = 0, \forall\, m = \{1, \cdots, M\}, n = \{1, \cdots, N\}$$

$$(4.57)$$

In writing the above equation, it is assumed that the transmitted powers are all the same and unitary ($P_1 = P_2 = \cdots = P_M = 1$). The optimization problem given by (4.57) is not in a convex form and therefore cannot be solved using the standard approaches. The following theorem reformulates the optimization problem in (4.57) as a SDP:

Theorem 4.4.1 *Consider a single-target scenario with a collocated MIMO radar being used as the measurement tool. Defining $T^* = \{T_{11}, \cdots, T_{nm}\}$, $S^* = \{\mathbf{s}_{t1}, \cdots, \mathbf{s}_{rN}\}$, and $\mathbf{t} = [t_{11} \;\; \cdots \;\; t_{nm}]'$, the optimal placement of transmitters and receivers that maximizes the determinant of FIM is found by solving the following SDP optimization problem:*

$$\max_{T^*, S^*, \mathbf{t}} \sum_{m=1}^{M} \sum_{n=1}^{N} t_{nm}$$

$$S.T. \qquad \sum_{m=1}^{M} \mathbf{s}_{tm} + \sum_{n=1}^{N} \mathbf{s}_{rn} = 0$$

$$\mathcal{T}(T_{nm} P) \geq t_{nm}$$

$$\begin{bmatrix} -I_{2\times 2} & \mathbf{s}_{tm} - \mathbf{s}_{rn} \\ \mathbf{s}'_{tm} - \mathbf{s}'_{rn} & -e_{nm}^2 \end{bmatrix} \preceq 0, \quad \begin{bmatrix} I_{2\times 2} & \mathbf{s}_{tm} - \mathbf{s}_{rn} \\ \mathbf{s}'_{tm} - \mathbf{s}'_{rn} & d_{nm}^2 \end{bmatrix} \preceq 0$$

$$\begin{bmatrix} 1 & \mathbf{s}'_{tm} - \mathbf{s}'_{rn} \\ \mathbf{s}_{tm} - \mathbf{s}_{rn} & T_{nm} \end{bmatrix} \preceq 0, \; \forall\, m = \{1, \cdots, M\}, n = \{1, \cdots, N\}$$

with $P = \mathbf{p}^c (\mathbf{p}^c)'$, and $\preceq$ as the generalized inequality operator.

Proof See Appendix 6.3.

The above optimization problem can be now efficiently solved using standard packages [44].

Remark 4.4.1 *The optimization problem in (4.57) proves dependency on the parameters of the target through the matrix P. The following proposition shows how the optimal structure is affected by changing the DOA of the target:*

Proposition 4.4.1 *Consider a single-target scenario with a collocated MIMO radar being used as the measurement tool. Defining θ_1 and θ_2 as two different DOAs and $\{S_t^{o1}, S_r^{o1}\}, \{S_t^{o2}, S_r^{o2}\}$ as the assigned optimal antenna allocations, respectively, the following equations are valid:*

$$\boldsymbol{s}_{tm}^{o2} = G_{\Delta\theta}\boldsymbol{s}_{tm}^{o1} \tag{4.58}$$

$$\boldsymbol{s}_{rn}^{o2} = G_{\Delta\theta}\boldsymbol{s}_{rn}^{o1} \ \forall \ m = \{1, \cdots, M\}, n = \{1, \cdots, N\} \tag{4.59}$$

with $\Delta\theta = \theta_2 - \theta_1$ and $G_{\Delta\theta}$ as the rotation matrix defined as follows:

$$G_{\Delta\theta} = \begin{bmatrix} \cos(\Delta\theta) & -\sin(\Delta\theta) \\ \sin(\Delta\theta) & \cos(\Delta\theta) \end{bmatrix} \tag{4.60}$$

Proof See Appendix 6.4.

Remark 4.4.2 *The SDP formulation given by Theorem 1 does not provide any information regarding the uniqueness of the optimal solutions for the location of antennas. The uniqueness of solutions is now discussed in the following proposition.*

Proposition 4.4.2 *Consider a single-target scenario with a collocated MIMO radar being used as the measurement tool. Then, there are at least two solutions for the optimization problem in (4.57) as $\{S_t^{o1}, S_r^{o1}\}$ and $\{S_t^{o2}, S_r^{o2}\}$. In*

addition, each optimal configuration can be obtained from the second one by a simple rotation as follows:

$$\boldsymbol{s}_{ti}^{o2} = G_\pi \boldsymbol{s}_{ti}^{o2}, \ i = \{1, \cdots, M\} \tag{4.61}$$

$$\boldsymbol{s}_{rj}^{o2} = G_\pi \boldsymbol{s}_{rj}^{o2}, \ j = \{1, \cdots, N\} \tag{4.62}$$

where G_π is a rotation matrix with π as the angle of rotation.

Proof See Appendix 6.5.

4.4.2 Multiple Target Case

When multiple targets fall inside the same resolution cell (or consecutive cells), the individual entries of the FIM in (4.26) are no longer convex.

Proposition 4.4.3 *Consider a collocated MIMO radar system with M transmitters and N receivers with $d_{nm} \leq ||\Delta \boldsymbol{s}_{nm}|| \leq e_{nm}, \ \forall \ m = \{1, \cdots, M\}, n = \{1, \cdots, N\}$. Also, assume a scenario with two targets fallen in the c-th resolution cell with parameters Θ_1^c and Θ_2^c, respectively. Then, the term $(\omega_1^c(:, l) - \omega_2^c(:, l))$ falls in the following interval:*

$$\frac{2\pi}{\lambda} d_{nm} \sqrt{2\left(1 - \cos(\theta_2^c - \theta_1^c)\right)} \leq \omega_1^c(:, l) - \omega_2^c(:, l) \leq \frac{2\pi}{\lambda} e_{nm} \sqrt{2\left(1 - \cos(\theta_2^c - \theta_1^c)\right)} \tag{4.63}$$

with $l = \{1, \cdots, MN\}$.

The above proposition states that the more separated the DOA of targets, the wider the difference $(\omega_1^c(:, l) - \omega_2^c(:, l))$. For example, defining $\Delta\omega$ as the difference between the upper and lower bounds of $(\omega_1^c(:, l) - \omega_2^c(:, l))$ in (4.63), Figure 4.3 shows how $\Delta\omega$ changes by varying the difference between the DOA of targets. It is observed that when the targets are well-separated in the DOA space, the difference between the maximum and minimum bound is significant.

This also highlights the contribution of the sinusoid terms in each entry of the FIM, which might result in several local optimum points. On the other hand, the convex relaxation approach used for the single target case cannot be applied to the cost function derived for the case with multiple targets in the same cell. The above problems make the optimization problem nonconvex when there are more than one target inside each resolution cell (consecutive cells).

To handle the above problem, the optimization algorithm for different initial locations of the antennas is run. However, a large number of initial points are required to capture the nonconvexity of the cost function. The sampling approach is now proposed in Algorithm 2. In the proposed algorithm, Q denotes the covariance of the normal density function that is used to generate new initial points. While the covariance matrix is chosen experimentally, a small variance might get the algorithm to be trapped in the local optimum point. Therefore, an intelligent choice of the covariance matrix can enhance the efficiency of the algorithm. The main idea behind the proposed approach is to, first, find an estimate of the optimal antenna location, which might be a local solution. Then, initial points are generated based on the obtained optimal location. The samples are generated until the algorithm reaches the global optimum point and therefore, no new location is found with the assigned cost lower than the previous step. Note that this algorithm does not always guarantee that the optimization algorithm captures the global solution. However, as it is shown in the simulations, it is observed that regardless of the initial selection of the antenna location, the algorithm always converges to a unique solution.

Remark 4.4.3 *The procedure given in Algorithm 2 is terminated when the*
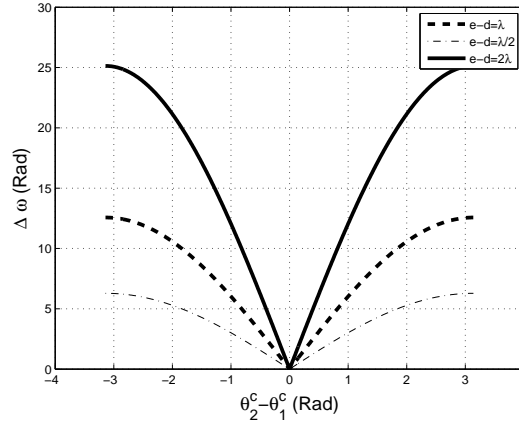
Figure 4.3: Variation of the sinusoid argument by changing the difference between the DOA of targets.

cost function is not reduced in more than μ iterations where the parameter μ is empirically chosen. If the algorithm finds the global solution of the cost function, randomly-generated initial conditions around the optimal point does not give a lower cost and, therefore, the algorithm does not advance in the subsequent iterations. In this case, the procedure is stopped after μ unsuccessful trials.

4.5 Simulation Results

In this section, it is studied how the optimal allocation of antennas in the surveillance region affects the localization performance of the MIMO radar system. To do this, a collocated MIMO radar is first designed with the parameters being shown in Table 4.7. In the following subsections, the performance of the optimization algorithm is first studied for a single target scenario. Then, the simulations results will be provided for a scenario with multiple targets occupying the same resolution cell.

Algorithm 2 The Optimization Algorithm For the Case With Multiple Targets In the Same Resolution Cell

---

Initialization: Generate an initial location of antennas as $\mathbf{s}_{tm}^0, \mathbf{s}_{rn}^0$ with $m = \{1, \cdots, M\}$ and $n = \{1, \cdots, N\}$.

Optimization: Find an optimal distribution of antennas by minimizing the following cost function:

$$
\begin{aligned}
\min_{\mathbf{s}_{t1}, \cdots, \mathbf{s}_{rN}} \quad & \mathcal{T}(C_{XX'}) \\
S.T. \quad & ||\Delta \mathbf{s}_{nm}|| \geq d_{nm} \\
& ||\Delta \mathbf{s}_{nm}|| \leq e_{nm} \\
& \sum_{m=1}^{M} \mathbf{s}_{tm} + \sum_{n=1}^{N} \mathbf{s}_{rn} = 0, \ \forall \ m = \{1, \cdots, M\}, \ n = \{1, \cdots, N\}
\end{aligned}
\tag{4.64}
$$

Optimal Cost: Initialize $\mathbf{s}_{tm}^o$ and $\mathbf{s}_{rn}^o$ and calculate the assigned cost as $\mathcal{C}^o = \mathcal{T}(C_{XX'})_{\mathbf{s}_{t1}^o, \cdots, \mathbf{s}_{rN}^o}$.

Sampling: While $u \leq U$ or $NA < \mu$:

- Sample $\mathbf{s}_{tm}^0 \sim \mathcal{N}(\mathbf{s}_{tm}^o, Q)$ and $\mathbf{s}_{rn}^0 \sim \mathcal{N}(\mathbf{s}_{rn}^o, Q)$ with $m = \{1, \cdots, M\}$ and $n = \{1, \cdots, N\}$.

- Run the optimization algorithm and find the new distribution of antennas $\mathbf{s}_{tm}^\star, \mathbf{s}_{rn}^\star$ and associated cost $\mathcal{C}^\star$.

- **if** $\frac{\mathcal{C}^\star}{\mathcal{C}^0} \leq 1$ **then**
  $\mathbf{s}_{tm}^o = \mathbf{s}_{tm}^\star, \mathbf{s}_{rn}^o = \mathbf{s}_{rn}^\star$ with $m = \{1, \cdots, M\}$ and $n = \{1, \cdots, N\}$.
  $\mathcal{C}^o = \mathcal{C}^\star$.
  $NA = 0$.

- **else**
  $NA = NA + 1$.

- **end if**

Report $\mathbf{s}_{tm}^o$ and $\mathbf{s}_{rn}^o$ as the optimal distribution of antennas.

Table 4.7: Simulation Parameters For the Antenna Allocation in a Collocated MIMO Radar

Parameter	Description	Value
r_{max}	Maximum coverage range of transmitters	5(km)
r_{bin}	Range width	30(m)
λ	Wave-length	30(cm)
K	Number of snapshots	128
σ_α^2	Variance of the scatterers	10^{-4}
σ_w^2	Variance of the additive noise	1
P_m	Transmitted power	1 (w)

4.5.1   A Single-target Scenario

Initially, consider a single target being located at $[410 \;\; -710]'(\text{m})$. The parameters of the target are also chosen to be as follows:

$$\Theta = [-\frac{\pi}{3} \; .33 \; 3 \; 3] \tag{4.65}$$

In the first experiment, assume that there are M antennas available where each antenna can both transmit and receive signals. Two antenna configurations are considered in this part. First, the Uniform-Linear-Array (ULA) structure is taken where the distance between each two antennas is $\frac{\lambda}{2}$. The second configuration is the optimal geometry found by the optimization algorithm proposed in this paper. For simulations, it is assumed that $d_{mn} = \lambda, e_{mn} = 2\lambda \; \forall\{m, n\}$. The optimization algorithm is now implemented and the optimal configuration of antennas is shown in Figure 4.4 for different number of antennas. In addition, Figure 4.5 presents the CRLB of localization for the optimal and the ULA structure separately. It can be observed that the CRLB of the optimal configuration is much lower than that of the ULA structure. The improvement becomes more significant when the number of antennas is smaller. For example, for the case with $M = 2$ antennas, the CRLB of the optimal structure is around 6 times lower than that of the ULA configuration while the
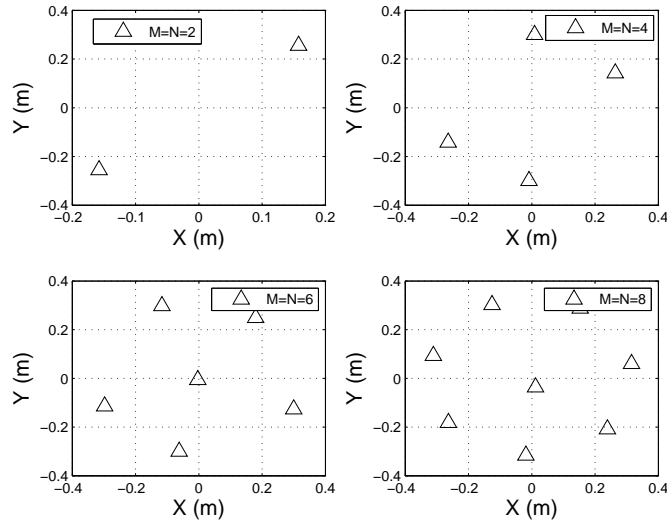
Figure 4.4: The obtained optimal configuration of antennas for a single-target case. The optimal configuration is found for different number of antennas where each antenna can both transmit and receive signals.

improvement decays to 2 times lower at $M = 5$ antennas. When the number of antennas increases, the gap between the optimal and ULA CRLB becomes tighter because the Signal-to-Noise Ratio (SNR) is large enough to make up the poor geometry of antennas.

Furthermore, in order to study how the DOA of the target affects the optimal configuration of antennas, consider the above-designed scenario with $M = 4$ antennas. While the target is still assumed to fall in the same cell defined in the above experiment, its DOA varies in the interval $\left[\frac{-\pi}{2}, \frac{\pi}{2}\right]$. The optimization algorithm is now implemented to find the optimal configuration of antennas. Figure 4.6 shows the results for four different target DOAs. The results shown in Figure 4.6 imply that the optimal configuration with θ_1 as the DOA can be obtained from the optimal structure with θ_2 by rotating the geometry $(\theta_2 - \theta_1)(\mathrm{Rad})$ around the mass center, which confirms proposition
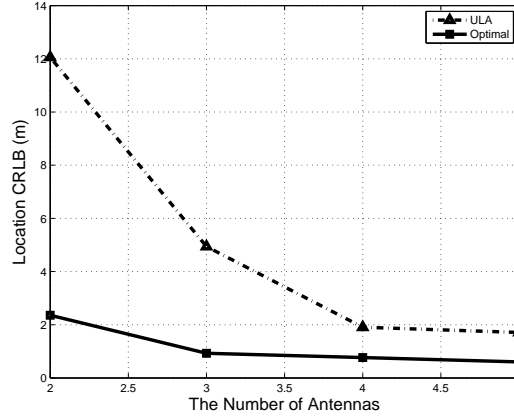
126

Figure 4.5: Localization CRLB for the ULA configuration and the optimal structure. The CRLB is found for a single-target scenario and different number of antennas.

4.4.1.

It is also beneficial to study the performance of the localization algorithm with the designed optimal configuration. To do this, assume $M = 3$ is fixed as the number of antennas. Besides the optimal and ULA configurations, a random antenna allocation is also used for the test where the antennas are randomly distributed in the underlying surveillance region. The localization Root-Mean-Squared-Error (RMSE) is now calculated at different target SNRs where all results are obtained after 100 Monte Carlo simulations. Figure 4.7 presents the resulting RMSE for each of the above-represented configurations. It is observed that the optimal configuration achieves the lowest RMSE while the ULA provides the worst results. The random allocation also gives an RMSE between the optimal and ULA configurations although other random distributions of antennas may provide higher RMSE results.

In the last experiment, simulation results were provided for a scenario in which each antenna can either transmit or receive signals. Consider a single-target scenario with $\theta^c = -\frac{\pi}{3}(\text{Rad})$ as the DOA. The optimal structure is

127

now found for two cases with $M = N = 2$ and $M = N = 6$ antennas. Figure 4.8 presents the obtained optimal structures where, for each case, the results are given for scenarios with the same and separate transmitters and receivers, respectively. It can be observed that the optimal structure obtained for each case (e.g. the same and separate transmitters and receivers) is the same with transmitters and receivers being clustered in a way that the mutual distances between the same-type antennas (e.g. transmitter or receiver) is minimized. To test this hypothesis, assume that 6 antennas are available and there are two scenarios with $M = 4$ and $M = 3$ as the number of transmitters at each scenario. The optimal structure is now found for each scenario and the final results are shown in Figure 4.9. It can be observed that the same optimal structure is obtained for both cases with antennas being clustered based on the mutual distances between the antennas with the same type. Note that although the obtained optimal structures in Figure 4.9 are similar, the optimum cost function might be different based on the number of signal paths ($M \times N$). For example, for the configurations given in Figure 4.9, the optimum cost is calculated to be .7545 and .6393 for $M = 4$ ($M \times N = 8$) and $M = 3$ ($M \times N = 9$) antennas, respectively. The obtained optimum cost values also confirm the fact that the more the diversity gain, the lower the achieved optimum cost.

4.5.2 Multiple Target Case

In this subsection, the optimization algorithm is applied to a scenario with more than one target being located in the same resolution cell. Let us assume
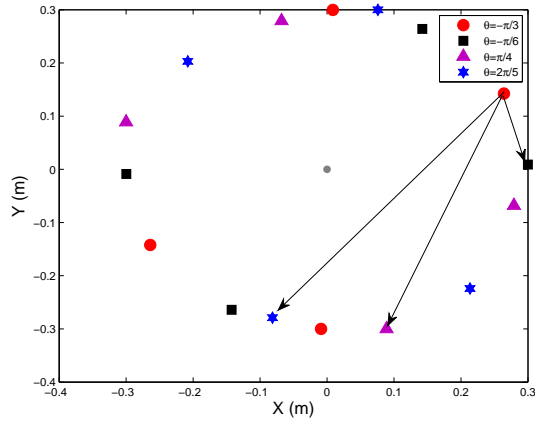
Figure 4.6: The obtained optimal configuration of antennas for a single-target case, and for four different target DOAs.
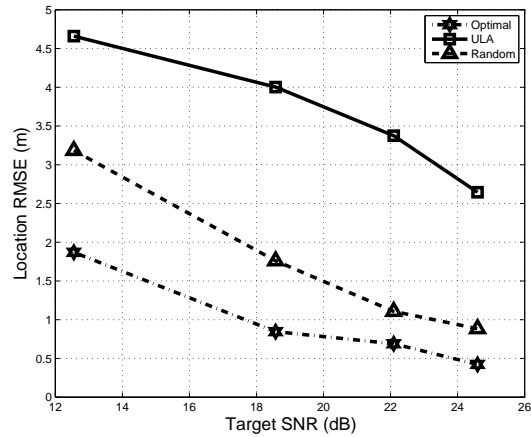
Figure 4.7: Location RMSE for different target SNRs and for the MIMO radar with $M = 3$ antennas. The RMSE results are obtained for three different structures (ULA, optimal, and randomly-distributed configurations).

129
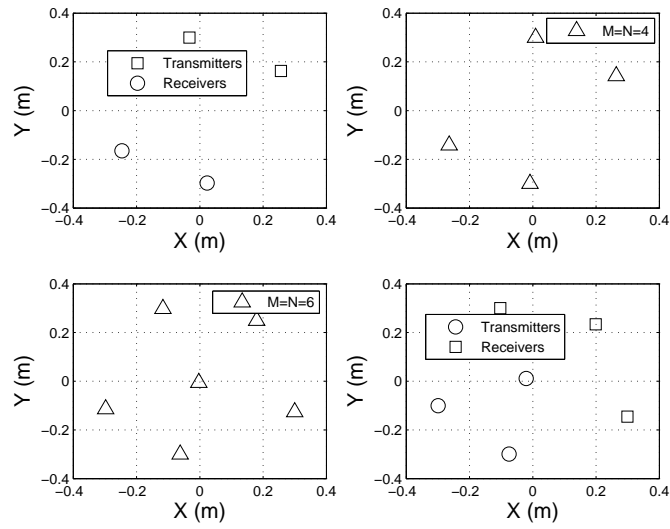
Figure 4.8: The obtained optimal configuration of antennas for a single-target case. The optimal configuration is found for different number of antennas where each antenna can either transmit or receive signals.

Figure 4.9: The obtained optimal antenna configuration for the single-target scenario when $M + N = 6$ antennas are available. The optimal structure is found for two cases with $M = 4$ and $M = 3$ antennas as the number of transmitters.

130

there are two targets falling in the same cell with the following parameters:

$$
\begin{aligned}
\Theta_1^c &= \left[-\frac{\pi}{3}\ .33\ 3\ 3\right]' \\
\Theta_2^c &= \left[+\frac{\pi}{3}\ .66\ 3\ 3\right]'
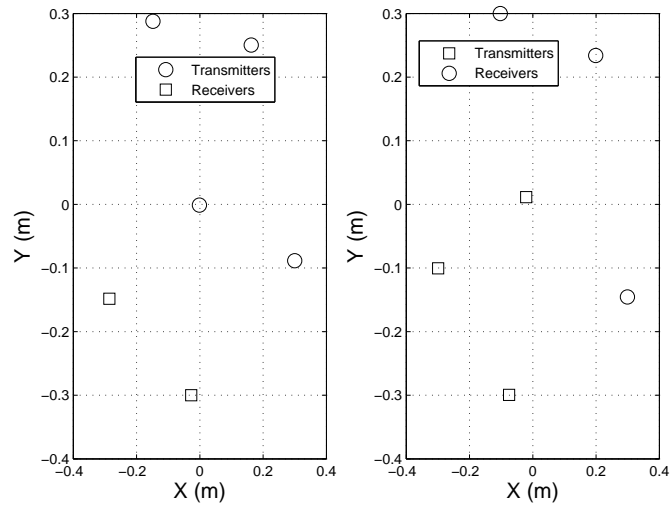\end{aligned}
\tag{4.66}
$$

Based on the results in Figure 4.3, it is now evident that the effect of sinusoid terms in the cost function cannot be ignored due to the large value for $\Delta\theta$. First, the optimization framework given by Algorithm 2 is applied to the two-target scenario with different initial conditions. Figure 4.10 shows the obtained cost values at different iterations of the algorithm and for different initial conditions. It is observed that the algorithm captures the global minimum after a number of iterations. While each initial condition leads to a different cost value, the sampling approach finally finds the structure corresponding to the global minimum. Note that without the sampling procedure, each initial condition leads to a different optimal cost as shown in Figure 4.11. However, when the sampling approach is used, regardless of the initial condition, the same optimal cost is finally obtained.

Now, the impact of the angular separation between the targets in the performance of the optimization algorithm is studied. The optimal structure is found for different values of $\Delta\theta = \theta_2^c - \theta_1^c$. The optimal configurations are now depicted in Figure 4.12 for four different values of $\Delta\theta$. It is observed that when $\Delta\theta \to 0$, the obtained structure resembles the one given in Figure 4.4 for the scenario with $M = 4$ antennas. Nevertheless, for other values of $\Delta\theta$, a new structure is obtained whose geometry depends on the distribution of targets in the resolution cell. Figure 4.13 also presents the cost function (e.g. the trace of the location CRLB) for different values of $\Delta\theta$ where the results are obtained for both optimal and ULA configurations. The graph states that the closer the targets, the poorer the performance. For example, the cost at $\Delta\theta = \frac{\pi}{100}$ is
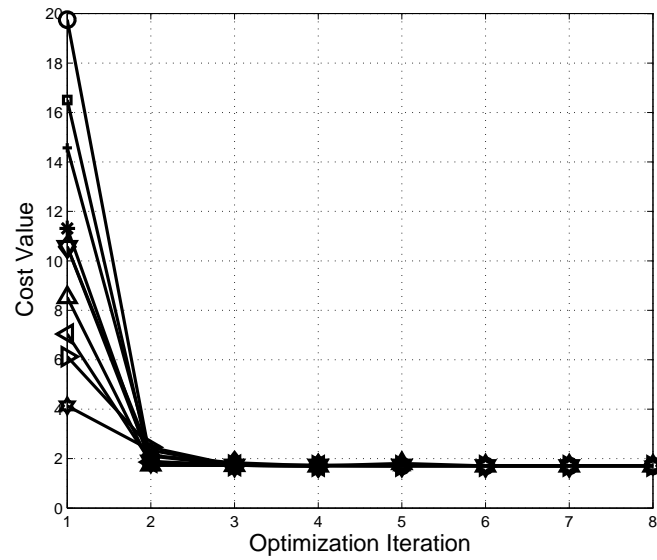
Figure 4.10: The obtained cost for 10 different initial antenna locations. The simulations are done for a two-target scenario fallen in the same resolution cell.
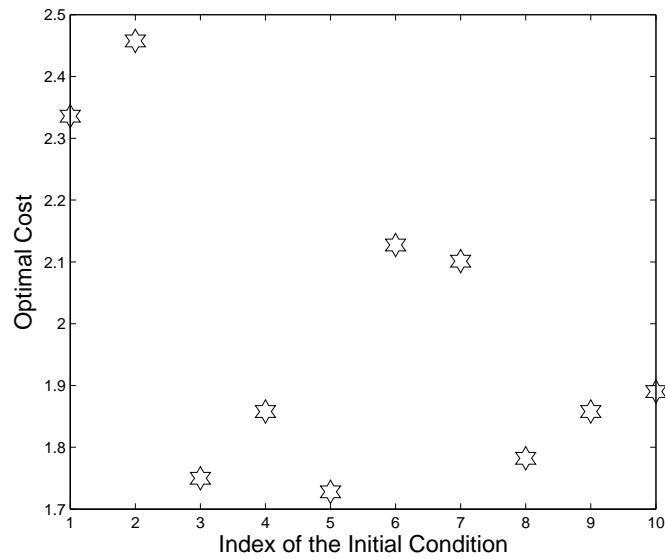

Figure 4.11: The optimal cost for 10 different initial antenna locations without using the sampling-based approach.

100% more than the one at $\Delta\theta = \frac{\pi}{50}$ when the optimal structure is taken. In addition, Figure 4.13 confirms the superiority of the optimal structure to the ULA. The rate of the improvement also increases when targets become closer, with 10 times lower cost at $\Delta\theta = \frac{\pi}{100}$ compared to 5-time lower cost achieved at $\Delta\theta = 2\frac{\pi}{3}$. The obtained results in Figures 4.4 and 4.13 imply that although the optimization algorithm can be implemented more efficiently when the angular separation between two targets becomes tighter, the performance of the localization is degraded once the target becomes closer. In other words, there is a trade-off between the quality of the localization and the efficiency of the optimization algorithm. Smaller values of $\Delta\theta$ makes the FIM entries in (4.26) less dependent on the sinusoid terms.

The performance of the optimization algorithm can be also evaluated for a scenario with more than two targets fallen inside the same resolution cell. It is known that there is a bound on the maximum number of targets that can be uniquely detected in the same resolution cell [59]. Assume different number of targets are placed in the c-th resolution cell with the same SNR being assigned to each target. Also, consider the MIMO structure with $M = N = 4$ antennas where each antenna can both transmit and receive signals. We find the optimal structure for each case with a different number of targets inside the same resolution cell. For the comparison, the localization algorithm is also applied to the obtained structures and the location RMSE is calculated by taking an average of individual estimates in 100 Monte Carlo runs. The RMSE results as well as the location CRLB are now depicted in Figure 4.14 where the graphs for the case with the ULA MIMO structure are also included. While the localization performance degrades by increasing the number of targets, the optimal structure always shows the lower RMSE compared to the ULA configuration. In addition, when more targets fall inside the same resolution

133
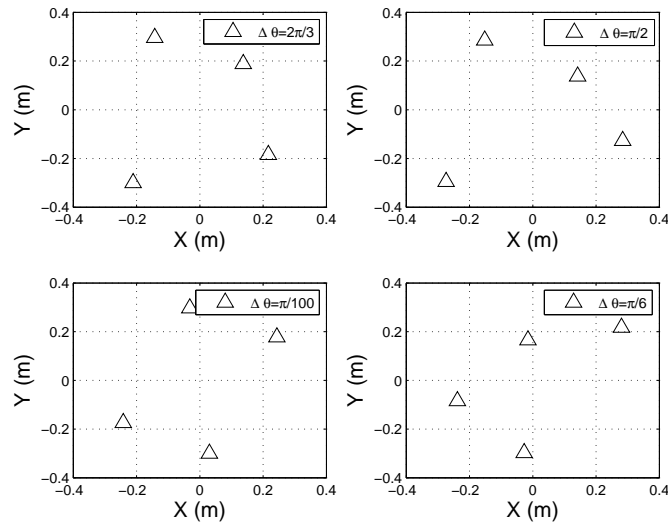
Figure 4.12: The optimal antenna configuration for the two-target scenario. The optimal structure is found for different values of $\Delta\theta$.

cell, the difference between the obtained RMSE of the ULA structure and that of the optimal configuration becomes higher. For example, for the scenario with $T = 2$ unresolved targets, the optimal RMSE is 53% lower than the RMSE obtained by the ULA structure. Nevertheless, the gap widens to 123% when 5 targets occupy the same resolution cell. Although the distribution of targets in the cell also affects the localization performance [43], this experiment shows the superiority of the optimal structure compared to the ULA configuration, specially, when more targets are placed in the same resolution cell.
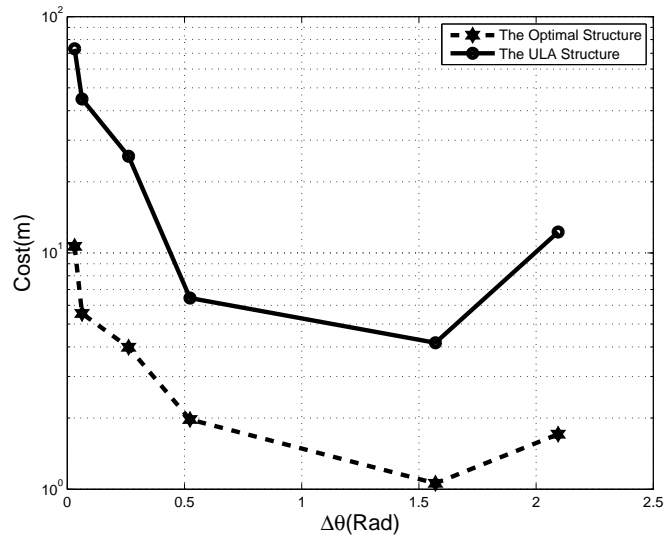
Figure 4.13: The calculated cost for the two-target scenario. The cost was calculated for different values of $\Delta\theta$ and scenarios with the optimal and ULA structure.
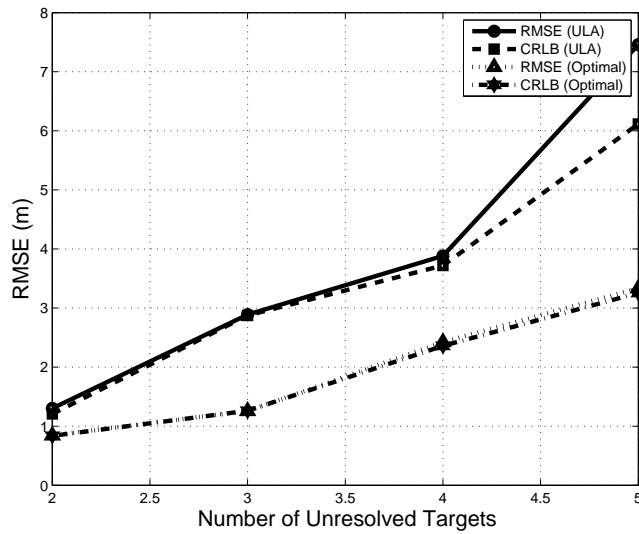
Figure 4.14: Location RMSE and CRLB for both optimal and ULA structures. The results are obtained for scenarios with different number of targets being located inside the same resolution cell.

Chapter 5

Conclusions

This thesis dealt with a number of challenging topics in the new emerging MIMO radar structures. Two well-known collocated and widely-separated MIMO radar systems were first presented. Signal models were derived for each structure and the advantages and disadvantages of each configuration compared to the traditional phased-array and multistatic radars were described.

It was observed that the traditional signal models for collocated MIMO radars suffer from the lack of observability. Therefore, a new signal model was proposed to incorporate range information in the received data in order to maintain the observability of the signal model and providing an estimate of range for targets of interest. Then, a localization algorithm was developed for the new model to estimate the number and parameters of targets. To do this, an MDL criterion was employed to find the correct number of targets inside each cell. Afterwards, the likelihood function was derived for the new model and an ML method was applied to estimate the states of targets. The parameter identifiability problem was also defined as the maximum number of unique targets that can be detected in one cell. The maximum bound for localization was derived and it was shown that, even, with the number below

the bound localization results may not be satisfactory due to the poor geometry of targets. Therefore, a multiple hypothesis based tracking method using the UKF algorithm in the filtering stage was formulated to deal with the limitation on the maximum number of uniquely detectable targets. Simulations showed that localization RMSE is affected by the geometry and number of targets located in the same cell. For comparison, simulations were done using the new signal-level tracking method and the localization-level algorithm using localization results as the measurements. Results showed the superiority of the signal-level tracking over the localization-level method even when the number of targets in the cell is below the maximum bound. Also, the the signal-level method is much more computationally efficient than the localization-level tracking method is. Finally, the new method was applied to a scenario in which the number of targets in one cell exceeds the maximum bound. Results showed the capability of the signal-level tracking method in estimating the states of unresolved targets while the localization CRLB becomes unbounded in the intervals that all targets enter the same cell. From the simulations, the efficiency of the signal-level tracking approach applied to the new developed model for co-located MIMO radars can be concluded.

This thesis also studied the impact of the distribution of antennas on the localization performance of a collocated MIMO radar. A novel derivation of the CRLB was presented where both range and DOA information were included in the CRLB. A well-known SDP was then formulated for the antenna allocation problem when a single target is available inside the resolution cell. Then, the antenna allocation was extended to the multiple unresolved target scenarios, and it was shown that the final cost function is non-convex. A sampling-based approach was then proposed to capture the global minimum of the proposed cost function. Simulation results were also presented

for both scenarios with the single-target and multiple targets occupying the same resolution cell. The obtained results confirmed the superiority of the optimal configuration compared to the common ULA structure in both single and multiple target scenarios.

The other main contribution of this thesis was to provide a general framework to analyze the performance of MIMO radars with widely-separated antennas in detecting, localizing, and tracking multiple targets with multiple scatterers. The detection capability of MIMO radars in handling multiple-scatterer targets was evaluated and their performance was compared to that of traditional multistatic radar systems. A new multiple hypothesis-based algorithm was also proposed in order to estimate the number and states of targets even when they become closely-spaced (or unresolved) in the measurement space. While the localization results can be used for track initiation, a tracking algorithm using the particle filter algorithm was presented for multitarget tracking. Using a number of simulations, the superior performance of MIMO radars over the multistatic systems was demonstrated. It was also concluded that MIMO radars are more suitable for scenarios with low target SNRs and low rate of visibility while multistatic radars are preferred at high SNRs. Finally, the performance of the tracking algorithm was evaluated using a two-target scenario. Simulations show that the proposed tracking algorithm is efficient in that it meets the PCRLB.

Chapter 6

Appendices

6.1 Partial Derivatives in the FIM of Collocated MIMO

Without loss of generality, derivatives are found for the t-th target parameters. Assume the target is located in the c-th cell. Derivatives are found for the case $c > 1$. When $c = 1$, the same equations can be used with zero derivative for $(c - 1)$-th cell. For the mean vector, the following equations are immediately obtained

$$\frac{\partial \mu_{c-1:c}}{\partial \theta_t} = [\left(\beta_t \alpha_t \dot{\mathbf{d}}_t\right)^H \ \left((1 - \beta_t)\alpha_t \dot{\mathbf{d}}_t\right)^H]^H \tag{6.1}$$

$$\frac{\partial \mu_{c-1:c}}{\partial r_t} = \frac{1}{r_{bin}}[(\alpha_t \mathbf{d}_t)^H \ (-\alpha_t \mathbf{d}_t)^H]^H \tag{6.2}$$

$$\frac{\partial \mu_{c-1:c}}{\partial \hat{\alpha}_t^R} = [(\beta_t \mathbf{d}_t)^H \ ((1 - \beta_t)\mathbf{d}_t)^H]^H \tag{6.3}$$

$$\frac{\partial \mu_{c-1:c}}{\partial \hat{\alpha}_t^I} = j\frac{\partial \mu_{c-1:c}}{\partial \hat{\alpha}_t^R} \tag{6.4}$$

where $\dot{\mathbf{d}}_t = \frac{d\mathbf{d}_t}{d\theta_t}$ that can be computed using the equation given for system matrix $\mathbf{d}_t$. For the covariance matrix, derivative is zero for DOA and scatters.

Therefore, the following equation is given for range

$$
\begin{aligned}
\frac{\partial \Sigma_{(c-1)(c-1)}}{\partial r_t} &= -4 \frac{1}{r_{bin}^2}(1-\beta_t)\sigma_\alpha^2 \mathrm{diag}(\mathbf{d}_t \mathbf{d}_t^H) \\
\frac{\partial \Sigma_{cc}}{\partial r_t} &= 4 \frac{1}{r_{bin}^2}\beta_t \sigma_\alpha^2 \mathrm{diag}(\mathbf{d}_t \mathbf{d}_t^H) \\
\frac{\partial \Sigma_{c(c-1)}}{\partial r_t} &= 2 \frac{1}{r_{bin}^2}(1-2\beta_t)\sigma_\alpha^2 \mathrm{diag}(\mathbf{d}_t \mathbf{d}_t^H)
\end{aligned}
\tag{6.5}
$$

Finally, derivatives of range and DOA can be also easily found by the following equations

$$
\frac{\partial r_t}{\partial x_t} = \frac{x_t}{r_t}, \frac{\partial r_t}{\partial y_t} = \frac{y_t}{r_t}, \frac{\partial \theta_t}{\partial x_t} = -\frac{y_t}{r_t^2}, \frac{\partial \theta_t}{\partial x_t} = \frac{x_t}{r_t^2}
\tag{6.6}
$$

6.2 Proof of Proposition 4.3.1

Consider the n-th target and the m-th target that are located in the c_1-th cell and the c_2-th cell, respectively. First, assume that $c_1 = c_2 - 1$. The unknown term $J_{\theta_n^{c_1} \theta_m^{c_2}}$ is first calculated where the proof sketch for other terms is similar. The entry $J_{\theta_n^{c_1} \theta_m^{c_2}}$ can be found using the following equality:

$$
J_{\theta_n^{c_1} \theta_m^{c_2}} = \left(\frac{\partial \bar{\rho}_*}{\partial \theta_n^{c_1}} \right)' \Sigma_*^{-1} \left(\frac{\partial \bar{\rho}_*}{\partial \theta_m^{c_2}} \right) + \mathcal{T}\left(\left(\frac{\partial \Sigma_*}{\partial \theta_n^{c_1}} \right) \Sigma_*^{-1} \left(\frac{\partial \Sigma_*}{\partial \theta_m^{c_2}} \right) \Sigma_*^{-1} \right)
\tag{6.7}
$$

Based on the definition of the covariance matrix in (4.13), it is evident that the second term in the right-hand side of the above equation equals zero. Now, according to the definition of $\bar{\rho}_*$ in (4.33), the following equations can be derived for the partial derivative terms in (6.7):

$$
\frac{\partial \bar{\rho}_*}{\partial \theta_n^{c_1}} = \left[\frac{\partial \Re(\bar{\eta}_{c_1-1})}{\partial \theta_n^{c_1}} \frac{\partial \Im(\bar{\eta}_{c_1-1})}{\partial \theta_n^{c_1}} \frac{\partial \Re(\bar{\eta}_{c_1})}{\partial \theta_n^{c_1}} \frac{\partial \Im(\bar{\eta}_{c_1})}{\partial \theta_n^{c_1}} 0 \right]
\tag{6.8}
$$

$$
\frac{\partial \bar{\rho}_*}{\partial \theta_m^{c_2}} = \left[0 \frac{\partial \Re(\bar{\eta}_{c_1})}{\partial \theta_m^{c_2}} \frac{\partial \Im(\bar{\eta}_{c_1})}{\partial \theta_m^{c_2}} \frac{\partial \Re(\bar{\eta}_{c_2})}{\partial \theta_m^{c_2}} \frac{\partial \Im(\bar{\eta}_{c_2})}{\partial \theta_m^{c_2}} \right]
\tag{6.9}
$$

After some straightforward algebraic operations, the FIM in (6.7) can be written in the following form:

$$
\begin{aligned}
J_{\theta_n^{c_1}\theta_m^{c_2}} &= k_2 \left\{ \left(\frac{\partial\Re(\bar{\eta}_{c_1})}{\partial\theta_n^{c_1}}\right)\left(\frac{\partial\Re(\bar{\eta}_{c_1})}{\partial\theta_m^{c_2}}\right)' + \left(\frac{\partial\Im(\bar{\eta}_{c_1})}{\partial\theta_n^{c_1}}\right)\left(\frac{\partial\Im(\bar{\eta}_{c_1})}{\partial\theta_m^{c_2}}\right)' \right\} \\
&+ k_4 \left\{ \left(\frac{\partial\Re(\bar{\eta}_{c_1-1})}{\partial\theta_n^{c_1}}\right)\left(\frac{\partial\Re(\bar{\eta}_{c_1})}{\partial\theta_m^{c_2}}\right)' + \left(\frac{\partial\Im(\bar{\eta}_{c_1-1})}{\partial\theta_n^{c_1}}\right)\left(\frac{\partial\Im(\bar{\eta}_{c_1})}{\partial\theta_m^{c_2}}\right) \right\} \\
&+ k_5 \left\{ \left(\frac{\partial\Re(\bar{\eta}_{c_1-1})}{\partial\theta_n^{c_1}}\right)\left(\frac{\partial\Re(\bar{\eta}_{c_2})}{\partial\theta_m^{c_2}}\right)' + \left(\frac{\partial\Im(\bar{\eta}_{c_1-1})}{\partial\theta_n^{c_1}}\right)\left(\frac{\partial\Im(\bar{\eta}_{c_2})}{\partial\theta_m^{c_2}}\right)' \right\} \\
&+ k_6 \left\{ \left(\frac{\partial\Re(\bar{\eta}_{c_1})}{\partial\theta_n^{c_1}}\right)\left(\frac{\partial\Re(\bar{\eta}_{c_2})}{\partial\theta_m^{c_2}}\right)' + \left(\frac{\partial\Im(\bar{\eta}_{c_1})}{\partial\theta_n^{c_1}}\right)\left(\frac{\partial\Im(\bar{\eta}_{c_2})}{\partial\theta_m^{c_2}}\right)' \right\} \quad (6.10)
\end{aligned}
$$

Using (4.10) and (4.11) and the notations given by definitions 4.3.3 and 4.3.4, the following expressions can be derived for the derivatives in (6.10):

$$
\begin{aligned}
\left(\frac{\partial\Re(\bar{\eta}_{c_1})}{\partial\theta_n^{c_1}}\right)\left(\frac{\partial\Re(\bar{\eta}_{c_1})}{\partial\theta_m^{c_2}}\right)' &= K\left(\frac{2\pi}{\lambda}\right)^2 \beta_n^{c_1}(1-\beta_m^{c_2})\sum_{l=1}^{MN}(\mathbf{p}_n^{c_1})'\Omega(:,l)\Omega'(:,l)\mathbf{p}_m^{c_2} \times \\
&\times \left(\bar{\xi}_n^{c_1}\cos(\omega_n^{c_1}(l)) - \bar{\zeta}_n^{c_1}\sin(\omega_n^{c_1}(l))\right) \times \\
&\times \left(\bar{\xi}_m^{c_2}\cos(\omega_m^{c_2}(l)) - \bar{\zeta}_m^{c_2}\sin(\omega_m^{c_2}(l))\right) \\
\left(\frac{\partial\Im(\bar{\eta}_{c_1})}{\partial\theta_n^{c_1}}\right)\left(\frac{\partial\Im(\bar{\eta}_{c_1})}{\partial\theta_m^{c_2}}\right)' &= K\left(\frac{2\pi}{\lambda}\right)^2 \beta_n^{c_1}(1-\beta_m^{c_2})\sum_{l=1}^{MN}(\mathbf{p}_n^{c_1})'\Omega(:,l)\Omega'(:,l)\mathbf{p}_m^{c_2} \times \\
&\times \left(\bar{\xi}_n^{c_1}\sin(\omega_n^{c_1}(l)) + \bar{\zeta}_n^{c_1}\cos(\omega_n^{c_1}(l))\right) \times \\
&\times \left(\bar{\xi}_m^{c_2}\sin(\omega_m^{c_2}(l)) + \bar{\zeta}_m^{c_2}\cos(\omega_m^{c_2}(l))\right)
\end{aligned}
$$

$$(6.11)$$

Therefore, the first term in the right hand side of (6.10) can be written as

$$
\begin{aligned}
k_2 \left\{ \left(\frac{\partial\Re(\bar{\eta}_{c_1})}{\partial\theta_n^{c_1}}\right)\left(\frac{\partial\Re(\bar{\eta}_{c_1})}{\partial\theta_m^{c_2}}\right)' + \left(\frac{\partial\Im(\bar{\eta}_{c_1})}{\partial\theta_n^{c_1}}\right)\left(\frac{\partial\Im(\bar{\eta}_{c_1})}{\partial\theta_m^{c_2}}\right)' \right\} &= K\left(\frac{2\pi}{\lambda}\right)^2 \beta_n^{c_1}(1-\beta_m^{c_2}) \times \\
\times \left\{ \sum_{l=1}^{nm}(\mathbf{p}_n^{c_1})'\Omega(:,l)\Omega'(:,l)\mathbf{p}_m^{c_2}\left(\kappa_{c_1c_2}^{nm}\cos(\omega_m^{c_2}(l) - \omega_n^{c_1}(l)) + \iota_{c_1c_2}^{nm}\sin(\omega_m^{c_2}(l) - \omega_n^{c_1}(l))\right) \right\}
\end{aligned}
$$

$$(6.12)$$

141

Other terms in the right-hand side of (6.10) can be similarly found. The final form can be now written as follows:

$$
\begin{aligned}
J_{\theta_n^{c_1}\theta_m^{c_2}} &= K\left(\frac{2\pi}{\lambda}\right)^2 \sum_{l=1}^{MN} (\mathbf{p}_n^{c_1})'\Omega(:,l)\Omega'(:,l)\mathbf{p}_m^{c_2} \times \\
&\quad \times \left(\kappa_{c_1 c_2}^{nm}\cos(\omega_m^{c_2}(l)-\omega_n^{c_1}(l)) + \iota_{c_1 c_2}^{nm}\sin(\omega_m^{c_2}(l)-\omega_n^{c_1}(l))\right) \times \\
&\quad \times \left(k_2\beta_n^{c_1}(1-\beta_m^{c_2}) + k_4(1-\beta_n^{c_1})(1-\beta_m^{c_2}) + k_5\beta_n^{c_1}\beta_m^{c_2} + k_6\beta_n^{c_1}(1-\beta_m^{c_2})\right)
\end{aligned}
$$
(6.13)

where the term in the second line of the above equation can be written as follows:

$$
\begin{aligned}
\left(k_2\beta_n^{c_1}(1-\beta_m^{c_2}) + k_4(1-\beta_n^{c_1})(1-\beta_m^{c_2}) + k_5\beta_n^{c_1}\beta_m^{c_2} + k_6\beta_n^{c_1}(1-\beta_m^{c_2})\right) &= \\
= \left[(\breve{\beta}_n^{c_1})'\ 0\right]\Sigma_*^{-1}&\left[0\ (\breve{\beta}_m^{c_2})'\right]'
\end{aligned}
$$
(6.14)

which is the coefficient $C_{\theta_n^{c_1}\theta_m^{c_2}}$. For the case with $c_1 = c_2$, the same procedure can be followed and the expression in the proposition is similarly found.

6.3 Proof of Theorem 4.4.1

We begin with the optimization formulation given by (4.57). Define the new matrix T_{nm} and the new variable t_{nm} with $\{m = 1, \cdots, M\}, \{n = 1, \cdots, N\}$, and rewrite the optimization problem as follows:

$$
\begin{aligned}
\max_{\{\Delta\mathbf{s}_{11},\cdots,\Delta\mathbf{s}_{nm},\mathbf{t},T^*\}} \quad & \sum_{m=1}^{M}\sum_{n=1}^{N} t_{nm} \\
\text{S.T} \quad & \|\Delta\mathbf{s}_{nm}\|_2 \geq d_{nm} \\
& \|\Delta\mathbf{s}_{nm}\|_2 \leq e_{nm} \\
& \sum_{m=1}^{M}\mathbf{s}_{tm} + \sum_{n=1}^{N}\mathbf{s}_{rn} = 0 \\
& (\mathbf{p}^c)'T_{nm}\mathbf{p}^c \geq t_{nm} \\
& (\Delta\mathbf{s}_{nm})(\Delta\mathbf{s}_{nm})' \succeq T_{nm}, \forall\ m = \{1,\cdots,M\}, n = \{1,\cdots,N\}
\end{aligned}
$$
(6.15)

where $\mathbf{t} = [t_{11} \cdots t_{nm}]'$, and $T^* = \{T_{11}, \cdots, T_{nm}\}$. The second-norm terms in the constraints can be written into the following form:

$$\begin{bmatrix} -I_{2\times 2} & \Delta\mathbf{s}_{nm} \\ \Delta\mathbf{s}'_{nm} & -e^2_{nm} \end{bmatrix} \preceq 0, \quad \begin{bmatrix} I_{2\times 2} & \Delta\mathbf{s}_{nm} \\ \Delta\mathbf{s}'_{nm} & d^2_{nm} \end{bmatrix} \preceq 0 \qquad (6.16)$$

In addition, using the Schur-complement of a square matrix, the last constraint in (6.15) is written as

$$\begin{bmatrix} 1 & \Delta\mathbf{s}'_{nm} \\ \Delta\mathbf{s}_{nm} & T_{nm} \end{bmatrix} \preceq 0 \qquad (6.17)$$

Inserting the new forms provided by (6.16) and (6.17) in (6.15) and using the fact that $(\mathbf{p}^c)'T_{nm}\mathbf{p}^c = \mathcal{T}(T_{nm}P)$ with $P = \mathbf{p}^c(\mathbf{p}^c)'$, the following new form is derived for the optimization problem:

$$\max_{\{T^*, S^*, \mathbf{t}\}} \qquad \sum_{m=1}^{M} \sum_{n=1}^{N} t_{nm}$$

$$\text{S.T} \qquad \sum_{m=1}^{M} \mathbf{s}_{tm} + \sum_{n=1}^{N} \mathbf{s}_{rn} = 0$$

$$\mathcal{T}(T_{nm}P) \geq t_{nm}$$

$$\begin{bmatrix} -I_{2\times 2} & \Delta\mathbf{s}_{nm} \\ \Delta\mathbf{s}'_{nm} & -e^2_{nm} \end{bmatrix} \preceq 0, \quad \begin{bmatrix} I_{2\times 2} & \Delta\mathbf{s}_{nm} \\ \Delta\mathbf{s}'_{nm} & d^2_{nm} \end{bmatrix} \preceq 0$$

$$\begin{bmatrix} 1 & \Delta\mathbf{s}'_{nm} \\ \Delta\mathbf{s}_{nm} & T_{nm} \end{bmatrix} \preceq 0, \forall \; m = \{1, \cdots, M\}, n = \{1, \cdots, N\}$$

where $S^* = \{\mathbf{s}_{t1}, \cdots, \mathbf{s}_{rN}\}$. Now, the difference vector is written as

$$\Delta\mathbf{s}_{nm} = \mathbf{s}_{rn} - \mathbf{s}_{tm} \qquad (6.18)$$

Replacing the above equation in (6.18), the form given by the theorem is obtained.

6.4   Proof of Lemma 4.4.1

Consider the optimal structure found for the case with θ_1. Assuming θ_2 as the new DOA the cost function in (4.57) can be rewritten as follows:

$$\sum_{m=1}^{M}\sum_{n=1}^{N}\Delta\mathbf{s}'_{nm}P^*\Delta\mathbf{s}_{nm} \tag{6.19}$$

with $P^* = (\mathbf{p}^*)'\mathbf{p}^*$ and $\mathbf{p}^* = [\cos(\theta_1 + \Delta\theta) \ -\sin(\theta_1 + \Delta\theta)]'$. The vector $\mathbf{p}^*$ can be expanded as

$$\mathbf{p}^* = \begin{bmatrix} \cos(\Delta\theta) & \sin(\Delta\theta) \\ -\sin(\Delta\theta) & \cos(\Delta\theta) \end{bmatrix} \begin{bmatrix} \cos(\theta_1) \\ -\sin(\theta_1) \end{bmatrix} \tag{6.20}$$

Defining the first term in the right-hand side of the above equation as $G_{\Delta\theta}$, the cost function can be rewritten as follows:

$$\sum_{m=1}^{M}\sum_{n=1}^{N}\Delta\mathbf{s}'_{nm}G_{\Delta\theta}PG'_{\Delta\theta}\Delta\mathbf{s}_{nm} \tag{6.21}$$

We know that $\Delta\mathbf{s}^{o1}_{nm} = (\mathbf{s}^{o1}_{tm} - \mathbf{s}^{o1}_{rn})$ maximizes the cost function in (4.57) where P is the matrix corresponding the target with θ_1 as the DOA. Therefore, an optimal solution of the optimization problem with θ_2 as the DOA of the target can be obtained as

$$G'_{\Delta\theta}\mathbf{s}^{o2}_{tm} = \mathbf{s}^{o1}_{tm} \tag{6.22}$$

$$G'_{\Delta\theta}\mathbf{s}^{o2}_{rn} = \mathbf{s}^{o1}_{rn}, \ \forall \ m = \{1,\cdots,M\}, n = \{1,\cdots,N\} \tag{6.23}$$

Consequently, the new optimal solution is written as follows:

$$\mathbf{s}^{o2}_{tm} = G_{\Delta\theta}\mathbf{s}^{o1}_{tm} \tag{6.24}$$

$$\mathbf{s}^{o2}_{rn} = G_{\Delta\theta}\mathbf{s}^{o1}_{rn}, \ \forall \ m = \{1,\cdots,M\}, n = \{1,\cdots,N\} \tag{6.25}$$

Now, we have to check whether the new solution holds in the constraints. It can be easily shown that:

$$||\Delta\mathbf{s}^{o2}_{nm}||_2 = ||\Delta\mathbf{s}^{o1}_{nm}||_2 \tag{6.26}$$

144

In addition, it is known that:

$$\sum_{m=1}^{M} \mathbf{s}_{tm}^{o2} + \sum_{n=1}^{N} \mathbf{s}_{rn}^{o2} = G_{\Delta\theta} \left(\sum_{m=1}^{M} \mathbf{s}_{tm}^{o1} + \sum_{n=1}^{N} \right) = 0 \qquad (6.27)$$

which implies that the new optimal solution also meets the constraints.

6.5   Proof of Proposition 4.4.2

Consider the optimization problem in (4.57) without including the constraint on the mass center. In this case, the cost function is quadratic with respect to the unknown difference vectors. The unique optimal solution obtained by solving the resulting optimization problem can be written as $\{\Delta\mathbf{s}_{nm}^{o}\}$ with $m = \{1, \cdots, M\}$ and $n = \{1, \cdots, N\}$. It is evident that there are an infinite number of location solutions for which the above set of difference vectors are obtained. Let us define the i-th and the j-th sets as $\{S_t^{oi}, S_r^{oi}\}$ and $\{S_t^{oj}, S_r^{oj}\}$, respectively. It is known from the geometry that:

$$\mathbf{s}_{tl}^{oi} = G_\theta \mathbf{s}_{tl}^{oj} + \mathbf{b}_{tl} \qquad (6.28)$$

where G_θ denotes a rotation matrix with θ as the angle of the rotation, and $\mathbf{b}$ refers to an arbitrary translation. Note that the above equation can be written for every other antenna in the array of receivers as well. Considering the mass center constraint given by (4.2.3), we show that the translation should be zero in (6.28). To show this, we first assume that there is a nonzero translation as $\mathbf{b}_{tl}$. Then, it is observed that such an assumption leads to the contradiction. It is known that the center of the mass of the array is located in the origin. Therefore, there should be another translation $\mathbf{b}_{tv}$ where $\mathbf{b}_{tv} = -\mathbf{b}_{tl}$. Under the new translations, the new difference vector is written as

$$(\mathbf{s}_{tl}^{oi} - \mathbf{s}_{tv}^{oi}) = (\mathbf{s}_{tl}^{oj} - \mathbf{s}_{tv}^{oj} + 2\mathbf{b}_{tl}) \qquad (6.29)$$

It is now evident that the new configuration gives a different set of difference vectors, which is a contradiction to our initial assumption (e.g. the same set of difference vectors). Therefore, the translation part in (6.28) is zero. Now, consider the rotation part in (6.28). It is known that the rotation transform does not change the distance between each two points. Rewrite the cost function in (4.57) into the following form:

$$\sum_{m=1}^{N}\sum_{n=1}^{N}(\mathbf{s}_{nm}^{oi})'P^c\Delta\mathbf{s}_{nm}^{oi} = \sum_{m=1}^{N}\sum_{n=1}^{N}(\mathbf{s}_{nm}^{oj})'G_\theta'P^cG_\theta\Delta\mathbf{s}_{nm}^{oj} \tag{6.30}$$

Using formal matrix operations, the new matrix $U = G_\theta'P^cG_\theta$ can be written in the following form:

$$U = \begin{bmatrix} \cos^2(\theta + \theta^c) & -\sin(\theta + \theta^c)\cos(\theta + \theta^c) \\ -\sin(\theta + \theta^c)\cos(\theta + \theta^c) & \sin^2(\theta + \theta^c) \end{bmatrix} \tag{6.31}$$

The cost produced by each of two sets of optimal solutions is equal if the following condition is held:

$$\sum_{m=1}^{M}\sum_{n=1}^{N}(\Delta\mathbf{s}_{nm}^{oi})'V\Delta\mathbf{s}_{nm}^{oi} = 0 \tag{6.32}$$

with $V = U - P^c$. The equality in (6.32) is valid if either $V = 0$ or V is neither positive nor negative semi-definite. First, assume $V = 0$. Based on the given form in (6.31) for the matrix U, it can be inferred that $U = P^c$ when $\theta = n\pi$. In other words, a rotation with $n\pi$ as the angle of rotation provides the same cost function. Now, assume the other case where $V \neq 0$. It can be shown that matrix V has two eigenvalues $\{\lambda, -\lambda\}$ where the value of λ depends on the rotation angle and θ^c. Therefore, the zero inequality in (6.32) leads to a number of solutions for the difference vectors. The rotated configuration can be then another solution of the optimization problem if $\{S_t^{oi}, S_r^{oi}\}$ belongs to the set of solutions of (6.32). The above discussions state that the optimization problem provides at least two solutions for the optimum configuration of antennas.

Bibliography

[1] M. Akcakaya and A. Nehorai, "Adaptive MIMO radar design and detection in compound-Gaussian clutter", *IEEE Transactions on Aerospace and Electronic Systems*, Vol. 47, No. 3, pp. 2200-2207, July 2011.

[2] S. Ahmed, J. S. Thompson, Y. R. Petillot, and B. Mulgrew, "Unconstrained synthesis of covariance matrix for MIMO radar transmit beampattern", *IEEE Transactions on Signal Processing*, Vol. 59, No. 8, pp. 3837-3849, August 2011.

[3] M.S. Arulampalam, S. Maskell, N. Gordon, and T. Clapp, "A tutorial on particle ?lters for online nonlinear/non-Gaussian Bayesian tracking", IEEE Transcations on Signal Processing, Vol. 50, No. 2, pp. 174-188, February 2002.

[4] V. Balasubramanian, *MDL, Bayesian inference and the geometry of the space of the probability distributions.* In P. D. Grunwald, I. J. Myung and M. A. Pitt (Eds.), Advances in Minimum Description Length: Theory and Applications, pp. 81–98, The MIT Press, 2006.

[5] Y. Bar-shalom and X. R. Li, *Multitarget-multisensor tracking: Principles and techniques*, Storrs, CT: YBS Publishing, 1995.

[6] Y. Bar-Shalom, X.R. Li, and T. Kirubarajan, *Estimation, Tracking and Navigation: Theory, Algorithms and Software*, John Wiley & Sons, New York, 2001.

[7] I. Bekkerman, and J. Tabrikian, "Target detection and localization using MIMO radars and sonars", *IEEE Transactions on Signal Processing*, Vol. 54, No. 10, pp. 3873–3883, October 2006.

[8] E. Biglieri, J. Proakis, and S. Shamai, "Fading channels: information-theoretic and communication aspects", *IEEE Transactions On Information Theory*, Vol. 44, No. 6, pp. 2619–2692, Octobe 1998.

[9] E. Biglieri, R. Calderbank, A. Constantinides, A. Goldsmith , A. Paulraj, and H. V. Poor, "An introduction to wireless communication", *Cambridge University Press*, New York, June 2006.

[10] A. N. Bishop, B. Fidan, B. D. O. Anderson, K. Dogancay, and P. N. Pathirana, "Optimality analysis of sensor-target localization geometries", *Automatica*, Vol. 46, pp. 479–492, 2010.

[11] E. Bjrnson, D. Hammarwall, B. Ottersten, "Exploiting quantized channel norm feedback through conditional statistics in arbitrarily correlated MIMO systems", *IEEE Transactions on Signal Processing*, Vol. 57, No. 10, pp. 4027–4041, October 2009.

[12] S.S. Blackman, "Multiple hypothesis tracking for multitarget tracking", *IEEE Aerospace and Electronic Systems Magezine*, Vol. 19, No. 1, pp. 5-18, January 2004.

[13] S. Boyd, and L. Vandenberghe, "Convex optimization", *Cambridge University Press*, 2004.

[14] D. Bruyere and N. Goodman, "Adaptive detection and diversity order in multistatic radar", *IEEE Transactions on Aerospace and Electronic Systems*, Vol. 44, No. 4, pp. 1615-1623, October 2008.

[15] C. Chen, and P. P. Vaidyanathan, "MIMO radar ambiguity properties and optimization using frequency-hopping waveforms", *IEEE Transactions on Signal Processing*, Vol. 56, No. 12, pp. 5926–5936, December 2008.

[16] C. Chen, and P. P. Vaidyanathan, "MIMO Radar Waveform Optimization with Prior Information of the Extended Target and Clutter", *IEEE Transactions on Signal Processing*, Vol. 57, No. 9, pp. 3533–3544, September 2009.

[17] W. J. Chen and R. M. Narayanan, "Antenna placement for minimizing target localization error in UWB MIMO noise radar", *IEEE Antennas and Wireless Propagation Letters*, Vol. 10, pp. 135-138, 2011.

[18] C. Y. Chong, F. Pascal, J. P. Ovarlez, and M. Lesturgie, "MIMO radar detection in non-Gaussian and heterogeneous clutter", *IEEE Journal of Selected Topics in Signal Processing*, Vol. 4, No. 1, pp. 115-126, February 2010.

[19] C. Chuah, D. Tse, J. Kahn, and R. Valenzuela, "Capacity scaling in MIMO wireless systems under correlated fading", *IEEE Transactions On Information Theory*, Vol. 48, pp. 637-650, March 2002.

[20] G. Cui, L. Kong, and X. Yang, "Multiple-input multiple-output radar detectors design in non-Gaussian clutter", *IET Radar, Sonar & Navigation*, Vol. 4, No. 5, pp. 724-732, October 2010.

[21] E. DAddio and A. Farina, "Overview of detection theory in multistatic radar", *IEE Proceedings of Communications, Radar, and Signal Processing*, Vol. 133, No. 7, pp. 613-623, December 1986.

[22] F. Daum, "MIMO radar: snake oil or good idea?", Proc. of IEEE Conference on Waveform Diversity and Design, pp. 113–117, February 2009.

[23] E. Martos-Naya, J. F. Paris, U. Fernandez-Plazaola, and A. Goldsmith, "Exact closed-form performance analysis for MIMO beamforming with MRC under prediction errors", Submitted to *IEEE Transactions on Wireless Communications*, February 2007.

[24] M. Evans, N. Hastings, and B. Peacock, "Erlang distribution", Ch. 12 in *Statistical Distributions*, 3rd ed. New York: Wiley, pp. 71–73, 2000.

[25] E. Fishler, A. Haimovich, R. Blum, L.J. Cimini, D. Chizhik, and R.A. Valenzuela, "Spatial diversity in radars- models and detection performance", *IEEE Transactions on Signal Processing*, Vol. 54, No. 3, pp 823–838, March 2006.

[26] P. H. Foo, "Combining the interacting multiple model method with particle filters for manoeuvring target tracking with a multistatic radar system", *IET Radar, Sonar & Navigation*, Vol. 5, No. 7, pp. 697-706, August 2011.

[27] G. J. Foschini and M. J. Gans, "On limits of wireless communications in a fading environment when using multiple antennas", *Wireless Personal Commun.: Kluwer Academic Press*, No. 6, pp. 311-335, 1998.

[28] D. R. Fuhrmann, G. San Antonio, "Transmit beamforming for MIMO radar systems using signal cross-correlation", *IEEE Transactions on*

Aerospace and Electronic Systems, Vol. 44, No. 1, pp. 171–186, January 2008.

[29] D. R. Fuhrmann, J. P. Browning, and M. Rangaswamy, "Signaling strategies for the hybrid MIMO Phased-Array radar", *IEEE Journal of Selected Topics in Signal Processing*, Vol. 4, No. 1, pp. 66-78, February 2010.

[30] A.A.E. Fuste, A.B. Ibars, J.P. Antequera, and J.C.M. Yuste, "CFAR data fusion center with inhomogeneous receivers", *IEEE Transactions on Aerospace and Electronic Systems*, Vol. 28, No. 1, pp. 276–285, January 1992.

[31] D. Gesbert, M. Kountouris, R. W. Heath, Jr., C.-B. Chae, and T. Salzer, "Shifting the MIMO Paradigm: From Single User to Multiuser Communications", *IEEE Signal Processing Magazine*, vol. 24, no. 5, pp. 36-46, October 2007.

[32] F. Gini, F. Lombardini, and P.K. Varshney, "On distributed signal detection with multiple local free parameters", *IEEE Transactions on Aerospace and Electronic Systems*, Vol. 35, No. 4, pp. 1457–1466, October 1999.

[33] H. Godrich, A. M. Haimovich, and R. S. Blum, "Target localisation techniques and tools for multiple-input multiple-output radar", *IET Radar, Sonar & Navigation*, Vol. 3, No. 4, pp. 314-327, August 2009.

[34] H. Godrich, A. M. Haimovich, and R. S. Blum, "A MIMO radar system approach to target tracking", Proc. Asilomar Conference on Signals, Systems, and Computers, pp. 11861190, USA, November 2009.

[35] H. Godrich, A. M. Haimovich, and R. S. Blum, "Target localization accuracy gain in MIMO radar-based systems", *IEEE Transactions on Information Theory*, Vol. 56, No. 6, pp. 2783–2803, June 2010.

[36] H. Godrich, V. M. Chiriac, A. M. Haimovich, and R. S. Blum, "Target tracking in MIMO radar systems: Techniques and performance analysis", Proc. IEEE Radar Conference, pp. 1111-1116, Arlington, USA, May 2010.

[37] H. Godrich, A. P. Petropulu, and H. V. Poor, "Sensor selection in distributed multiple-radar architectures for localization: a knapsack problem formulation", *IEEE Transactions on Signal Processing*, Vol. 60, No. 1, pp. 247–260, January 2012.

[38] S. Gogineni and A. Nehorai, "Polarimetric MIMO radar With distributed antennas for target detection", *IEEE Transactions on Signal Processing*, Vol. 58, No. 3, pp. 1689-1697, March 2010.

[39] S. Gogineni and A. Nehorai, "Target estimation using sparse modeling for distributed MIMO radar", *IEEE Transactions on Signal Processing*, Vol. 59, No. 11, pp. 5315-5325, November 2011.

[40] S. Gogineni and A. Nehorai, "Monopulse MIMO radar for target tracking", *IEEE Transactions on Aerospace and Electronic Systems*, Vol. 47, No. 1, pp. 755-768, January 2011.

[41] A. Goldsmith, S. A. Jafar, N. Jindal, and S. Vishwanath, "Capacity limits of MIMO channels", *IEEE Journal on Selected Areas in Communications*, Vol. 21, No. 5, pp. 684–702, June 2003.

[42] N. A. Goodman and D. Bruyere, "Optimum and decentralized detection for multistatic airborne radar", *IEEE Transactions on Aerospace and Electronic Systems*, Vol. 43, No. 2, pp. 806-813, April 2007.

[43] A. A. Gorji, R. Tharmarasa, W. D. Blair, and T. Kirubarajan, "Multiple unresolved target localization and tracking using collocated MIMO radars", *IEEE Transactions on Aerospace and Electronic Systems*, Accepted in the Final Form, October 2011.

[44] M. Grant, and S. Boyd, "CVX user's guide", Technical Report, Standford University, February 2002.

[45] B. Habtemariam, R. Tharmarasa, and T. Kirubarajan, "Multitarget track-before-detect with MIMO radars", Proc. IEEE Aerospace Conference, Big Sky, pp. 19, USA, March 2010.

[46] A. M. Haimovich, "Coherent MIMO radar: high resolution applications", Presentation, Princeton, November 2007.

[47] A. M. Haimovich, R. S. Blum, and L. J. Cimini, "MIMO radar with widely separated antennas", *IEEE Signal Processing Magazine*, Vol. 25, No. 1, pp. 116-129, 2008.

[48] A. Hassanien, and S. A. Vorobyov, "Phased-MIMO radar: a tradeoff between Phased-array and MIMO radars", *IEEE Transactions on Signal Processing*, Vol. 58, No. 6, pp. 3137–3151, June 2010.

[49] Q. He, R. S. Blum, H. Godrich, and A. M. Haimovich, "Target velocity estimation and antenna placement for MIMO radar with widely separated antennas", *IEEE Journal of Selected Topics in Signal Processing*, Vol. 4, No. 1, pp. 79-100, February 2010.

[50] Q. He, N. Lehmann, R. S. Blum, A. M. Haimovich, "MIMO radar moving target detection in homogeneous clutter", *IEEE Transactions on Aerospace and Electronic Systems*, Vol. 46, No. 3, pp. 1290-1301, July 2010.

[51] Q. He, R. S. Blum, H. Godrich, and A. M. Haimovich, "Target velocity estimation and antenna Placement for MIMO Radar with widely separated antennas", *IEEE Journal of Selected Topics in Signal Processing*, Vol. 4, No. 1, pp. 79–100, February 2010.

[52] Q. He and R. S. Blum, "Diversity gain for MIMO Neyman-Pearson signal detection", *IEEE Transactions On Signal Processing*, Vol. 59, No. 3, pp. 869–881, March 2011.

[53] H. He, P. Stoica, and J. Li, "Wideband MIMO systems: signal design for transmit beampattern synthesis", *IEEE Transactions on Signal Processing*, Vol. 59, No. 2, pp. 618–628, February 2011.

[54] T. Jeffery, "Phased-array radar design: application of radar fundamentals", *Scitech Pub Inc*, January 2009.

[55] S. Julier, J. Uhlmann and H. Durrant-Whyte, "A new approach for ?ltering nonlinear systems", Proceedings of the American Control Conference, Seattle, USA, June 1995.

[56] T. Kirubarajan, H. Wang, Y. Bar-Shalom and K. R. Pattipati, "Efficient multisensor fusion using multidimensional data association", *IEEE Transactions on Aerospace and Electronic Systems*, Vol. 37, Issue 2, pp. 386–400, April 2001.

[57] N. H. Lehmann, E. Fishler, A. M. Haimovich, R. S. Blum, D. Chizhik, L. J. Cimini, and R. A. Valenzuela, "Evaluation of transmit diversity in MIMO radar direction finding", *IEEE Transactions on Signal Processing*, Vol. 55, No. 5, pp. 2215-2225, May 2007.

[58] J. Li, and P. Stoica, "MIMO radar with collocated antennas", *IEEE Signal Processing Magezine*, Vol. 24, No. 5, pp. 106-114, September 2007.

[59] J. Li, P. Stoica, X. Luzhou, and W. Roberts, "On parameter identifiability of MIMO radar", *IEEE Signal Processing Letters*, Vol. 14, No. 2, pp. 968–971, December 2007.

[60] J. Li, L. Xu, P. Stoica, K. W. Forsythe, and D. W. Bliss, "Range compression and waveform optimization for MIMO radar: a Cramer-Rao bound based study", *IEEE Transactions on Signal Processing*, Vol. 56, No. 1, pp. 218–232, January 2008.

[61] J. Li, and P. Stoica, "MIMO Radar Signal Processing", *Hoboken, NJ: John Wiley Sons*, 2009.

[62] M. Malanowski and K. Kulpa, "Two methods for target localization in multistatic passive radar", *IEEE Transactions on Aerospace and Electronic Systems*, Vol. 48, No. 1, pp. 572-580, January 2012.

[63] A.V. Mrstik, "Multistatic-radar binomial detection", IEEE Transactions on Aerospace and Electronic Systems, Vol. 14, No. 1, pp. 103108, January 1978.

[64] R. U. Nabar, H. Bolcskei, and A. J. Paulraj, "Diversity and outage perfor-
mance in space-time block coded Ricean MIMO channels", *IEEE Transac-
tions on Wireless Communications*, Vol. 4, No. 5, pp. 2519–2532, Septem-
ber 2005.

[65] R. Niu, R.S. Blum, P.K. Varshney, and A.L. Drozd, "Target tracking in
widely separated non-coherent multiple-input multiple-output radar sys-
tems", Proc. of Asilomar Conference on Signals, Systems, and Computers,
pp. 11811185, USA, November 2009.

[66] A. Papoulis, *Probability, Random Variables, and Stochastic Processes*,
McGraw-Hill, Inc., 1991.

[67] W. Roberts, P. Stoica, J. Li, T. Yardibi, and F. A. Sadjadi, "Iterative
adavptive approaches to MIMO radar imaging", *IEEE Journal of Selected
Topics in Signal Processing*, Vol. 4, No. 1, pp. 5–20, February 2010.

[68] G. San antonio, D. R. Fuhrmann, and F. C. Robey, "MIMO radar ambi-
guity functions", *IEEE Journal of Selected Topics in Signal Processing*,
Vol. 1, No. 1, pp. 167-177, June 2007.

[69] F. Septier, Sze Kim Pang, S. Godsill and A. Carmi, "Tracking of co-
ordinated groups using marginalised MCMC-based Particle algorithm",
Proceedings of IEEE Aerospace Conference, Mnotana, USA, March 2009.

[70] H. Shin and M. Z. Win, "MIMO diversity in the presence of double scat-
tering", *IEEE Transactions on Information Theory*, Vol. 45, No. 7, pp.
2976–2996, July 2008.

[71] S. Simakov, "Localization in airborne multistatic sonars", *IEEE Journal
of Oceanic Engineering*, Vol .33, No. 3, pp. 278-288, July 2008.

[72] M. Skolnik, "Introduction to radar systems", 3rd ed. *New York: McGraw-Hill*, 2002.

[73] A. Soysal, and S. Ulukus, "Joint channel estimation and resource allocation for MIMO systems-part II: multi-user and numerical analysis", *IEEE Transactions on Wireless Communications*, Vol. 9, No. 2, pp. 632–640, February 2010.

[74] P. Stoica, J. Li, and X. Zhu, "Waveform synthesis for diversity-based transmit beampattern design", *IEEE Transactions on Signal Processing*, Vol. 56, No. 6, pp. 2593–2598, June 2008.

[75] P. Swerling, "Radar probability of detection for some additional ?uctuating target cases", *IEEE Transactions on Aerospace and Electronic Systems*, Vol. 33, No. 2, pp. 698-709, April 1997.

[76] X. Tan, W. Roberts, J. Li, and P. Stoica, "Sparse learning via iterative minimization with application to MIMO radar imaging", *IEEE Transactions on Signal Processing*, Vol. 59, No. 3, pp. 1088–1101, March 2011.

[77] E. Telatar, "Capacity of Multi-antenna Gaussian channels", *European Transactions on Telecommunications*, Vol. 10, No. 6, pp. 585–595, December 1999.

[78] R. Tharmarasa, T. Kirubarajan, M. L. Hernandez, and A. Sinha, "PCRLB-based multisensor array management for multitarget tracking", *IEEE Transactions on Aerospace and Electronic Systems*, Vol. 43, No. 2, pp. 539–555, April 2007.

157

[79] P. Tichavsky, C. Muravchik and A. Nehorai, "Posterior Cramer-Rao bounds for discrete-time nonlinear filtering", *IEEE Transactions on Signal Processing*, Vol. 46, No. 5, pp. 1386–1396, 1998.

[80] J. Vermaak, S. Godsill and P. Perez, "Monte Carlo filtering for multi-target tracking and data association", *IEEE Transactions on Aerospace and Electronic Systems*, Vol. 41, Issue 1, pp. 309–332, January 2005.

[81] L. Xu, and J. Li, "Iterative generalized-likelihood ratio test for MIMO radar", *IEEE Transactions on Signal Processing*, Vol. 55, No. 6, pp. 2375–2385, June 2007.

[82] L. Xu, J. Li, and P. Stoica, "Target detection and parameter estimation for MIMO radar systems", *IEEE Transactions on Aerospace and Electronic Systems*, Vol. 44, No. 3, pp. 927–939.

[83] H. Yan, J. Li, and G. Liao, "Multitarget identification and localization using bistatic MIMO radar systems", *Eurasip Journal on Advances in Signal Processing*, Vol. 2008, 2008.

[84] Y. Yang, R. S. Blum, and S. Sfar, "Antenna selection for MIMO systems with closely spaced antennas", *EURASIP Journal on Wireless Communications and Networking*, Vol. 2009, March 2009.

[85] H. Yong, and G. Jian, "A track-before-detect algorithm for statistical MIMO radar multitarget detection", Proc. IEEE Radar Conference, Arlington, USA, May 2010.

[86] T. Yu, and A. Goldsmith, "Capacity and power allocation for fading MIMO channels with channel estimation error", *IEEE Transactions on Information Theory*, Vol. 52, No. 5, pp. 2203–2214, May 2006.

[87] P. Wang, L. Hongbin, and B. Himed, "Moving target detection using distributed MIMO radar in clutter with nonhomogeneous power", *IEEE Transactions on Signal Processing*, Vol. 59, No. 10, pp. 4809-4820, October 2011.

[88] L. Zheng and D. N. C. Tse, "Diversity and multiplexing: A fundamental tradeoff in multiple antenna channels", *IEEE Transactions On Information Theory*, Vol. 49, No. 5, pp. 1073-1096, May 2003.

[89] X. Zhang, P. Willet and Y. Bar-Shalom, "Detection and localization of multiple unresolved extended targets via monopulse radar signal processing", *IEEE Transactions on Aerospace and Electronic Systems*, Vol. 45, No. 2, pp. 455-472, June 2009.

[90] J. Zhang, H. Wang, and Z. Zhu, "Adaptive waveform design for separated transmit/receive ULA-MIMO radar", *IEEE Transactions on Signal Processing*, Vol. 58, No. 9, pp. 4936-4942, September 2010.

[91] X. J. Zhang, Y. Gong, and K. B. Letaief, "On the diversity gain in MIMO channels with joint power and rate control based on noisy CSITR", *IEEE Transactions On Wireless Communications*, Vol. 10, No. 1, pp. 68–72, January 2011.